Charles University in Prague
2nd Faculty of Medicine

Field of study: Medical Biophysics

Mgr. Martin Plencner

Nanofiber Scaffolds for Incisional Hernia Regeneration

Nanovlákenné nosiče pro regeneraci incisionální kýly

PhD Thesis

Supervisor: Prof. RNDr. Evžen Amler, CSc.

Prague, 2015

Statement of originality:

I hereby declare that this thesis and the work reported herein was composed by and originated entirely from me. This thesis has not been submitted for any degree or other purposes. Information derived from the published and unpublished work of others has been acknowledged in the text and references are given in the list of sources.

I agree with prolonged accumulation of an electronic version of my work in the Theses.cz interuniversity database system project for the purposes of systematic checks on similarities among theses.

Prague,

Martin Plencner

PLENCNER, Martin. *Nanovlákenné nosiče pro regeneraci incisionální kýly (Nanofiber Scaffolds for Incisional Hernia Regeneration).* Praha, 2015, S138, 3 příl. Disertační práce (Ph.D.). Univerzita Karlova v Praze, 2. Lékařská fakulta, Ústav biofyziky. Vedoucí práce Amler, Evžen.

Key words: Nanofibers, Polypropylene surgical mesh, hernia regenerarion, Growth factors, Platelet Rich Plasma, Drug Delivery System.

Klíčová slova: Nanovlákna, Polypropylénova chirurgická síťka, Regenerace hernie, Růstové faktory, Plasma bohatá na trombocyty, Systém dodávání léčiv.

First of all, I would like to express my gratitude to my supervisor, Prof. RNDr. Evžen Amler, CSc., for his valuable advice and for many suggestions concerning my experimental work.

I would like to thank the Institute of Biophysics, 2nd Faculty of Medicine, Charles University in Prague and the Institute of Experimental Medicine of the Academy of Sciences of the Czech Republic, with whose support I was able to carry out all the experiments.

I very appreciate the help of my colleagues from Institute of Experimental Medicine, Mgr. Eva Prosecká, Mgr. Michala Rampichová, Ph.D., Mgr. Eva Filová, Ph.D., Mgr. Andrea Míčková, Mgr. Matej Buzgo, Mgr. Jana Benešová, Mgr. Věra Sovková and MUDr. Ing. Karolína Vocetková. My thanks also belong to prof. MUDr. Jiří Hoch, CSc. and MUDr. Barbora East both from Department of Surgery, 2nd Faculty of Medicine, Charles University in Prague for the valuable advice and participating in *in vivo* tests, to MVDr. Andrej Litvinec, Ph.D. for the surgeries on animals, to Doc. MUDr. Mgr. Zbyněk Tonar, Ph.D. and Doc. MUDr. Milena Králíčková, Ph.D. for their great work in the histological analyses, and to Ing. Martin Otáhal, Ph.D. for measuring the mechanical properties of the scaffolds.

I am grateful to my reviewers and opponents for revising my thesis and for their comments.

I owe a great debt of gratitude to my entire family and friends for their support throughout all my studies.

List of Abbreviations

Abbreviation	Explanation
Aa	Area fraction
AU	Absorbance unit
BCECF-AM	2´,7'-Bis[2carboxyethyl]-5[6]-carboxyfluorescein acetoxymethyl ester
bFGF	Basic fibroblast growth factor
BMP	Bone morphogenic protein
BrdU	5-bromo-2'-deoxyuridine
BSA	Bovine serum albumin
DiOC6	3,3'-Dihexyloxacarbocyanine iodide
DMEM	Dulbecco's modified Eagle's medium
DMSO	Dimethyl sulfoxide
DNA	Deoxyribonucleic acid
E	elasticity in traction
ECM	Extracellular matrix
EDTA	Ethylenediaminetetraacetic acid
EGF	Epidermal growth factor
EMA	European Medicine Agency
ePTFE	Expanded polytetrafluoroethylene
ε_{max}	Proportional elongation
FBS	Fetal bovine serum
FDA	Food and Drug Administration
FESEM	Field emission scanning electron microscopy
GF	Growth factor
HA	Hyaluronic acid
hr	Human recombinant
HRP	Horseradish peroxidase
IGF	Insulin growth factor

IL	Interleukin
i.m.	Intra-muscular
i.v.	Intra-venous
MSC	Mesenchymal stem cells
MTS	3-[4,5-dimethylthiazol-2-yl]-(3-(4,5-dimethylthiazol-2-yl)-5-(3-carboxymethoxyphenyl)-2-(4-sulfophenyl)-2H-tetrazolium bromide
MTT	3-[4,5-dimethylthiazol-2-yl]-2,5-diphenyltetrazolium bromide
n.s.	No significance
PBS	Phosphate buffered saline
PCL	Poly-ε-caprolactone
PDGF	Platelet-derived growth factor
PEG	Polyethylene glycol
PEO	Polyethylene oxide
PET	Polyethylene terephthalate
PLA	Polylactic acid
PLGA	poly(lactic-co-glycolic) acid
PP	Prolene™
PPP	Platelet-poor plasma
PRP	Platelet-rich plasma
PTFE	Polytetrafluoroethylene
PU	Polyurethane
PVA	Polyvinyl alcohol
Qa	Section area
®	Registered trademark
s.c.	Subcutaneous
SD	Standard deviation
SDF	Stromal cell-derived factor
SDS	Sodium dodecyl sulphate
SEM	Scanning electron microscopy
SMC	Smooth muscle cells

$\sigma_{max.}$	Maximum strength force
TGF	Transforming growth factor
TM	Trademark
TRS	Thrombocytes-rich solution
VEGF	Vascular endothelial growth factor
vWF	Von Willebrand factor

Contents

1 Introduction

The development of tissue engineering as a new promising discipline for the repair of various defects and injuries is primarily connected with the production of new tissues or whole organs *in vitro.* In the preparation of new tissue prosthetics it is crucial to use an appropriate scaffold as a carrier of different kinds of new cells. Highly-porous scaffolds with interconnected pores are favoured in tissue-engineering applications (Sato T. et al., 2004). Biodegradable nanofibers produced by electrospinning are receiving much attention nowadays. These scaffolds contain fibers in the diameter of the extracellular matrix (ECM; Khil M.S., et al., 2005), which plays a pivotal role in cell adhesion, proliferation, migration and differentiation (Khil M.S. et al., 2011). The optimal scaffold in tissue engineering should mimic the natural ECM and thus provide an appropriate microenvironment for the cells of new formed tissues. The big advantages in using nanofibers as a scaffold for tissue regeneration are found in their topographical features, which can be easily adjusted to fit specific applications (Lukas D. et al., 2009; Bhardwaj N. and Kundu S.C., 2010; Grafahrend D. et al., 2011).

More than a hundred surgical meshes have been designed for use in abdominal wall hernia repair procedures (Shankaran V. et al., 2011). However, no single mesh has yet demonstrated the ability to simultaneously promote host tissue remodelling and the high-strength repair of abdominal wall defects (Ebersole G.C et al., 2012). The ideal mesh does not yet exist, and still needs to be developed. One of the possibilities on how to effectively improve the properties of the surgical meshes for incisional hernia repair that has been used till now is to combine them with other promising tissue engineered scaffolds, or to completely replace the meshes through them.

1.1 Hernia in general

An abdominal hernia is an abnormal protrusion of the intra-abdominal contents through a defect in the abdominal wall. This defect may occur either as an indirect hernia that is congenital or a direct hernia that is acquired. Abdominal wall hernias are very common. Approximately 50,000 hernioplasties are performed each year in Germany alone (Bittner R. et al., 2014) and 100,000-200,000 incisional hernia repairs are performed annually in the United States (Flum D.R. et al., 2003). Operations for abdominal wall hernia are important from the medical and socio-economical perspective because of their high frequency, especially in the elderly, and the potential to cause more serious complications.

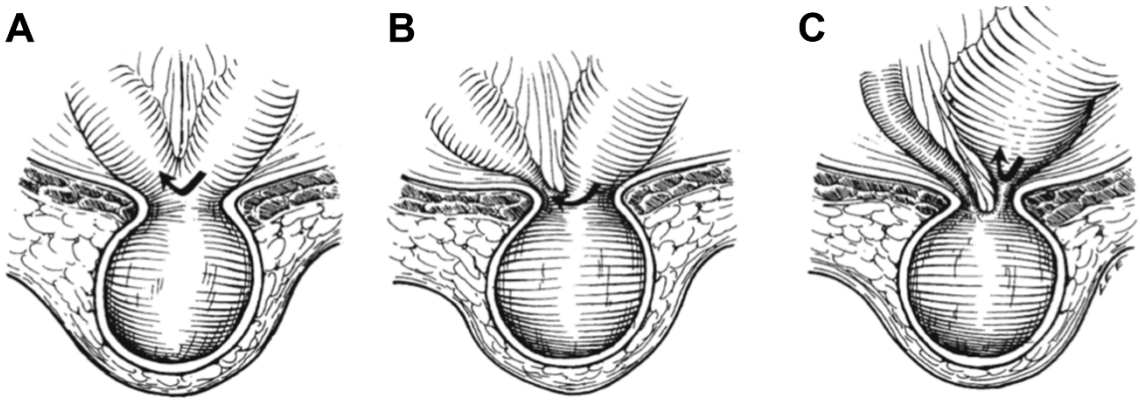

Figure 1. Abdominal wall hernia. The circumference of the bowel and progressive situation. (A) partial involvement of the bowel circumference without obstruction. (B) Subacute obstruction. (C) Complete obstruction and strangulation.

Notes: Adapted from Bay-Nielsen M., 2013.

Complications of abdominal wall hernias can lead to incarceration with a subsequent acute obstruction and strangulation, which even could cause a life threatening situation (Figure 1). Incarceration is the state when an external hernia cannot be reduced into the abdomen. Incarceration is caused by (a) a tight hernia sac neck; (b) adhesion between the hernia contents and the sac lining, with the possible

development of previous ischemia and inflammation; (c) development of pathology in the incarcerated viscus, e.g. a carcinoma or diverticulitis in the incarcerated colon; (d) the impaction of faeces in an incarcerated colon (Bay-Nielsen M., 2013).

1.1.1 Types of hernias

Abdominal wall hernias are classified as external either when the hernia sac is clinically palpable or occult external due to the presence of ansa within the abdominal wall, which do not emerge on the surface (Fisch A.E. and Brodey P.A., 1981). It could be congenital or acquired through trauma or after surgery. Abdominal wall hernias are considered the most frequent external hernias (Lee G.H. and Cohen A.J., 1993; Miller P.A. et al., 1995).

Inguinal hernia could be classified as an oblique external (indirect) hernia or a direct hernia. Both of them occur due to the acquired weakness and dilatation of the internal inguinal ring. Inguinal hernias are more prevalent in males. An indirect hernia is localized laterally to the inferior epigastric vessels whereas a direct hernia is localized medially (Ekberg O. and Kesek P., 1987).

Femoral hernias are rare in comparison with inguinal hernias. They are more common in women between 30 and 60 years of age who have been pregnant or are obese, but they can also arise in men. They usually occur on the right side (Ianora A.A., 2000).

Ventral hernias, also called **primary** abdominal wall hernias, include all hernias localized in the anterior abdominal wall except for inguinal hernias (Harrison L.A. et al., 1995).

Umbilical hernia is a very common type of ventral hernia. This hernia represents a protrusion through the *linea alba* in the region of the umbilicus. Umbilical hernias are

most common in females (Lee G.H. and Cohen A.J., 1993). Frequent risk factors are obesity, multiple pregnancies and ascites (Miller P.A. et al., 1995).

Epigastric hernias are less common and can develop in both women and men. It occurs along the xipho-umbilical line through the stretching of the *linea alba* and usually develops in people born with a weak spot in the abdominal muscle (Miller P.A. et al., 1995).

Spigelian hernias are truly rare and occur in less than 2% of patients with any anterior abdominal wall hernias (Hiller N. et al., 1994). They are generally acquired lateral to the rectus muscle and below the umbilicus.

Parastromal hernias are caused by the protrusion of a bowel ansa near an ileostomy or a colostomy (Etherington R.J. et al., 1990; Lee G.H. and Cohen A.J., 1993). Most of these hernias occur as a consequence of technical errors during surgery. Other risk factors are obesity, chronic coughing and a distended abdomen (Lee G.H. and Cohen A.J., 1993). These types of hernias are excluded from the group of incisional abdominal wall hernias although they are by definition incisional hernias. Parastromal hernias are included in a different group requiring specific properties and treatments (Muysoms F.E. et al., 2009).

The last main type of hernia is an **incisional hernia.**

1.2 Incisional hernia

For an incisional hernia there was the decision to use the definition proposed by Korenkov et al. An incisional hernia is: “Any abdominal wall gap with or without a bulge in the area of a postoperative scar perceptible or palpable by clinical examination or imaging” (Korenkov M. et al., 2001).

1.2.1 Classification of incisional abdominal wall hernia

A general classification of incisional abdominal wall hernias is important for an objective comparison of publishing results and future hernia studies. It is necessary to know whether various medical cases described in different studies are comparable. Until 2009 there were suggested several classifications in the literature primarily for incisional hernias but the authors were uncertain for a long time. For example the classification proposed by Chervrel and Rath in 2000 was simple and the required data to match the classification were easily obtained (Chevrel J.P. and Rath A.M., 2000). Unfortunately, this classification has not been commonly used in the literature. Thus several members of the European Hernia Society suggested the current classification for incisional abdominal wall hernias (Figure 2; Muysoms F.E. et al., 2009).

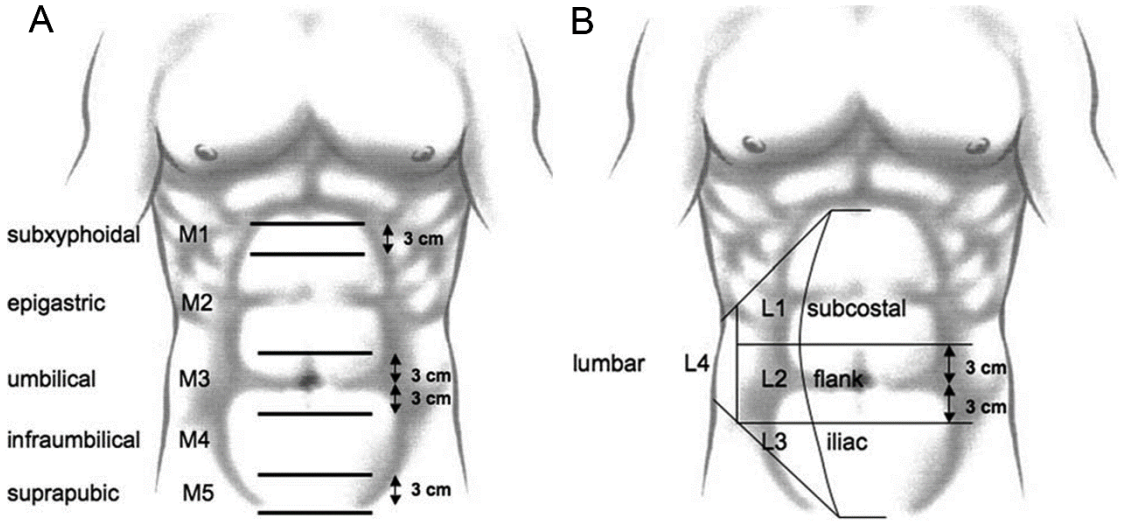

Figure 2. Classification of an incisional abdominal wall hernia according to localisation. (A) Five midline subgroups. (B) Four lateral subgroups.

Notes: Adapted from Muysoms F.E. et al., 2009.

Muysoms et al. divide an incisional hernia according to main localisation into a midline and lateral group. The midline group is subsequently divided into 5 subgroups named M1- M5, moving from the xiphoid to the pubic bone (Figure 2A). The lateral

group is divided into 4 other groups named L1-L4, and is presented in Figure 2B (Muysoms F.E. et al., 2009).

Complementary classification includes information about the size of a hernia when the weight and height is measured or it was accepted to use a semi-quantitative division, taking only the width as a measurement. The size of the hernia is then divided into 3 groups (W1 $<$ 4 cm; W2 ≥ 4-10 cm; W3 ≥ 10 cm). The last parameter included the information if an incisional hernia is a recurrence and how many time after previous repair (Muysoms F.E. et al., 2009).

1.2.2 Incidence of incisional hernia and the need for using prosthetic repair

An incisional hernia is the most common postoperative complication, affecting up to 20% of patients after a midline incision and is associated with high morbidity and significant socio-economic costs (Sugerman H.J. et al., 1996; Hoer J. et al. 2002). The treatment of incisional hernias using primary wound closure (simple suture) and fascia doubling in Mayo's technique had a recurrence rate of more than 40% (Mayo W.J., 1899; Paul A. et al., 1998). Progress in the knowledge of reinforcements of the abdominal wall using prosthetic meshes has reputedly reduced the rate up to 10% in relation to the type of hernia and the technique used (Conze J. et al., 2005). In contrast to this data there is the often cited randomised controlled trial study from Holland revealing the 10-year cumulative rate of recurrence after incisional hernia repair even at an unacceptable level of 63% for suture repair and 32% for prosthetic repair (Burger J.W. et al, 2004). In 2008 Cochrane's review of 3 trial studies comparing open primary suture repair of incisional hernia and open prosthetic repair showed recurrence rates of 54% and 16%, respectively (den Hartog D. et al., 2008). The cumulative incidence

of re-operation after incisional hernia repair, with or without a surgical mesh, has exhibited a linear rise over the years. An implantation of a mesh did not reduce the risk of recurrence – it only delayed the onset of hernia recurrence by 2-3 years (Flum D.R. et al., 2003).

Synthetic meshes have become a standard aspect of care in ventral and incisional hernia repair, even though the recurrence rates are still very high (Usher F.C. et al.,1958). Incorporating polymeric meshes during hernia repair has demonstrated the reduction of recurrence rates, minimizing of pain, improving patient outcomes postoperatively in general, and is not associated with the increased incidence of complication (Luijendijk R.W. et al., 2000; Burger J.W. et al, 2004).

1.2.3 The basic operation technique in prosthetic incisional hernia repair

Worldwide, there is insufficient coherence on the terminology for a prosthetic mesh position either during a laparoscopic or open approach to incisional hernia repair. Thus the European Hernia Society has attempted to unite the existing terminology and proposethe definition of positions listed in Table 1 and the illustration represented by Figure 3 (Muysoms F. et al., 2012).

Another discussed topic related to ventral and incisional hernia repair techniques is the use of the laparoscopic approach. The laparoscopic repair of hernias was introduce in the 1990s with potential advantages such as the need for smaller incisions, a decrease in wound infection, less consumption of narcotics after surgeries and a shorter hospital stay (Park A. et al., 1998; Ramshaw B.J. et al., 1999). The 5-year recurrence rates of laparoscopic repair and open mesh repair are nearly the same, 29% and 28%, respectively (Ballem N. et al., 2008). However, Ballem et al. also

revealed that patients who required conversion from laparoscopic to open repair had a higher rate of immunosuppression, ascites and a larger size defect. All these complications contributed to the 5year rate of recurrence at a level of up to 60% (Ballem N. et al., 2008).

Table 1. Definitions of the mesh position in ventral and incisional hernia repair

Position	Definition
Onlay	The mesh is positioned above the abdominal wall muscles and fascia, behind the subcutaneous fat
Inlay	The mesh is positioned in the hernia defect, without overlap, and fixed to the margins of the defect
Retromuscular Medial	The mesh is positioned behind the *rectus abdominis* muscle and in front of the posterior rectus fascia or in front of the peritoneum
Retromuscular Lateral	The mesh is placed in the plane between the lateral abdominal wall muscles
Preperitoneal	The mesh is placed in the plane behind all the abdominal wall muscles in front of the peritoneum
Intraperitoneal	The mesh is placed behind all layers of the abdominal wall, including the parietal peritoneum

Notes: Adapted from Muysoms F. et al., 2012

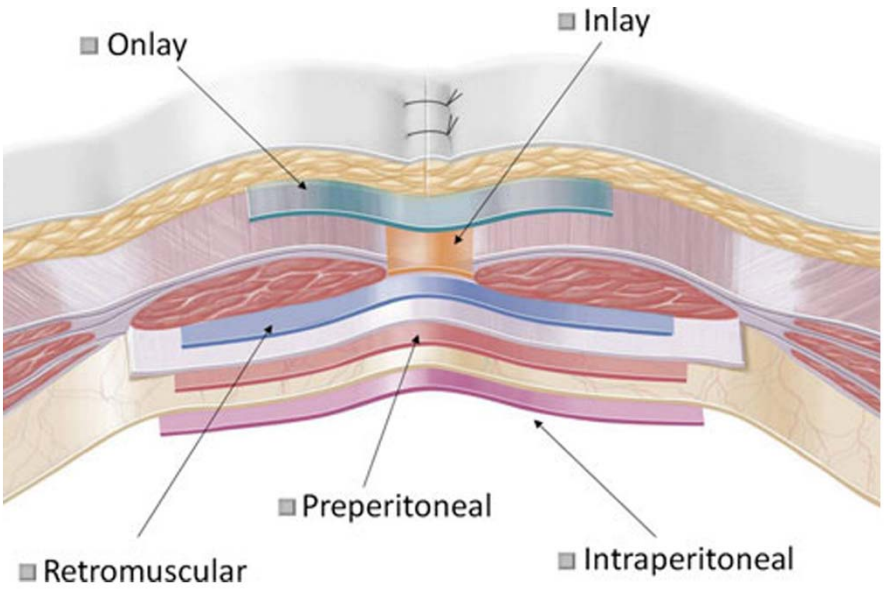

Figure 3. Terminology of mesh position in ventral and incisional hernia repair.

Notes: Adapted from Muysoms F. et al., 2012

1.2.4 The main risks of an incisional hernia developing after prosthetic repair

Repairs to a large incisional defect often requires the use of a prosthetic implant, which can cause various long-term complications, e.g. adhesion formation, graft infection/rejection, erosions, migration, loss of bio-compliance, fistula formation and hernia recurrence (Vrijland W.W. et al., 2000; Jacob B.P. et al., 2007; Losanoff J.E. et al., 2002; Jezupovs A. and Mihelsons M., 2006; Jacob B.P. and Ramshaw B., 2013). Other studies have also revealed different complications such as the shrinkage, contraction and distortion of the surgical meshes, which could lead to chronic pain and recurrence (Klinge U. et al., 1998a; Cozad M. et al., 2010). The optimal mesh should minimize the complications connected with the wound healing process. This process consists of five overlapping stages: haemostasis, inflammation, proliferation, contraction, and remodelling (Figure 4; Franz M.G., 2006; Binnebosel M. et al., 2011). Implanting a material into a living body can be considered an injury, and likewise evokes a cascade of host reactions, including blood-material interactions with the formation of a fibrin matrix, inflammation, cellular infiltration, new tissue formation and remodelling. After the initial inflammatory response, blood vessels and mesenchymal cells will start to approach and eventually invade the implant. The kind of tissue that is finally formed depends on the microenvironment to which the migrated cells will be exposed (Cobb W.S. et al., 2009; Voskerician G. et al., 2010).

Important risk factors, besides choosing the proper type of prosthetics and operation technique in the abdominal wall hernia development, is the lifestyle patients have. The most detrimental negative influence is smoking tobacco. Smokers have a four-time higher recurrence rate of ventral hernias in comparison with non-smokers. Knuutinen et al. showed that a synthesis of collagen type I and type III are negatively

affected by smoking (Knuutinen A. et al, 2002). That can result in a reduction of the collagen I/III ration, which causes a decrease of abdominal wall tissue stability (Birk D.E. and Mayne R., 1997). The negative ratio of those collagens was also described by Klosterhalfen and Klinge, who revealed that tissues surrounding the explanted surgical meshes because of hernia recurrence showed a lowered collagens ratio of 70% (Klosterhalfen B. and Klinge U., 2013). In addition, smokers have matrix metalloproteinase enzymes, which degrade the collagens expressed in higher levels, possibly causing a decrease in the final tensile strength of the new healed wound tissue (Knuutinen A. et al, 2002).

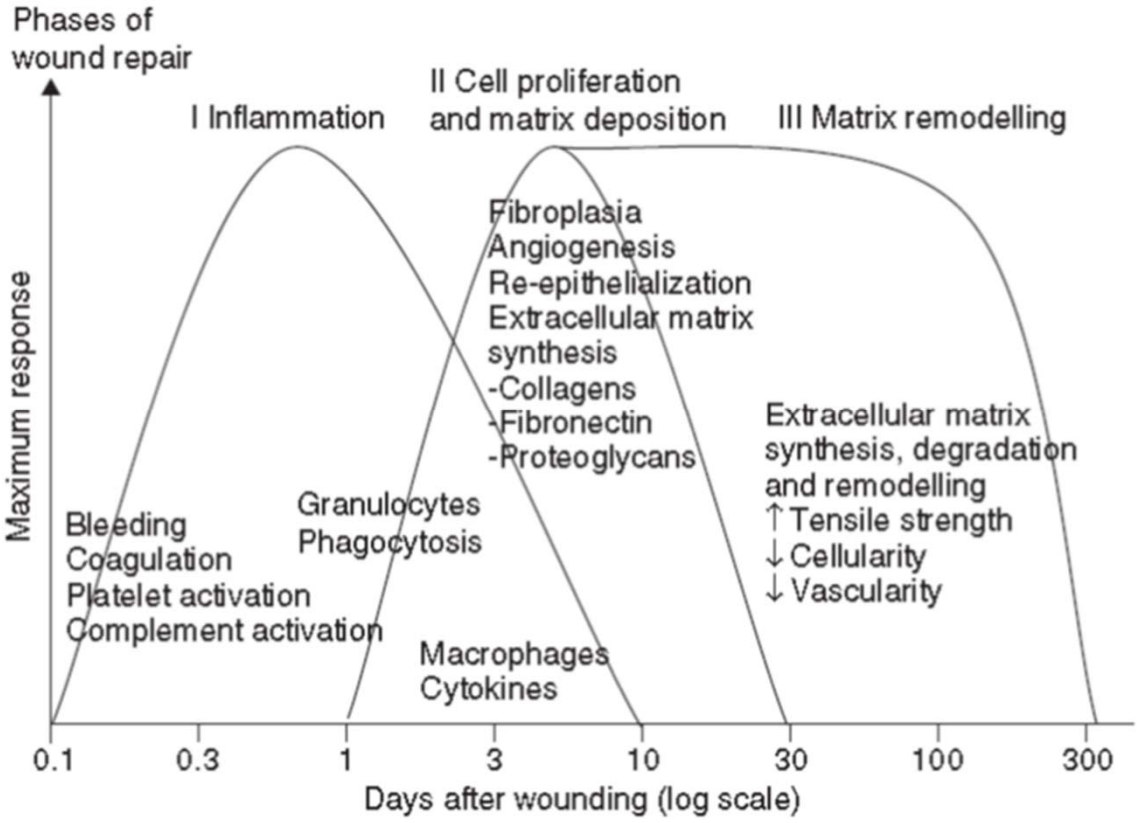

Figure 4. Phases of wound repair.

Notes: Adapted from Ather S. and Harding K.G., 2009.

Other risk factors concerning either the genetic constitution of the collagen synthesis and remodelling or other inherited disorders of the connective tissue playing

a significant role in hernia development are the Marfan and Ehlers-Danlos syndromes, homocystinuria, elastosis and others (Antoniou G. A. et al., 2011). The classic risk factors causing impaired wound healing are malnutrition, obesity, diabetes mellitus and the use of corticosteroids and immunosuppression (Heniford B.T. et al., 2003; Brem H. and Tomic-Canic M., 2007).

1.3 Basic prosthetics used for incisional hernia repair

An ideal mesh for use in ventral hernia regeneration should meet a number of criteria. The mesh has to be chemically inert, biocompatible, non-carcinogenic, capable of being sterilized, should not cause inflammation or an allergic response and be unlikely to produce a significant host immune response (Read R.C., 2004; Shankaran V. et al., 2011). From the biomechanical point of view the mesh should withstand at least tensile strength equivalent to that of the abdominal wall, which is 16 Ncm^{-1} (Klinge U. et al., 1996). In addition, the mesh should be largely producible in an affordable manner (Shankaran V. et al., 2011).

1.3.1 History of prosthetics in abdominal wall hernia repair

The very first surgical mesh for hernia repair was developed in 1900 in Germany by Witzel and Goepel. They made the mesh as a silver filigree by hand (Figure 5; Witzel O., 1900; Goepel R., 1900). Silver was assumed to be bactericidal, but the mesh was rigid, corrodible when in contact with tissue fluids, and with a higher risk of fistula forming, caused problems. Another mesh was made from the inert metal tantalum in the 1940s (Jefferson N.C. and Dailey U.G., 1948; Koontz A.R., 1948). Unfortunately, tantalum caused small bowel fistula, ulceration and the metal fragments eroded

through the peritoneum and skin after the repeated flexion of the tissues (Thorbjarnarson B. and Goulian D., 1967; Bothra R., 1973).

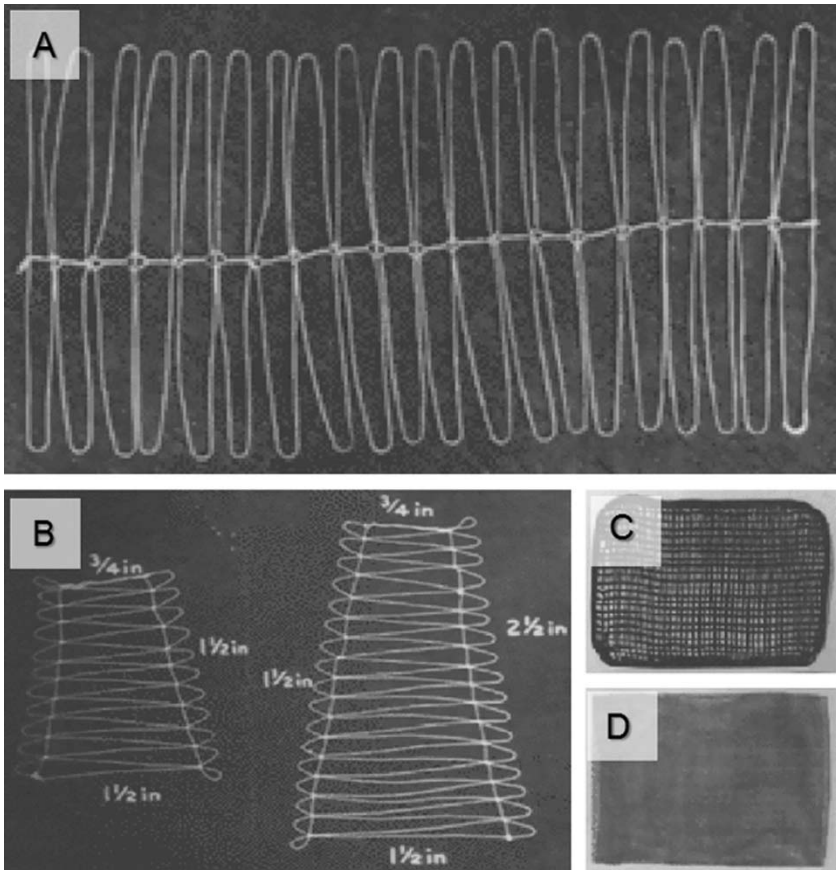

Figure 5. Different previous prosthetics made from either silver filigree or tantalum. (A, B, C) Silver filigree meshes. (D) Tantalum gauze.

Notes: Adapted from Mayer W.,1902; McGavin L., 1907; Burke G.L., 1940.

At the same time, Nylon, the first plastic prosthesis, became widely available. The first reported use of Nylon as a suture in herniology was reported by Melick (Melick D.W., 1942). A monofilamtous nylon suture successfully used by Moloney et al. (Moloney G.E. et al., 1948) replaced silk, which was associated with a foreign body reaction and sepsis (Handley W.S., 1918). Aquaviva and Bounet began using it in France in the form of a mesh during World War II (Aquaviva D. and Bounet P., 1944). Nylon was later replaced by other plastics because it lost 80% of the tensile strength during its hydrolysis and denaturation in time and had to be removed in the presence

of infection (Koontz A.R. and Kimberly R.C, 1959; Adler R.H. and Firme C.N., 1957). The use of another synthetic polymer in the form of a knitted mesh for incisional hernia repair was described in animal studies by Usher et al. in 1958 (Usher F.C. et al., 1958). This surgical mesh made from polypropylene with the present commercial names Marlex® or Prolene® are the most widely-used prosthetic material for repairing ventral hernias to date (Amid P.K. et al., 1995, Cobb W.S. et al., 2009).

A second synthetic polymeric material with the commercial name Dacron® or Mersilene® commonly used to date is based on polyesters (Wolstenholme J.T., 1956; Shankaran V. et al., 2011). Rives and Stoppa successfully used polyesters for “pre-peritoneal” placement in hernia repairs (Rives J., 1967; Stoppa R.E., 1989). A third very often used prosthetic material was developed from polytetrafluoroethylene (PTFE) to its expanded porous form in the 1970s (Gore R.W. et al., 1976). The last main group of surgical meshes includes biologic meshes and different composites that have become increasingly popular in recent years.

1.3.2 The most widely used prosthetics nowadays

In general, non-resorbable synthetic meshes could be divided into 4 main groups. Polypropylenes (Prolene®, Marlex®, Vypro®, ProLite™, etc.), polyesters (Dacron®, Mersilene®, etc.), expanded polytetrafluoroethylenes (ePTFE, Goretex®, etc.) and composites (Sepramesh™, Proceed®, Parietex™, etc.) The group of absorbable synthetics includes glycolic acid (Vicryl®), polyglycolic acid (Dexon™), and carboxycellulose (Seprafilm®). It is very difficult to choose a proper one from the large number of classifications of surgical meshes. Many different ways of classifying have been presented (Klinge U. and Klosterhalfen B., 2012; Coda A. et al., 2012).

In addition to synthetic meshes, there are a few commercially-available biological meshes with appropriate biocompatible features, e.g. derived bovine pericardium (Tutomesh®), acellular porcine dermis (Permacol™) and an acellular analogue of the human dermis (AlloDerm®). However, the use of xenografts is nowadays on the decline, and the production of this type of mesh is limited by the extremely high cost.

1.3.2.1 Polypropylenes

Polypropylene-based meshes are the most widely-used prosthetics for hernia repair, with more than 1 million implantations each year in the United States (Cobb W.S., et al., 2005, Cobb W.S., et al., 2009). Polypropylene is a hydrophobic polymer extremely resistant to biological degradation by tissue enzymes (Read R.C., 2004) and in general represent non-degradable polymers. However, its degradation occurs through free radicals and the oxygen attack of the methyl groups that produce small chain fractures and chemical by-products such as aldehydes and carboxylic (Costello C.R. et al., 2010; Cozad M.J. et al., 2010). Polypropylene is most often used in the form of a knitted mesh because it allows the increase of porosity and flexibility, as well as having identical mechanical properties in all directions (Cobb W.S., et al., 2009). Although the most commonly used polypropylene prosthetics are monofilament heavyweight meshes Marlex® and Prolene® (Amid P.K. et al., 1995, Cobb W.S. et al., 2009), the lightweight polypropylene meshes e.g. Vypro® or ProLite™ appear to have some significant advantages such as large pore size, a reduced amount of alloplastic material and lower foreign body reaction, with the preservation of appropriate tensile strength (Klosterhalfen B. et al., 2005). In addition, Klinge et al. compared the elasticity of the human abdominal wall obtained from cadavers with both types of polypropylene meshes and discovered that a lightweight mesh imitates human tissue more closely (Klinge U. et al., 1998b). Moreover, patients who underwent hernia repair using the

Vypro® mesh complained of chronic pain and a stiff abdomen less often than patients with heavyweight hernia repair (Schmidbauer S. et al., 2005). This results are in concordance with the study of Klosterhalfen and Klinge, who showed that large pore polypropylene meshes (Vypro®, Ultrapro®) in comparison with small pore polypropylene meshes (Marlex®, Prolene®, Atrium®) caused relatively less inflammation, less infection and chronic pain (Klosterhalfen B. and Klinge U., 2013).

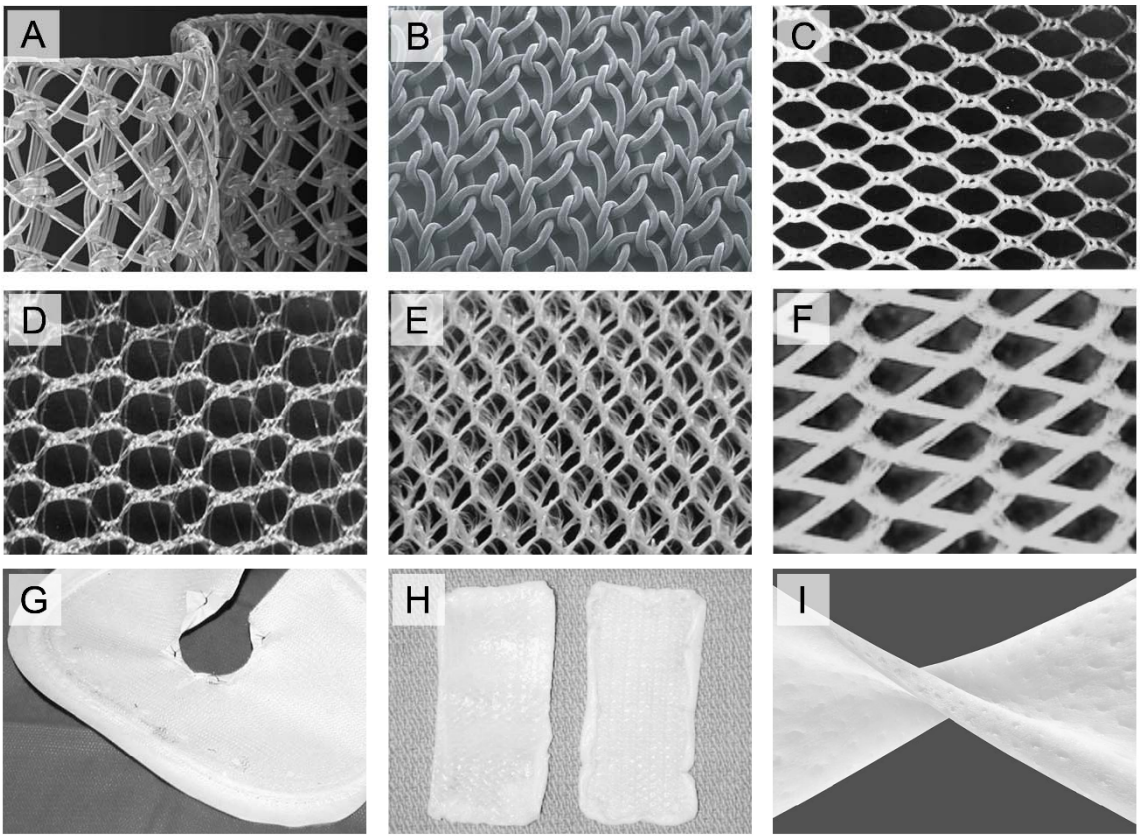

Figure 6. Different kinds of currently used surgical meshes. (A) Prolene® polypropylene mesh. (B) Marlex® polypropylene mesh. (C) Mersilene® polyester mesh. (D) Proceed® composite mesh. (E) Parietex™ composite mesh. (F) Knited Vicryl® absorbable mesh. (G) ePTFE polypropylene composite mesh. (H) AlloDerm® polypropylene composite biologic mesh. (I) Permacol™ biologic mesh.

Notes: Adapted from LeBlanc K.A., 2013; Klosterhalfen B. et al., 2005; Klinge U., 2008; Deeken C.R., 2011; Abaza R., 2005; Butler C.E. and Prieto V.G, 2004.

1.3.2.2 Polyesters

Polyethylene terephthalate (PET) is a multifilament, non-resorable, hydrophilic polymer produced by polymerisation from ethylene glycol and terephthalic acid. Dacron® was the first commercial polyester for inguinal and abdominal hernia repairs used by Wolstenholme (Wolstenholme J.T., 1956). Its newer elastic macroporous form was called Mersilene® (Knott J.I., 1961). Current study results regarding the effectiveness and safety of using polyesters for hernia repairs are very confusing. On the one hand Wantz successfully used Mersilene® and showed its ability to adapt to abdominal wall curves and guarantee encapsulation due to a fibroblastic response (Wantz G.E., 1991). In addition, short-term swine studies demonstrated significantly less contraction, higher incorporation and lower visceral adhesion rates with a polyester mesh in comparison with a polypropylene mesh (Gonzalez R. et al., 2005; Burger J.W. et al., 2006). On the other hand, in the study of Leber et al., Mersilene® hernia repairs revealed higher infection, recurrent rates and levels of fistula formation in comparison with the polypropylene mesh (Leber G.E. et al., 1998).

1.3.2.3 ePTFEs

PTFEs provides chemical inertness due to their covalent bond between carbons and fluorides in a long carbon chain backbone. The expanded form was fabricated through a combination of the PTFE nodes interconnected by the PTFE fibrils (Gore R.W. et al., 1976). Klinge et al. described a few advantages of using ePTFE in ventral hernia repair. ePTFE in that study demonstrated both a lesser adhesion formation and low inflammatory reaction of the human body in comparison with heavyweight polypropylene (Klinge U. et al., 1999). Unfortunately ePTFE also has a higher recurrence level and undergoes shrinkage at a range from 0 to 24% (Klinge U. et al.,

1999, Schoenmaeckers E.J. et al. 2009). Another comparison of the same kind of meshes in a rabbit animal study showed that polypropylene had superior tissue integration but it also incited a more intense inflammatory foreign body reaction (Bellon J.M. et al. 1996). In conclusion ePTFE is not entirely appropriate for preperitoneal placement due to its lower tensile strength and small pore size, which does not allow the ingrowth of the tissue. The intraperitoneal implantation of ePTFE seem to be more suitable because that allows exposing it to the viscera (Bellon J.M. et al. 1996, Shankaran V. et al., 2011).

1.3.2.4 Composite meshes

There are several composite meshes on the market based on e.g. polypropylenes and polyesters. These composites combine the tensile strength of the surgical mesh base with absorbable or permanent coatings. The coatings are tasked with reducing adhesion, inflammatory response, decreasing fibrosis and the contraction of the mesh (Scheidback H. et al., 2004). Several studies proved some of these effects by using some of the coated meshes.

Table 2. Different types of composite meshes and the description of their compound.

Name/Brand	Description
C-QUR™	Lightweight polypropylene coated with Omega-3 fatty acid
Parietex™	PET coated with collagen-polyethylene-glycerol
Proceed®	Lightweight polypropylene/polydioxanon coated with oxide regenerated cellulose
PolyPro Hydrocoat™	Polypropylene coated with polyether urethane urea
Sepramesh™	Polypropylene coated with carboxy-methylcellulose
Ti-Mesh	Lightweight polypropylene covalently covered with titanium
Ultrapro®	Lightweight polypropylene coated with polyglecapron

Notes: Adapted from Shankaran V. et al., 2011; Jacob B.P. and Ramshaw B., 2013.

In the short-term outcomes, most of the composite meshes successfully reduced adhesions and decreased the inflammatory response (Jacob B.P. et al., 2007; Judge T.W. et al., 2007), however the coatings were unstable over time and disintegrated (Sehreinemacher M.H. et al., 2009). The different types and the description of coatings of the composite meshes are summarised in Table 2.

1.3.2.5 Absorbable meshes

Absorbable prosthetics are generally applied for temporary abdominal closure, or are used in conjunction with permanent synthetics (Shankaran V. et al., 2011). These meshes demonstrated some advantages in the long-term outcomes. They reduce the risk of adhesion formation and foreign body reaction (Jacob B.P. and Ramshaw B., 2013). Absorbable meshes are mostly composed of polylactic acid and polyglycolic acid in the form of their copolymers (Dexon™, TIGR®) in potential combination with e.g. polyglycin or trimethylene carbonate (Vicril®, GORE® Bio-A®), or carboxycellulose (Seprafilm®) and polyglycolic acid (Safil®) alone. The important feature of the absorbable meshes is also the different degradation rate. When the mesh degrades too fast it could lose the tensile strength and thus cause a recurrence. On the other hand when the mesh degrades too slowly it may induce a long-term foreign body reaction (Jacob B.P. and Ramshaw B., 2013; Bendavid R. et al., 2001).

1.3.2.6 Biologic meshes

Bioprosthetics belong among the newest materials used for wall hernia repair. These meshes are derived from the collagen-rich tissues of a human, porcine or bovine donor from different sites such as the dermis (AlloDerm®, Permacol™, Strattice™), small intestine submucosa (Surgisis®) and the pericardium (Tutomesh®, Peri-Guard®). The tissues are decellularized with different methods e.g. with sodium deoxycholate or

sodium hydroxide. With this treatment we obtain a collagen, elastin and laminin scaffold that can be repopulated and neo-vascularized. Precisely, the neo-vascularisation and incorporation into host tissue may allow a biological scaffold to use it in contaminated or infected surgical wounds (Milburn M.L. et al., 2008; Hiles M. et al., 2009). The biologic scaffolds may also be cross-linked to increase their cohesiveness and preserve the structure for a longer period (Gaertner W.B. et al., 2007). However, several studies demonstrated that the biologic matrix modified with specific manufacturing and/or crosslinking may lead to a negative response of the host to such material (Jarman-Smith M.L. et al., 2004; Sandor M. et al., 2008). A negative limitation of this type of meshes is their potential disease transmission (Peppas G. et al., 2010). There were reported cases in the literature about prion-related disease transmission from allografts or the risks of the host immune response development due to residues of deoxyribonucleic acid (DNA) fragments in the xenografts, despite the sterilisation and the decelularisation process (Peppas G. et al., 2010; Gilbert T.W. et al., 2009).

Despite the inalienable advantages of biologic scaffolds, most of them are xenografts subject to the strict control and approval of the Food and Drug Administration (FDA) and European Medicines Agency (EMA). Moreover, these grafts generally cost ten times more than the synthetic meshes. Heterografts cost approximately 20% less than allografts (Peppas G. et al., 2010; Rosen M.J., 2010). More specifically some sources compared the prices of a e.g. human acellular dermal matrix ($26.00/cm^2) and bovine or porcine-based scaffolds ($8.60 - $22.00/cm^2) with polypropylene mesh ($1.00/cm^2) or absorbable Vicryl® mesh ($0.20/cm^2; Bachman S. and Ramshaw B., 2008; Blatnik J. et al., 2008; Peppas G. et al., 2010).

1.4 Nanofibers in tissue engineering

As previously mentioned, the optimal prosthetic for abdominal wall repair should meet a number of criteria. The mesh has to be chemically inert, biocompatible with sufficient biomechanical properties, and should not cause inflammation or an allergic response (Read R.C., 2004; Shankaran V. et al., 2011). One way to improve the properties of the meshes used until now is to combine them with other tissue-engineered materials, or to replace the meshes completely through these materials.

Highly-porous scaffolds with interconnected pores are favoured in tissue engineering applications (Sato T. et al., 2004). Much attention has been paid to the application of biodegradable microfibers and nanofibers. Nanofiber scaffolds produced e.g. by electrospinning contain a large number of interconnected pores and fibers in the diameter of the ECM (Khil M.S. et al., 2005). In living systems, the ECM plays a pivotal role in controlling cell behaviour, such as adhesion, proliferation, migration, and differentiation (Kim S.H. et al., 2011). An optimal scaffold, particularly a surgical mesh designed in tissue engineering, should mimic natural ECM. Such a mesh would create the finest microenvironment for cell adhesion and proliferation. Clearly, nanofibrous scaffolds meet these requirements not only due to their topography, but also due to their high surface-to-volume ratio and the possibility of modifying their surface and also interior to improve biocompatibility (Ma Z. et al., 2005a; Agarwal S. et al., 2008). In recent years, for example, the electrospinning method has been applied for this purpose, as it is a simple and cost-effective way to fabricate fibers both from synthetic polymers and other substances (Lukas D. et al., 2009). The topographical features of the fibers can easily be adjusted to fit specific applications by controlling various

parameters (Lukas D. et al., 2009; Bhardwaj N. and Kundu S.C., 2010; Grafahrend D. et al., 2011).

1.4.1 Fabrication of nanofibers through the electrospinning method

Nanofibers for tissue engineering fabricated e.g. by electrospinning, are produced from materials that are biocompatible and mostly biodegradable or non-biodegradable. Nowadays, electrospinning has gained attention as one of the most efficient submicrometer fiber-forming fabrication processes (Cipitria A et al., 2011). To date more than 200 different polymeric materials have been successfully electrospun (Bhardwaj N. and Kundu S.C., 2010). These polymers may have a synthetic origin such as poly-ε-caprolactone (PCL; Kim T.G. and Park T.G., 2006), polyvinyl alcohol (PVA; Chuangchote S. and Supaphol P., 2006), polylactic acid (PLA; Yang F. et al., 2005), poly(lactic-co-glycolic) acid (PLGA; Kim T.G. and Park T.G., 2006), polyurethanes (PU; Khil M.S. et al., 2003) or natural origin such as collagen (Matthews J.A. et al., 2002), fibrin (Carlisle C.R. et al., 2009), silk (Ohgo K. et al. 2003) chitosan (Jayakumar R. et al., 2010), cellulose (Ma Z.W. et al., 2005b) and hyaluronic acid (Um I.C. et al., 2004).

1.4.1.1 Principles of electrospinning

The principle of the electrospinning method is based on the influence of a high voltage electric field to polymer solutions. The electrostatic forces are induced due to attractive forces between the charged electrode with the polymer and the conversely charged collecting electrode. A role is also played by the repulsion among identically charged molecules inside the polymer solution. Above a certain critical value of the applied electric field strength the surface of the polymeric liquid starts to form an instability. This instability results in the development of “Taylor cones” due to the

balance formed between electrostatic forces arising from a high voltage electric field and the surface tension of liquid. The electrospinning jets are formed on the wave crests of these “Taylor cones”. As the jets move towards the collecting electrode the solvent evaporates and the ultrafine fibers are produced (Lukas D. et al., 2008; Lukas D. et al., 2009).

The basic electrospinning device set-up requires a high-voltage source, a capillary tube or a syringe, a mattering pump for the continuous supply of the polymer solution, some polymer and a collecting electrode (Figure 7).

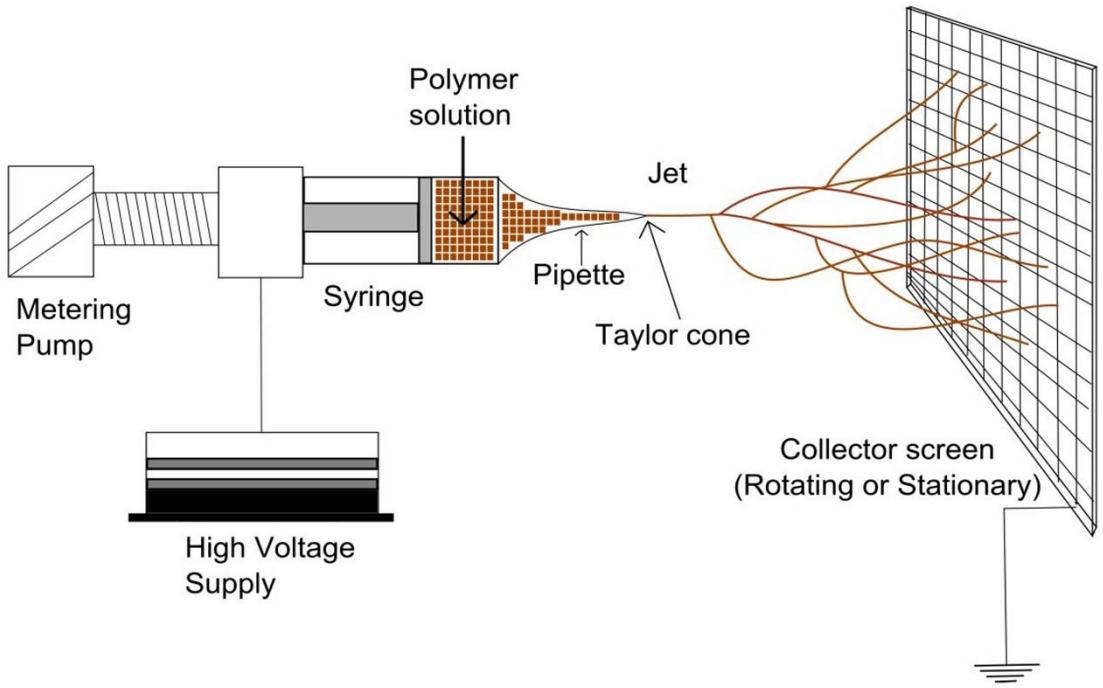

Figure 7. Schematic diagram of an electrospinning device set-up.

Notes: Adapted from Lukas D. et al., 2008.

1.4.1.2 Basic electrospinning methods

In general, electrospinning can be basically classified into either needle or needleless electrospinning according to the spinneret and spinning method. The group of needle electrospinning includes basic capillary electrospinning and sophisticated

core-shell electrospinning, which is divided into emulsion and coaxial electrospinning. Needleless electrospinning is using the self-organization of fiber jets on a free polymer liquid surface.

Capillary electrospinning using a needle-like spinneret is based on spinning from a droplet. Polymer solutions are supplied on the tip of a thin capillary where a droplet forms. The capillary is connected to a high voltage supply and thus the electrospinning process may occur between the droplet on the tip and a collecting electrode (Figure 7). The advantages of this system is its simplicity and the potential to electrospin many different polymers. On the other hand this system has low productivity and the maintenance of the apparatus is difficult (Teo W. and Ramakrishna S.A., 2006). Productivity can be increased with the parallel arrangement of the capillaries. However, the usage of more capillaries leads to the deformation of the electric field and the arising of adverse effects in the electrospinning process (Teo W. and Ramakrishna S.A., 2006).

Another basic type of electrospinning is based on the self-organization of fiber jets on a free liquid surface without using a capillary electrode (Lukas D. et al., 2008b). The simplest set-up consists of a bulky metallic rod with a diameter of approximately 1 cm serving as an electrode. On the top of the electrode there is deposited a very viscous hemispherical polymer droplet. The high voltage electric field results in the forming of many “Taylor cones “ and intensive nanofiber production (Figure 8; Lukas D. et al., 2009).

A less frequently used system consists of a container with a polymer solution and paramagnetic microparticles. The tips of the paramagnetic microparticles are raised from the solution in the electric field and allows the formation of polymer fiber jets (Yarin A.L. and Zussman E., 2004). Another interesting system is based on a perforated

cylinder as an electrode. The polymer solution flows through the holes to the surface of the cylinder. Within the electric field many fiber jets are formed and nanofibers are collected onto a cylindrical collector (Dosunmu O.O. et al., 2006).

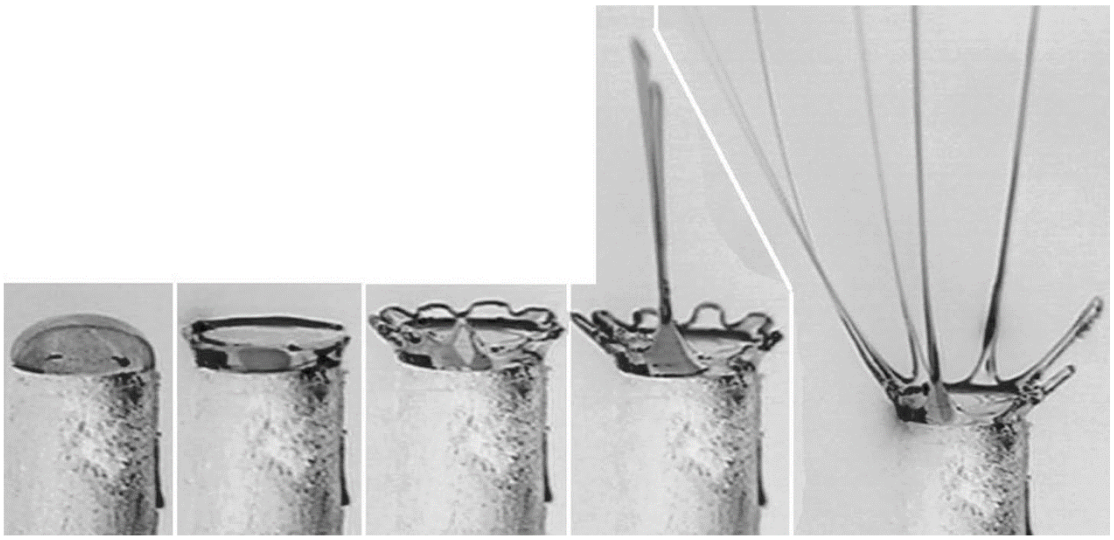

Figure 8. The self-organisation of fiber jets on a free liquid surface. At zero field strength, the viscous droplet has a hemispherical shape (left-hand side of the figure). In the critical value of the electric field intensity, the liquid polymer jets are self-organised (right-hand side of the figure).

Notes: Adapted from Lukas D. et al., 2009.

The most important system from needleless electrospinning is the Nanospider™ (Jirsak O. et al., 2006). This system is based on a rotating cylinder electrode rinsed directly in a polymer solution. Due to the rotation the polymer creates a thin layer on the electrode surface, resulting in the formation of many “Taylor cones” and the production of a big amount of nanofiber material (Figure 9). Therefore the Nanospider™ system is often used for high production and the industrial usage of the nanofibers. The competitive device is based on electrospinning from a rotating disk electrode (Figure 9, Niu H. et al., 2009). In these systems the extent of the nanofiber formation depends on the polymer concentration, the intensity of the electric field and the rotation speed.

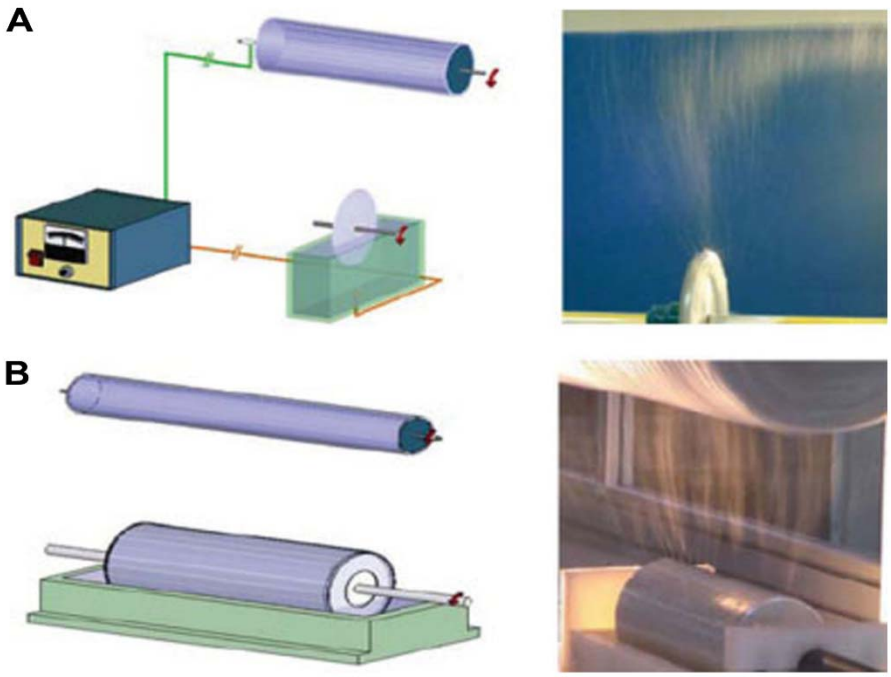

Figure 9. Schematic illustration of needleless electrospinning with a high productivity of nanofibers and photos of the electrospinning processes. (A) System based on the electrospinning from a rotating disk electrode. (B) The Nanospider™ system based on electrospinning from a rotating cylinder electrode.

Notes: Adapted from Niu H. et al., 2009.

One of the younger electrospinning methods that have gained attention among others due to the high potential of being used as drug delivery systems is core-shell electrospinning. Core-shell electrospinning could be basically divided into emulsion electrospinning from a blend and coaxial electrospinning. Emulsion electrospinning is based on nanofiber production depending on the immiscibility of the two polymer solutions, called a blend (Figure 10). One of the polymers is present in a continuous phase and another as droplets covering this continuous phase (Agarwal S. and Greiner A., 2011). Emulsion electrospinning can use needle or needleless electrospinning technique. The crucial point of emulsion electrospinning is the emulsification process of the core materials, including different soluble drugs in the fiber forming shell

materials and core-shell nanofibers from this emulsion in the electrospinning process (Figure 10; Qi H.X. et al., 2006; Agarwal S. and Greiner A., 2011).

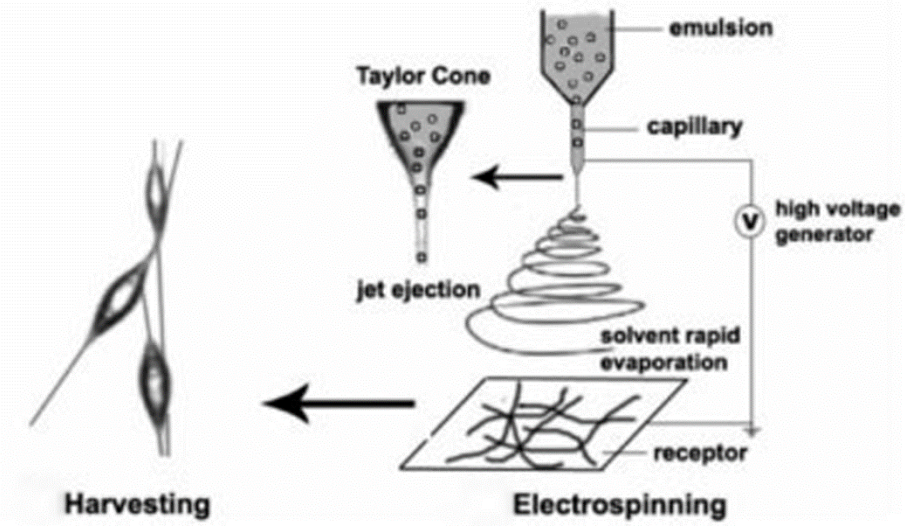

Figure 10. Schematic illustration of emulsion core-shell electrospinning. Important emulsification of a core material with a soluble drug in a fiber forming shell material allows the formation of core-shell nanofibers.

Notes: Adapted from Agarwal S. and Greiner A., 2011.

The coaxial electrospinning first introduced by Sun et al. is an especial type of capillary electrospining (Figure 11; Sun Z.C. et al., 2003). The spinning electrode consists of two capillaries that are placed together coaxially. This technique allows the production of nanofibers from polymers that either could not be electropun together (Teo W.E. and Ramakrishna S.A., 2006) or one of the polymers used as a core material being along non-spinnable (Lukas D. et al., 2009). Using a water soluble polymer as the core material during coaxial electrospinning allows the obtainment of hollow nanofibers after subsequent washing in a water solution (Sun Z.C. et al., 2003). Coaxial electrospinning finds a wide application in the field of drug delivery systems (Sun Z.C. et al., 2003; Zhang Y.Z. et al., 2004). It enables the incorporation of various bioactive substances such as antibiotics, drugs, DNA, proteins and even living cells and affords

protection from the environment by the shell material (Reznik S. et al., 2006; Townsend-Nicholson A. and Jayasinghe S.N., 2006; Yarin A.L. 2011).

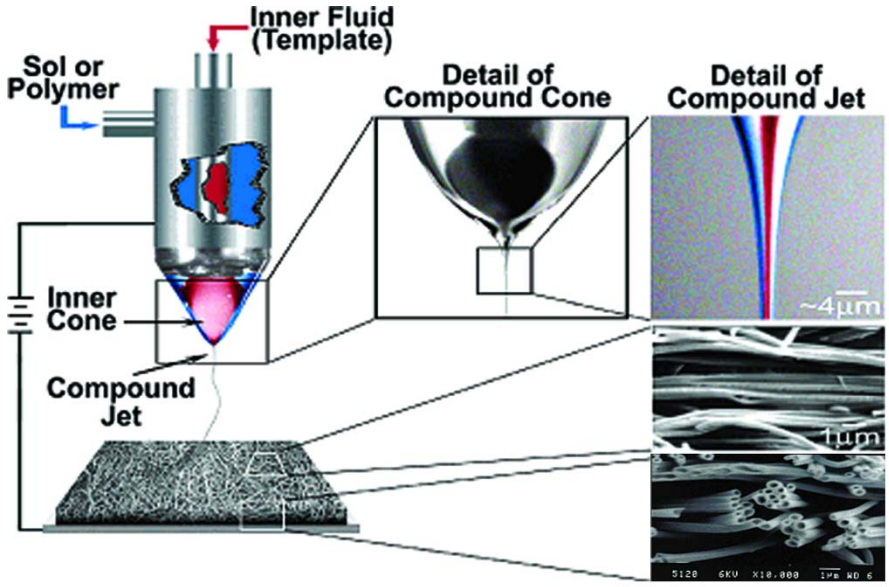

Figure 11. Coaxial electrospinning of nanofibers. Two immiscible polymer solutions (red and blue) are supplied through two concentric needles connected with a high voltage power supply. A compound "Taylor cone" is formed from which a coaxial fiber jet is emitted. On the lower right-hand side of the figure is a view of the sample after cutting

Notes: Adapted from Loscertales I.G. et al., 2004.

1.4.1.3 Collecting electrodes (collectors)

Grounded or charged collecting electrodes play important role in the productivity of nanofibers and can result in the final mesh properties. Using the simple non-structured collectors results in the formation of randomly oriented nanofiber meshes. As a collector most often a metal plate made from aluminium or copper is used (Lukas D et al., 2009; Teo W.E. and Ramakrishna S.A., 2006). Modified collectors enable the fabrication of a structured nanofibers layer. The depositing of the nanofibers onto the collector is affected by its shape and the arrangement of the conductive and non-conductive parts (Lukas D. et al., 2009; Teo W.E. and Ramakrishna S.A., 2006). One of those kinds of collectors has projections that affect the depositing of the nanofibers.

The nanofibers are deposited onto the collector not only as a planar mesh but form a specific 3D structure (Lukas D. et al., 2009). Another kind of collector is represented by a rotating cylinder or disk. With an appropriate speed setting the electrospun polymer forms an oriented layer of nanofibers (Matthews J.A. et al., 2002). The depositing of the oriented nanofiber is also the result of static collectors composed from parallel conductive wires, circles or slices (Teo W.E. and Ramakrishna S.A., 2006).

1.4.1.4 Basic controlling factors and parameters for the modification of nanofiber features

Electrospinning is affected by a large amount of parameters that can modify the features of a nanofiber scaffold.

The basic parameter is a voltage value applied for the electrospinning process. The increase in applied voltage results in the different structural morphology of nanofibers. Deitzel et al. observed that higher voltages cause the formation of bead fibers with a thick diameter (Deitzel J.M. et al., 2001).

The distance of the electrode from the collector affects the intensity of the electric field and thereby the morphology of the nanofibers. With increasing distance the intensity per square unit is decreasing, resulting in the weakening of the electrostatic forces and forming a thinner fiber. When the distance reaches a critical value the “electrospraying” phenomenon occurs and the polymer droplets instead of fibers are formed (Doshji J. and Reneker D.H., 1995).

The speed of the polymer solution supply affects the width and morphology of nanofibers. When using a high speed of supply the solvent is not completely evaporated, resulting in an accumulation of either the non-fiber layers or the fibers with

a changed morphology. The usage of the lower speed supply forms nanofiber with a smaller diameter (Yuan X.Y. et al., 2004)

The molecular weight and concentration of the polymer affects the rheological and electrical features of the polymer solution. Both the higher molecular weight and the higher concentration of polymer increases the thickness of the nanofibers (Haghi A.K. and Akbari M., 2007; Cui W.G. et al., 2010).

The volatility of the solvent is a very important factor that could change the nanofibers structure. In the case of insufficient solvent volatility the liquid polymer solution is deposited onto the collector and forms non-spun layers (Bhardwaj N. and Kundu S.C., 2010). When the volatility is too high the solvent quickly evaporates and the deposited nanofibers have a porous surface (Sill T.J. and von Recum H.A., 2008).

Electrospinning is also affected by environmental factors such as the temperature of polymer solution, ambient temperature, and humidity (Lukas D. et al., 2009)

1.4.2 PCL nanofibers in tissue engineering

In general, nanofibers prepared by electrospinning is one of the most promising scaffolds used in tissue engineering. Tissue engineering is focused on the reparation of damaged tissues and organs. The main field of PCL nanofibers scaffold use is the regeneration of cartilages, tendons, bones, nerves and skin. As mentioned before PCL nanofibers create the finest microenvironment for cell adhesion, proliferation and differentiation by mimicking natural ECM (Khil M.S. et al., 2005).

PCL is a semi-crystalline, aliphatic polyester that is non-toxic, biodegradable, biocompatible and is used in pharmaceutical products and wound dressings (Ng K.W. et al., 2001). In addition this polymer is relatively inexpensive, chemically stable, rather hydrophobic and highly elastic with good mechanical properties and a slow

degradation rate. It degrades within 6-24 months as a result of the hydrolysis of its ester linkages. The degradation process is non-enzymatic hydrolytic cleavage followed by intracellular degradation in the phagosomes of the macrophages and giant cells (Woodward SC et al., 1985). Moreover, PCL has frequently been chosen for scaffold fabrication in tissue engineering, because it is an FDA-approved material and has been shown to support the attachment and growth of chondrocytes (Jakubova R. et al., 2011), osteoblasts (Hutmacher D.W. et al., 2001; Kweon H. et al., 2002), smooth muscle cells (Thapa A. et al., 2003), fibroblasts (Hutmacher D.W. et al., 2001; Chen M. et al., 2007), myoblasts (Williamson M.R. and Adams E.F., 2006), and mesenchymal stem cells (MSC; Rampichova M. et al., 2013).

Tissue engineering focusing on cartilage regeneration is a promising tool for arthroses and mechanical cartilage impairs healing. The three-dimensional PCL nanofiber scaffold seeded with foetal bovine chondrocytes was prepared and tested by Li et al. Chondrocytes cultivated on this scaffold kept their phenotype and expression of chondrogene markers such as collagen type II and glycosaminoglycans (Li W.J., et al. 2003). A later work of this group demonstrated the differentiation of human MSCs cultivated on that scaffold from chondrocytes by using the addition of beta 1 transforming growth factor (TGF-β1; Li W.J. et al., 2005).

In bone tissue engineering the nanofiber scaffolds should meet the criteria for mechanical stability, morphology, porosity and prolonged biodegradability (Vasita R. and Katti D.S., 2006). Promising nanofiber scaffolds are fabricated by the electrospinning of a PCL solution, including hydroxyapatite particles (Wutticharoenmongkol P. et al., 2006).

Ligaments and tendons are created with dense ECM and tenocytes. The damages of tendons leads to the altered function of joints, which could cause

irreversible changes in the musculoskeletal system. The usage of a tissue engineered scaffolds enables the improvement of present surgical methods of damaged ligaments and tendon repair. For these purpose it seems most appropriate to use the nanofiber scaffolds formed with oriented PCL fibers (Kim G.H, 2008).

The regenerative potential of the nervous system is limited and its damage is difficult to treat. Oriented PCL nanofiber layers enable the growth of axonal dendrites and the migration of glial and Schwan cells (Schnell E. et al., 2007). Panseri et al. even proved that an electrospun micro-nanotube scaffold made from PCL and PLGA lead to the regeneration of a 10 mm long gap in rat ischiadic nerves (Panseri S. et al. 2008).

PCL appears to be a suitable material for scaffold preparation for reparative surgery. It has been used in several preclinical trials for wound healing (Venugopal J.R. et al., 2006; Ng K.W. et al., 2007; Liu X. et al., 2010; Kobsa S. et al., 2013), and could be used in combination with a surgical mesh in ventral hernia regeneration.

1.5 Drug delivery systems based on PCL nanofibers

Nanofibers in combination with drug delivery systems positively affect the physiological state of various cells and enable the creation of an appropriate microenvironment proximate to the tissue defect (Agarwal S. et al., 2008).

1.5.1 Adhesion of bioactive substances onto PCL nanofibers

Nanofibers in general have an interconnected porous structure and a high surface-area-to-volume ratio, permitting the adsorption and high immobilization of drugs (Canbolat M.F. et al., 2004), antibiotics (Dave R. et al., 2009) and growth factors (Matlock-Colangelo L. et al., 2014) as well as blood derivatives such as platelet-rich plasma (PRP; Hromadka M.C. et al., 2008). An interesting example of a scaffold with

adhered bioactive substances are nanofibers coaxially electrospun from a PCL core and a cationized gelatine shell (Lu Y et al., 2009). Onto the shell it is possible to adhere a negatively charged ligand such as heparin, hyaluronic acid, bovine serum albumin (BSA) or other proteins and nucleic acid. The adhesion of heparin and BSA enables the subsequent specific interaction with a vascular endothelial growth factor (VEGF) and basic fibroblast growth factor (bFGF; Lu Y et al., 2009). Another simple drug delivery system based on the adhesion of bioactive substances onto PCL nanofibers was developed in our group. Human platelets were adhered onto PCL nanofibers and scaffolds were tested *in vitro* by porcine chondrocyte cultivation (Figure 12; Jakubova R. et al., 2011). Growth factors were released from the platelet adhered to the nanofibers over a period of 1-14 days (Buzgo M. et al., 2013).

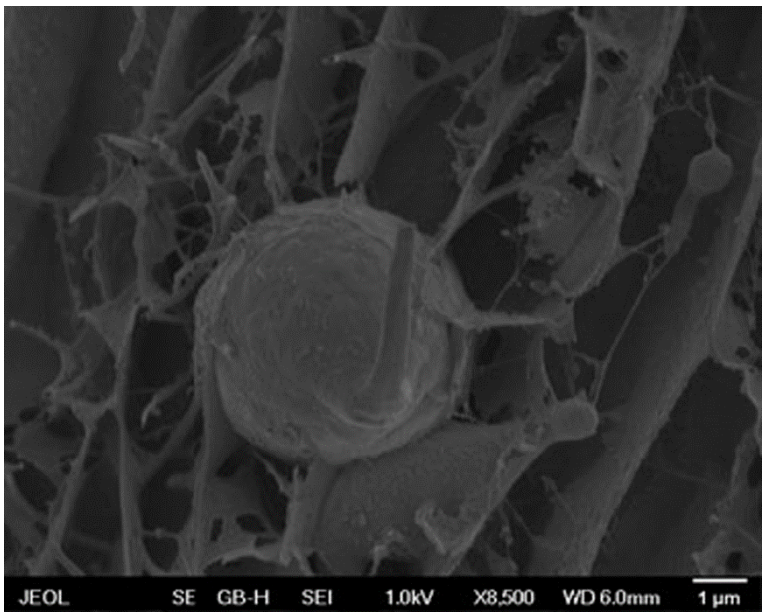

Figure 12. Cryo-Scanning electron microscopy (CryoSEM) visualization of a platelet adhered to PCL nanofibers.

Notes: Adapted from Jakubova et al., 2011.

1.5.2 Core-shell PCL nanofibers as a drug delivery system

Another option for fabricating a drug delivery system based on nanofibers is to use either electrospinning from a mixture of bioactive substance and electrospun polymer (composite blend) or coaxial electrospinning. Electrospinning from the blend is a simple one-step method enabling the incorporation of many bioactive substances (16). The limiting factor is the compatibility of a transferred bioactive substance with a polymer solvent. The most appropriate polymer for this type of drug delivery system fabrication is PVA and polyethylene glycol (PEG). These polymers can mimic the biomolecules and enable the development of secondary binding to the transferred substances and thus stabilise them (Wang Z.G. et al, 2009). The blend electrospinning technique was used for the incorporation of different antibiotics (Bolgen N. et al., 2007), drugs (Xie J. and Wang C.H. et al., 2006), proteins (Zeng J. et al., 2005) and DNA (Liang D. et al., 2005). The ability to preserve the bioactivity of proteins in the nanofibers were proven by the incorporation of e.g. alkaline phosphatase, β-galactosidase (Dror Y. et al., 2008) and horseradish peroxidase (HRP; Patel A.C. et al., 2006).

Coaxial electrospinning is a promising strategy for the delivery of required bioactive substances. One big advantage of this technique for producing core-shell nanofibers consist in the preservation of biomolecules during the electrospinning process. A second important advantage enables the combination of water non-soluble polymers with bioactive molecules not compatible with a non-polar solvent. The hydrophilic core polymers such as PVA, PEG or polyethylene oxide (PEO) enable the loading of biomolecules, whereas the hydrophobic shell e.g. PCL assigns fiber formation (Saraf A. et al., 2009). The rate of bioactive molecules released from the

nanofibers depends exactly on the content of the degradable core components (Jiang H.L. et al., 2006).

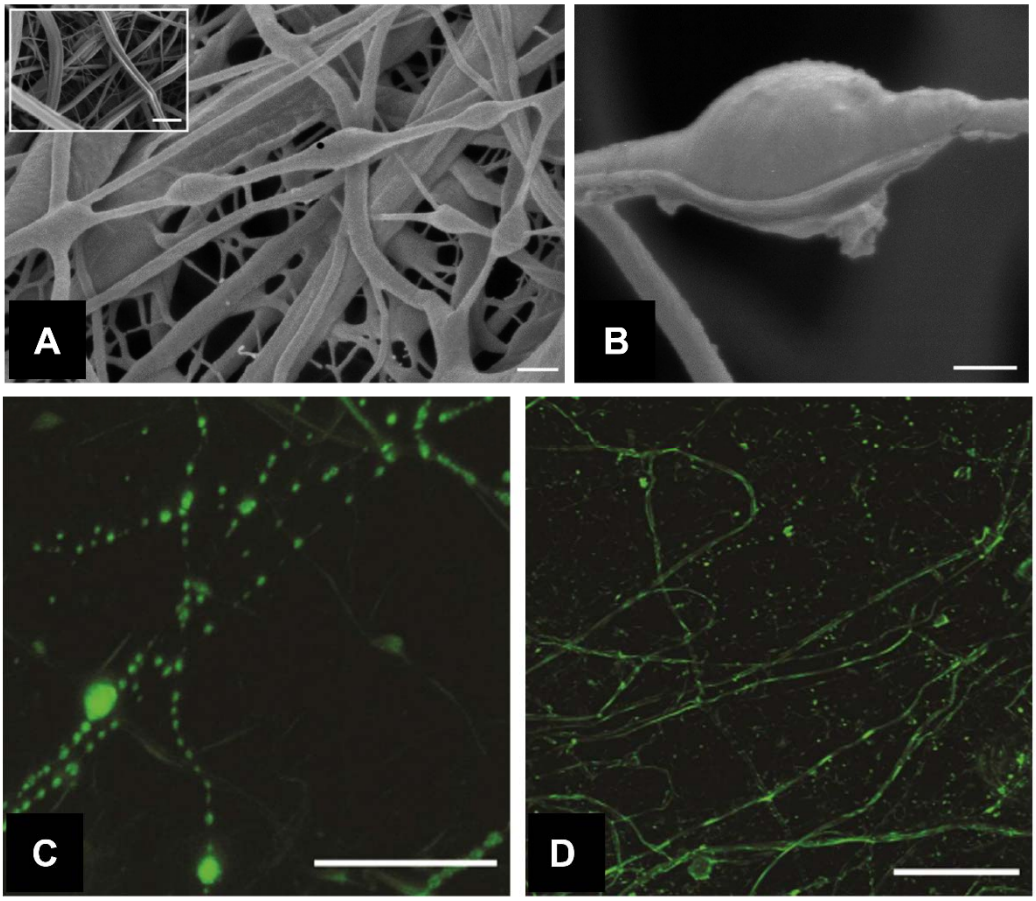

Figure 13. Coaxially electrospun PVA-core/PCL-shell nanofibers with encapsulated liposomes. (A, B) Field emission scanning electron microscopy (FESEM) of embedded liposomes within PVA/PCL nanofibers. (B) Detail of an incorporated intact liposome. (Insert) Pure PVA/PCL nanofibers without liposomes as a control. (C, D) Confocal microscopy of PVA/PCL nanofibers either (C) with encapsulated liposomes containing fluorescein or (D) without liposomes but with the addition of fluorescein in the core showing distribution throughout all nanofibers.

Notes: (A, B) scale bars 300 nm, (C) scale bar 20 μm, (D) scale bar 50 μm, (Insert) 2 μm. Adapted from Mickova A. et al. 2012.

Coaxial nanofibers have been used for the incorporation of various bioactive substances such as antibiotics, drugs, DNA, and proteins (Sill T.J. and von Recum H.A., 2008; Ji W. et al., 2010). In addition, Sahoo et al. prepared core-shell nanofibers

through a blend and coaxial electrospinning for the delivery of bFGF. The presence of the growth factor in coaxial nanofibers led to increasing MSC proliferation (Sahoo S. et. al., 2010). In another work bFGF encapsulation with BSA for fibroblast proliferation stimulation of PCL/PEO coaxial nanofibers were used (Rubert M. et al., 2014). Moreover, coaxial nanofibers based on a PCL shell and PVA core with encapsulated liposomes as a promising controlled drug delivery system was developed and analysed in our group (Figure 13; Mickova A. et al., 2012)

1.5.3 Other examples of drug delivery system based on nanofibers

The last main group of a drug delivery system using nanofibers is based on the covalent immobilisation of bioactive substances onto the scaffold surface. These types of systems are more difficult for preparation and their application is more specific. Monteiro et al. prepared a chitosan nanofiber mesh with gentamicin-loaded liposomes immobilised on their surface. The nanofiber surface was modified with thiol groups that enabled the covalent binding of the liposomes. This functionalised nanofiber could be used as a promoter of antibacterial activity in human wound dressing (Monteiro N et al., 2015). Another system based on nanofibers with covalent immobilised bioactive substances was prepared by Manahkov et al. and Oktay et al. (Manahkov A. et al., 2015; Oktay B. et al., 2015).

1.6 Platelets as a part of tissue engineering

Nowadays one of the very important widely used components of tissue engineered scaffolds are stimulating factors enabling the inducement, acceleration and enhancement of tissue regeneration. Synthetic growth factors (GF), platelet derivatives as a natural source of GF and other stimulating substances can be applied directly

during *in vitro* cultivation or through incorporation into the drug delivery systems, such as nanofiber scaffolds or liposomes.

Platelets play a primary role in the hemostasis and initiation of the wound healing process (White J.G., 1987). On the one hand, platelets are a natural source of various growth factors that stimulate healing (Vavken P. et al., 2011). On the other hand, they form a clot as a temporary matrix that fills the injury site and provides support for cell migration, tissue regeneration and remodelling (Vavken P. et al, 2011). That function of platelets could be enhanced or substituted by nanofiber scaffolds.

1.6.1 Composition of platelets

Platelets are formed by the fragmentation of big polyploid bone marrow cells with a large lobulated nucleus called a megacaryocyte (White J.G., 1987). Platelets fulfil their biologic activity mainly by releasing secretory granules. The bioactive substances are entrapped within 3 types of granules (a) alpha granules; (b) delta granules (dense granules); (c) lambda granules (lysosomes). Among these types the alpha granules are the most abundant, containing most of the platelet bioactive substances and essential for normal platelet activity (Blair P and Falumenhaft R., 2009).

Alpha granules are released from the platelets after activation. Physiologically the activation occurs after the adhesion of platelets at the injury site and is mediated through the existing collagen layer (Roberts D.E. et al., 2004). Biochemical changes in the platelets lead to the release of secretory granules and to changes in platelet morphology (Figure 14; Flaumenhaft R. et al., 2003). The release of the content of alpha and lambda granules has a positive feedback effect on other platelet activation and aggregation at the injury site. The activation of other platelets runs through

different mechanisms such as a thrombin haemostatic cascade, autocrine thromboxane pathway or through serotonin (Di Cera E., 2008, Nakahata N., 2008).

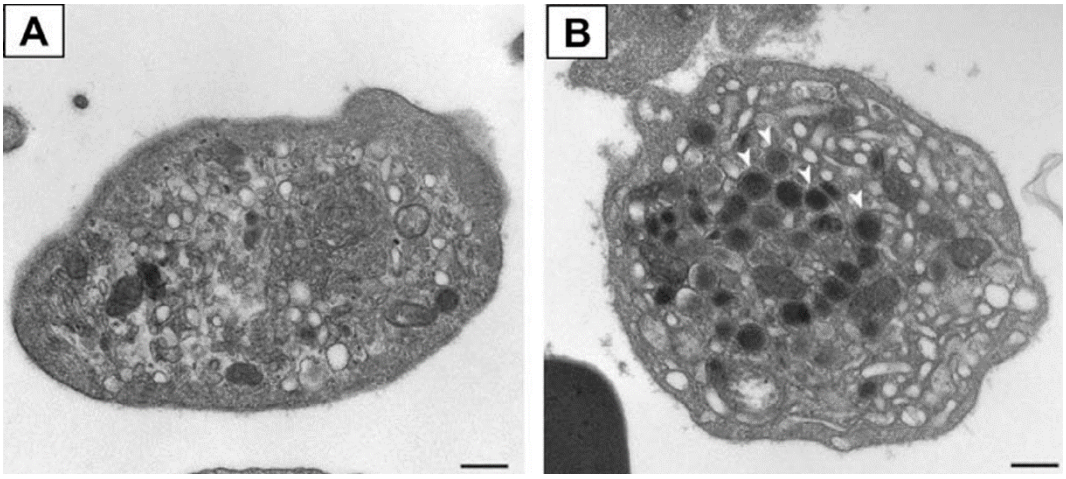

Figure 14. Transmission electron microscopy (TEM) of activated platelets. (A) Platelets from a foetus with a mutation in the VPS33B gene producing a membrane-associated protein involved in the activation pathway. (B) Platelet with alpha granules indicated with white arrows are presented only in an unaffected foetus.

Notes: Scale bars 500 nm. Adapted from Lo B. et al., 2005.

1.6.1.1 Alpha granules

Alpha granules contain various bioactive molecules such as growth factors, coagulation proteins, adhesive molecules, cytokines, integrins, angiogenic factors and other substances (Blair P and Falumenhaft R., 2009).

Alpha granules are an important source of protein from the TGF-β family, consisting of three isoforms (Lawrence D.A., 1996). TGF-β plays an important role in the initiation of proliferation and differentiation of the cells of mesenchymal origin. Conversely, these growth factors have an inhibitive effect on the proliferation of epithelial, endothelial and hematopoietic cells as well as B and T lymphocytes (Lawrence D.A., 1996). TGF-β family members enhance the proliferation of chondrocytes, stimulate the production of ECM and play regulatory roles in modulating

wound healing responses and scarring (Tuli R. et al., 2003). The bone morphogenic protein 2 (BMP-2) is also a member of the TGF-β family and plays a crucial role in bone epidermis repair (Blokhuis T.J., 2009).

The epidermal growth factor (EGF) and TGF-α belongs to the same family. The biological effect is to increase the glycolysis and synthesis of proteins. It acts as a potent mitogen for keratinocytes, other mesenchymal and epithelial cells and enhances the migration of cells to the acute wounds (Barientos S. et al., 2008).

bFGF, also known as FGF-2, induces proliferation in most of the mesenchymal cells, including progenitor mesenchymal stem cells, which helps to keep them in a non-differentiated state. FGFs also play a role in the re-epithelization, angiogenesis, granulation and remodelling of the new tissue (Friesel R.E. and Maciag T., 1995).

Insulin growth factor 1 (IGF-1) plays a role as a mitogen in the organism. It induces cell proliferation and the differentiation of mesenchymal, nervous and epithelial cell types. IGF-1 is involved in re-epithelization, the development of the granulation tissue and Hers at al. proved that it is essential for vascular wound healing (Madry H. et al., 2001; Hers I., 2007)

The major mitogen of osteoprogenitor cells, osteoblasts, fibroblasts, smooth muscle cells and glial cells is the platelet-derived growth factor (PDGF). PDGF plays an important role in wound healing, the stimulation of ECM synthesis and chemotactic induced MSC migration into the injury site (Heldin C.H. and Westermark B., 1990).

Some other proteins such as VEGF or thrombospondin-1 presented in the platelets are involved in angiogenesis regulation (Italiano J.E. et al., 2008). Platelets also contain the Stromal cell-derived factor 1 (SDF-1) involved in MSC and epithelial cell migration (Stellos K et al., 2008). The inflammation reaction is mediated by

chemokines such as Interleukin-8 (IL-8), CLXL-4, RANTES and CLXL-7 (Gleissner C.A. et al., 2008). Adhesion is induced by the Von Willebrand factor (vWF), fibrinogen and fibronectin (Italiano J.E., et al., 2008).

1.6.1.2 Delta and Lambda granules

The second type of secretory granules are delta or dense granules. As mentioned before they play an important role in the activation of other platelets at the injury site either through the non-metabolic fraction of ADP and ATP and purinergic receptors or through serotonin action (King S.M. and Reed G.L., 2002).

The last type of secretory granules are lambda granules. These granules play the role of lysozymes in the platelets and include acidic hydrolases, katepsin D, katepsin E and other proteins (King S.M. and Reed G.L., 2002).

1.6.2 Platelet rich plasma and thrombocyte-rich solutions

Growth factors abundantly present in platelet preparation such as PRP have been shown to be effective in promoting wound healing and regeneration in tissue engineering (Nauta A. et al., 2011). Preparations derived from platelets were originally designed for increasing their numbers in the transfusion therapy of coagulation disorders. PRP is defined as a relatively small volume of the plasma fraction with a platelet concentration above a certain value. PRP classically contains more than 0.5×10^{11} platelets per unit (Ehrenfest D.M et al., 2009).

At present, PRP is usually prepared through the centrifugation of the collected blood. During this procedure the blood is divided into four fractions with an anticoagulant, red blood cells found at the bottom, acellular plasma also known as platelet-poor plasma (PPP), in the supernatant and the “buffy coat”, including

leucocytes, appears in between. The “buffy coat” fraction may be either directly applied to the surgical site using thrombin for platelet activation and fibrin polymerisation, or may be resuspended in the small amount of plasma and used for *in vitro* application (Ehrenfest D.M et al., 2009). Another processing of the “buffy coat” uses the gradual depletion of the leucocytes through multistep centrifugation (Anitua E., 1999) with subsequent resuspending in a supplement buffer solution (Baenziger N.L. et al., 1971; Jakubova R et al., 2011). In the first case we can obtain the previously mentioned PRP products and in the second product, called a thrombocyte-rich solution (TRS). The big advantage of a TRS preparation not containing leucocytes is the minimizing of the immune response when applied. On the other hand the disadvantages is the low yield and reproducibility. Some studies also demonstrated the effectivity of using PPP in tissue engineering. PPP can improve wound healing when compared with untreated controls, but not as effectively as PRP (Pietrzak W.S. et al., 2007; Creeper F. et al., 2012).

The *in vitro* studies demonstrated the ability of different platelet preparation to stimulate the proliferation of osteoblasts (Clausen C. et al., 2006), fibroblasts, tenocytes (Anitua E. et al., 2005), chondrocytes and MSC (Drengk A. et al., 2009). The proliferative effect of the TRS on chondrocytes and on MSCs has been also confirmed in our laboratory (Jakubova R., et al., 2011; Buzgo M. et al., 2013).

The main problem with using different platelet preparations is the immediate release of GFs at the injury site, which could lead to some risk connected with high doses of GF application. The results from *in vitro* and *in vivo* studies indicated that the pro-inflammatory effect of platelet preparation could also have a negative effect and its dosage should be determined deliberately (Goutallier D. et al., 2003). Particularly, Graziani et al. showed that the best effect of the platelet on osteoblast and fibroblast

proliferation *in vitro* was achieved using a concentration 2.5 times higher than the physiological concentration of the platelet in human blood. The 2.5-time higher concentration caused reduction in the proliferation of those cells (Gaziany F. et al., 2006). In contrast Yamaguchi et al. had to use a much higher platelet concentration to promote anastomotic wound healing in a rat specimen. The effect of PRP was observed in the preparation with a concentration of 2×10^6 platelets/µl (approx. 8 times the physiological concentration). The inhibition of healing was observed in the preparation with a concentration of 5×10^6 platelets/µl (Yamaguchi R. et al., 2012). Another problem using different platelet preparations is the short-lived therapeutic effect of GFs in case they are washed out from the injury site. The solution for both complications is to use a platelet preparation in combination with other biomaterials, enabling their elimination. We have already mentioned the potential usage of a nanofiber scaffold for drug delivery systems. Other described scaffolds using platelet preparations are decellularizated bone matrix (Rodriguez A. et al., 2003), fibrin gels (Anitua E. et al., 2007) and hydrogel based on alginate and cationized gelatine (Hokugo A. et al., 2005).

2 Aims of the study

The study was focused on development and functionalization of scaffolds for incisional hernia repair.

The study includes the following stages:

1. Preparation and testing of a novel composite scaffold based on a polypropylene surgical mesh functionalized with the PCL nanofibers and adhered human platelets *in vitro.*

2. Testing the composite scaffold based on a polypropylene surgical mesh functionalized with the PCL nanofibers and adhered synthetic growth factors *in vivo* on rabbits as a small animal model.

3. Testing a scaffold based on the PCL nanofibers functionalized with adhered human platelets *in vivo* on minipigs as a large animal model.

4. Testing the scaffold base on cryogrinded PCL nanofibers with potential use as a drug delivery system for tissue engineering *in vitro*.

3 Material and methods

3.1 *In vitro* testing of the composite scaffold based on a polypropylene surgical mesh functionalized with PCL nanofibers and adhered human platelets

3.1.1 Scaffold preparation

PCL nanofibers were prepared by an electrospinning method from PCL with molecular weight MW 45 000 (Sigma-Aldrich, St. Louis, MO, USA; Lukas D. et al., 2009). Electrospinning was performed from a 14% solution of PCL dissolved in chloroform:ethanol with a ratio of 8:2. A high-voltage source generated voltages of up to 50 kV, and the polymer solution was connected to a high-voltage source. Electrospun nanofibers were deposited on the grounded collecting electrode. A polypropylene surgical mesh (PP; Prolene™, Ethicon Inc., Somerville, NJ, USA) was coated with PCL nanofibers. Prolene™ was attached to the grounded collector, and PCL nanofibers were deposited on the mesh from each side (Figure 15).

3.1.2 Thrombocyte-rich solution preparation

Human platelets in plasma was obtained from the Haematology Service of the General Teaching Hospital, Prague, Czech Republic. Platelets (volume 200 mL, thrombocyte concentration 106 × 10^7 platelets/mL) was centrifuged (2250 g, 15 min), the supernatant was discarded and the resulting platelets were washed in a washing buffer (113 mM NaCl, 4.3 mM K_2HPO_4, 4.3 mM Na_2HPO_4, 24.4 mM NaH_2PO_4 and 5.5 mM glucose, pH 6.5) as described by Baenziger et al (Baenziger N.L. et al., 1971). Contaminating leukocytes and erythrocytes were removed by further centrifugation (120 g, 7 min). The platelets were washed until the leukocytes and erythrocytes

contained in them were removed. The platelets were pelleted by centrifugation (2000 g, 15 min), and were then washed once and finally resuspended in 10 mL of a pH 7.5 resuspendation buffer (109 mM NaCl, 4.3 mM K_2HPO_4, 16 mM Na_2HPO_4, 8.3 mM NaH_2PO_4 and 5.5 mM glucose). TRS was stored and shaken in centrifuge tubes at 22 °C.

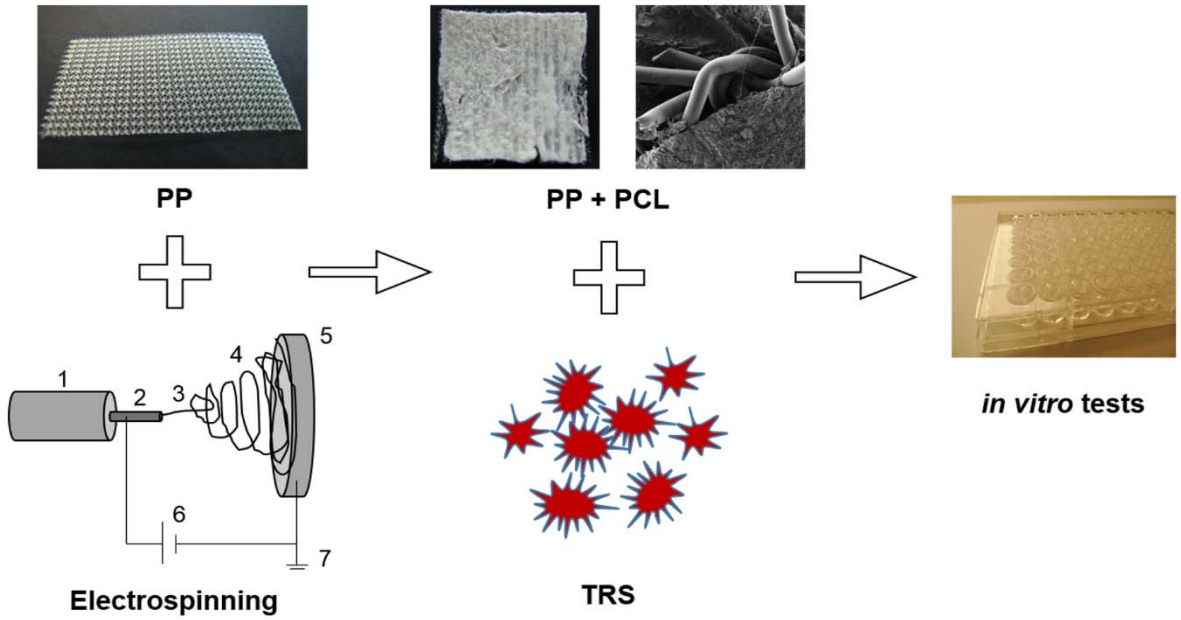

Figure 15. Methodology of the scaffold fabrication. PCL nanofibers were prepared by an electrospinning method. Electrospun nanofibers were deposited on a PP surgical mesh which was attached to the grounded collecting electrode from each side. PP covered with PCL nanofibers was cut into round patches of 6 mm in diameter, sterilized and immersed in TRS for 2 hours. The non-adhered platelets were removed by rinsing twice in phosphate buffered saline (PBS; pH 7.4). The composite scaffolds were placed in a new well, seeded with 3T3 fibroblasts and tested *in vitro.*

Notes: (1) syringe and metering pump, (2) needle serving as the electrode, (3) stable part of the jet, (4) whipping/coiling zone, (5) collector covered with PP, (6) ground and (7) high voltage supply.

Abbreviations: PP, Prolene™; PCL, poly-ε-caprolactone; TRS, thrombocytes-rich solution; PBS, phosphate buffered saline.

3.1.3 Composite scaffold preparation

Before cell seeding, PCL nanofibers and Prolene™ coated with PCL nanofibers were cut into round patches 6 mm in diameter and sterilized using ethylene oxide at 37°C. The scaffolds were used one week after sterilisation, in order to air out possible remnants of ethylene oxide. The scaffolds were immersed in TRS (106×10^6 platelets/mL) for 2 hours to enable adhesion of platelets (Figure 13; Jakubova R. et al., 2011). After the incubation time, non-adhered platelets were removed by rinsing twice in PBS (pH 7.4). Scaffolds without adhered platelets were incubated in PBS (pH 7.4) for 2 h. Then the composite scaffold was placed in a new well and was seeded with 3T3 fibroblasts. Growth factors were released from the platelets adhered to the nanofibers over a period of 1 - 14 days (Buzgo M. et al., 2013).

3.1.4 Scanning electron microscopy and stereological analysis of the scaffolds

Nanofibers were sputter-coated with a layer of gold approximately 60 nm in thickness using a Polaron Sputter-coater (SC510, Polaron, Quorum Technologies Ltd, East Gristead, UK). The samples were examined in an Aquasem scanning electron microscope (Tescan, Brno, Czech Republic) in secondary electron mode at 15 kV.

The electrospun scaffolds were characterized in terms of fiber diameter and pore size using mathematical stereological methods, as described in detail previously (Mickova A. et al., 2012). Briefly, the stereological parameters were measured from arbitrarily selected sections of the SEM images, using Ellipse software (Version 2001; ViDiTo, Kosice, Slovak Republic). The distribution of the fiber diameters and pore sizes were determined quantitatively from 200 measurements.

3.1.5 Cell cultivation and seeding

The mouse 3T3 fibroblast cells (line 3T3-Swiss albino CCL-92™, ATCC, Manassas, VA, USA) were routinely maintained in a humidified incubator (Shellab SS-2306; Sheldon Manufacturing, Inc., Cornelius, OR, USA) with an atmosphere of 5% CO_2 in air at 37°C with fresh medium added every 2 days. Cells were cultured in Dulbecco's modified Eagle's medium (DMEM; PAN-Biotech GmbH, Aidenbach, Germany) supplemented with 10% fetal bovine serum (FBS; PAA Laboratories GmbH, Pasching, Austria) and penicillin/streptomycin (100 IU/ml and 100 µg/mL, respectively, Sigma-Aldrich, St. Louis, MO, USA). When the cells reached 80-90% confluence they were suspended using Trypsin–Ethylenediaminetetraacetic acid (EDTA; PAA Laboratories GmbH, Pasching, Austria). The number of cells was determined using light microscopy. To detect the metabolic activity, proliferation and viability, fibroblasts were seeded on the scaffolds at a density of 3×10^3 cells/cm^2, and to determine cell adhesion at a density of 3×10^4 cells/cm^2, respectively. To eliminate any contribution from non-adherent cells, each scaffold was transferred to a new well on the plate before any *in vitro* tests. From each well, which contained 300 µL of medium, a volume of 150 µL of the medium was exchanged every second day.

3.1.6 Cell adhesion by DiOC6 staining

Staining with a 3,3'-Dihexyloxacarbocyanine iodide (DiOC6; Invitrogen, Carlsbad, CA, USA) fluorescent probe was used to detect adhesion of cells on the scaffolds. Samples were fixed with frozen methyl alcohol (–20˚C) for 10 min, and were rinsed with PBS followed by DiOC6 (0.1-1 µg/mL in PBS, pH 7.4). After 45-min incubation at RT, the samples were rinsed with PBS (pH 7.4), and propidium iodide (5 µg/mL in PBS, pH 7.4) was added for 10 min, rinsed with PBS (pH 7.4) again and visualized using a

Zeiss LSM 5 DUO confocal microscope (Zeiss, Oberkochen, Germany; λ_{exc} = 484 nm and λ_{em} = 482–497 nm). The areas of adhered cells were counted with Ellipse software (Version 2001; ViDiTo, Kosice, Slovak Republic). For each scaffold, an area of 100 cells was measured and averaged.

3.1.7 Cell metabolic activity analysis by the MTT test

Cell metabolic activity was measured using the 3-[4,5-dimethylthiazol-2-yl]-2,5-diphenyltetrazolium bromide (MTT) test. MTT (50 µL, 1 mg/mL; Sigma-Aldrich, St. Louis, MO, USA) in PBS (pH 7.4) was added to 150 µL of the sample medium and was incubated for 4 hours at 37°C. Using mitochondrial dehydrogenase of normally metabolizing cells, the MTT was reduced to purple formazan. The formazan crystals were solubilized with 100 µL of 50% N,N-dimethylformamide in 20% sodium dodecyl sulphate (SDS) at pH 4.7. The results were examined by spectrophotometry in an absorbance microplate reader (ELx800; BioTek, Winooski VT, USA) at 570 nm (reference wavelength 690 nm). The metabolic activity of 3T3 fibroblasts on a scaffold was tested on days 1, 3, 7, 10 and 14.

3.1.8 Cell proliferation analysis by PicoGreen® assay

The second proliferation analysis was carried out using the Invitrogen PicoGreen® assay kit (Quant-iT™ PicoGreen® dsDNA Reagent kit, Invitrogen, Carlsbad, CA, USA). The proliferation of 3T3 fibroblasts on the scaffolds was tested on days 1, 3, 7, 10 and 14. To process the material for an analysis of the DNA content, each scaffold was replaced in a vial with 500 µl of cell lysis solution (0.2% v/v Triton X-100, 10 mM Tris (pH 7.0), 1 mM EDTA). To prepare the cell lysate, the samples were processed through a total of three freeze/thaw cycles; the scaffold sample was first frozen at -70 °C and thawed at RT. Between each freeze/thaw cycle, the scaffolds

were roughly vortexed. The prepared samples were stored at -70 °C until analysis. To quantify the cell number on the scaffolds, a cell based standard curve was prepared using samples with a known number of cells (range 100 – 5×10^5 cells). The DNA content was determined by mixing 100 µL PicoGreen reagent and 100 µL of the DNA sample. The samples were loaded in triplicate and the florescence intensity was measured on a multi-mode microplate reader (Synergy HT; BioTek, Winooski VT, USA; λ_{ex} = 480–500 nm, λ_{em} = 520 – 540 nm).

3.1.9 Viability of cells seeded on scaffolds by live/dead staining

To detect cell viability, live/dead cell staining was performed. The cell viability of 3T3 fibroblasts on the scaffold was tested on days 1, 3, 7, 10, 14. The cells were stained with 2´,7'-Bis[2carboxyethyl]-5[6]-carboxyfluorescein acetoxymethyl ester [(BCECF-AM), storage solution 1 mg/mL in dimethyl sulfoxide (DMSO)], and were finally diluted 1:100 in a serum-free medium; (Sigma-Aldrich, St. Louis, MO, USA) and propidium iodide (5 µg/mL in PBS, pH 7.4; Sigma-Aldrich, St. Louis, MO, USA). BCECF-AM was added to the scaffolds and incubated for 45 min at 37°C and 5% CO_2 and subsequently rinsed in PBS (pH 7.4). After rinsing with PBS (pH 7.4), propidium iodide was added for 10 min, then the scaffolds were rinsed again with PBS (pH 7.4) and visualized using a Zeiss LSM 5 DUO confocal microscope (BCECF - AM λ_{ex} = 488 nm and λ_{em} = 505–535 nm, propidium iodide λ_{ex} = 543 nm and λ_{em} = 630–700 nm). BCECF-AM is an intracellular fluorescent pH indicator, which is hydrolysed to BCECF by cytosolic esterases. Thus, only live cells contribute to the staining results (green colour). Propidium iodide binds to double stranded DNA, but it can only cross the plasma membranes of non-viable cells (red colour). For each scaffold, the number of live/dead cells was counted with Ellipse software (Version 2001; ViDiTo, Kosice,

Slovak Republic) and was averaged. Viability was calculated as the percentage of live cells from the total cell count per unit area.

3.1.10 Cell proliferation analysis by colorimetric immunoassay

The proliferation activity of 3T3 fibroblasts seeded on the scaffolds was determined using a colorimetric immunoassay based on measurements of 5-bromo-2'-deoxyuridine (BrdU), which is incorporated during DNA synthesis (Cell proliferation ELISA, BrdU, colorimetric; Roche Applied Science, Penzberg, Germany). The assay was performed according to the manufacturer's instructions. Briefly, on days 1, 3, 7, 10 and 14, each scaffold 100 µL BrdU-labeling solution was added to each well containing a scaffold and was allowed to incorporate into the cells in a CO_2-incubator at 37°C for 2 h. Subsequently, the supernatant in each well was removed, and the scaffolds were incubated with FixDenat solution to fix the cells and denature the DNA at room temperature (RT) for 30 min. The supernatant was removed and, subsequently, 100 µL anti-BrdUperoxidase (dilution ratio = 1:100) was added and kept at RT for 60 min. After removing the unbound antibody conjugate, 100 µL of substrate solution was added, allowed to stand for 4 min, and the reaction was completed by adding 25 µL of H_2SO_4 solution (1M). Then, 100 µL of the solution was transferred to a 96-well plate and measured within 5 min at 450 nm with a reference wavelength of 690 nm, using an absorbance microplate reader (ELx800; BioTek, Winooski VT, USA). The blank corresponded to a scaffold without cells, with or without BrdU.

3.1.11 Statistical analysis of *in vitro* tests

Quantitative data are presented as mean ± standard deviation (SD). For the *in vitro* tests, average values were determined from four independently prepared samples. The results were evaluated statistically, using One Way Analysis of Variance

(ANOVA) and the Student-Newman-Keuls Method. The level of significance was set at 0.001 and 0.05.

3.2 *In vivo* testing of the composite scaffold based on a polypropylene surgical mesh functionalized with PCL nanofibers and adhered synthetic growth factors on a rabbit model

3.2.1 Preparation of the functionalized scaffolds and composite meshes

Preparation of the scaffold based on the polypropylene surgical mesh functionalized with PCL nanofibers is described in chapter 3.1.1.

For *in vivo* tests on a rabbit model PCL nanofibers, Prolene™ (PP) and P coated with PCL nanofibers were cut into rectangular shape with 4 cm and 8 cm sides. The scaffolds were sterilized using ethylene oxide at 37°C. The synthetic GF were bound to the scaffold by 12h incubation in a PBS (pH 7.4) solution, which contained 200 ng/mL IGF-I [human recombinant (hr), Sigma-Aldrich, St. Louis, MO, USA], 40 ng/mL bFGF (hr, Roche Applied Science, Penzberg, Germany), and 4 ng/mL TGF-β2 (from porcine platelets, Sigma-Aldrich, St. Louis, MO, USA). After incubation GFs were adhered on the surface of nanofibers. The release of synthetic growth factors from nanofibers were in the order of 1 to 3 weeks (Filova E. et al. 2013). Implanted scaffolds without the GF were incubated in PBS (pH 7.4) for 12h.

3.2.2 Rabbit animal model, study groups and animal care

A total of 27 rabbits were randomly divided into six groups. In Group I (the control group), the tissue defect in the fascia was primarily closed using a 4/0 PP suture. In

Groups II, III and V, the defect in the fascia was closed with a 4/0 PP suture, a 4×8 cm mesh was placed over the fascia in an onlay position, overlapping the incision by 2 cm circumferentially. Group II was treated with a PP mesh only (the second control group), while Group III was treated with a PP mesh functionalized with PCL nanofibers enriched with GF, and Group V was treated with a PP mesh functionalized with PCL nanofibers without GF. The mesh was then fixed with a continuous suture technique, using a 4/0 PP suture. The last continuous stitch was used to suture the mesh to the incision line. Groups IV and VI were treated with PCL nanofibers only, with adhered GF (Group IV) or without GF (Group VI). For better understanding, the groups are summarized in Table 3.

Table 3. Groups and meshes used

Group	Description
I	Suture only
II	PP
III	PP + PCL nanofibers + Growth Factors
IV	PCL nanofibers + Growth Factors
V	PP + PCL nanofibers
VI	PCL nanofibers

Abbreviations: PP, polypropylene; PCL, poly-ε-caprolactone.

Twenty seven Chinchilla rabbits (3.2±0.3 kg), 4 months old, were obtained from a conventional breed (CB Bio, Prague, Czech Republic) and bred in standard cages without bedding. The rabbits were fed *ad libitum* using the standard granular diet for rabbits (TM–MaK 1, Bergman, Karlovy Vary, Czech Republic). The Ethical Principles and Guidelines for Scientific Experiments on Animals were respected throughout this study. The maintenance and handling of the experimental animals followed EU Council

Directive (86/609 EEC), and the animals were treated in accordance with the principles of Care and Use of Animals.

3.2.3 Surgical procedure, euthanasia and sample collection

The animals were pre-medicated with intramuscular 15 mg Diazepamum *pro toto* (posteriorthigh – semitendinous and semimembranous muscles). The surgical procedure was conducted under general anesthesia using Ketamine (35 mg/kg) and Xylazine (3 mg/kg) and subsequently inhalation of O_2 + 1.5-2.0% Halothane during surgery. Following completion of all the preoperative preparations, a skin incision of about 6 cm was cut through the midline of the abdomen, starting 3 cm below the xyphoid. Another 5 cm long midline incision was made in the fascia as an abdominal closure model. Antibiotics (20 mg/kg/day s.c. of Cefalexinum monohydricum, Cefalexin ad us. vet.) and analgesics (0.1mg/kg/day s.c. of Butorphanol tartrate) were administered during the first 3 days. The rabbits were not limited in their movement after surgery. The animals were euthanized using T61 (Schering-Plough Corporation, Kenilworth, NJ, USA) 6 weeks later.

Samples for histological and immunohistochemical analysis were fixed in 10% phosphate-buffered formalin for 48 h. Two samples of 1×6 cm of full layer abdominal wall with mesh were removed for biomechanical testing (Figure 16), two samples from the suture line and two from the edge of the mesh were harvested for histological testing. All suturing material was explanted prior to all tests.

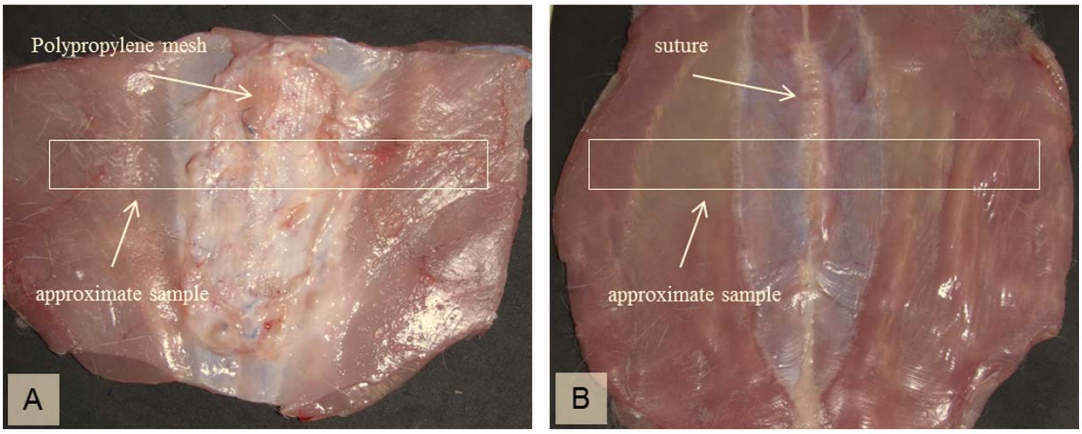

Figure 16. Full layer regenerated abdominal wall for biomechanical and histological analyses. (A) Incision of abdominal wall closed with PP mesh, (B) incision of abdominal wall closed with simple suture.

Abbreviations: PP, polypropylene.

3.2.4 Video-recorded biomechanical assay (tensile strength)

The hysteresis curve and the maximum tensile strength were determined on a Micro tester digital tension meter (the device was developed in Department of Anatomy and Biomechanics, Faculty of Physical Education and Sport, Charles University in Prague, Utility model with document/registration number 25008, Industrial Property Office, Czech Republic). The structure of each sample was scanned throughout the experiment by an Olympus SZX-12 microscope (Olympus Corporation, Tokyo, Japan) equipped with an ultrasensitive SensiCam video camera (PCO, Kelheim, Germany). The force response of each sample was detected at the branches of the tension meters during the whole cycle. Both static and dynamic properties of each of the samples were analysed. The following quantities were measured: elasticity in traction E [N/mm^2], maximum strength force $\sigma_{max.}$ per square unit [N/mm^2] and the corresponding proportional elongation value $\varepsilon_{max.}$. The localization and the character of the tear line were also analysed. The tissue samples (1×6 cm strips of regenerated abdominal wall) were individually attached to the branches of the tension meter in longitudinal manner,

not including the place covered with scaffolds of a particular type (Figure 17). The samples were stretched by 5 mm at a speed of 10 mm/s ten times and were then pulled at a speed of 0.5 mm/s until the sample broke (Figure 27).

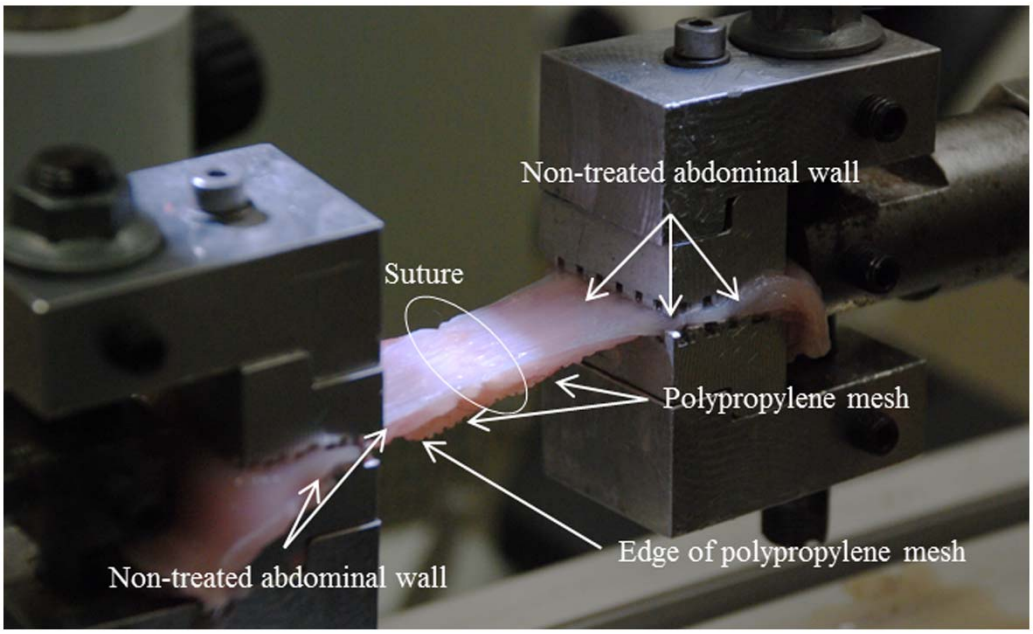

Figure 17. Tensiometer branches with anchored samples during biomechanical analyses.

3.2.5 Histological evaluation

The tissue samples were fixed with buffered formalin, dehydrated and embedded in paraffin blocks. Six serial histological sections 5 μm in thickness were processed from each paraffin-embedded tissue block. α-Smooth muscle actin was used as a marker of the contractile SMC phenotype and myofibroblasts, and CD31 was used as an endothelial marker (Table 4). Endogenous peroxidase activity was blocked with 3% H_2O_2 in PBS. Non-specific binding activity was blocked with normal goat or horse serum (Table 4) in a phosphate-buffered salt solution at room temperature. The sections were incubated overnight with primary antibodies (Table 4) at 4°C. Immunoreaction products were detected using the immunoperoxidase technique (Table 4), and the reactions were visualized with diaminobenzidine (Sigma-Aldrich, St.

Louis, MO, USA). All sections were counterstained with Gill's hematoxylin (Dr. Kulich Pharma, Otrokovice, Czech Republic). Quantification of area fractions of tissue constituents and quantification of microvessel density were done using stereological point counting method (Mouton P.R., 2002) and the unbiased counting frame provided by Ellipse software (ViDiTo, Kosice, Slovak Republic).

Table 4. Primary antibodies used for immunohistochemistry

Antibody	Blocking serum	Pre-treatment	Detection
Monoclonal Mouse Anti-Human Smooth Muscle Actin, Clone 1A4, (DakoCytomation, Glostrup, Denmark)	Normal goat serum (DakoCytomation) in PBS at room temperature	None	N-Histofine kit (Nichirei Biosciences, Tokyo, Japan)
Monoclonal Mouse Anti-Human and Anti-Rabbit CD31, Clone JC/70A (Vector Laboratories Ltd., Peterborough, UK) Dilution 1:25 *(endothelial marker)*	Normal horse serum for 20 min at room temperature	Enzyme-induced epitope retrieval with Proteinase K (DakoCytomation) for 6 min	ImmPress reagent kit with Anti-mouse Ig peroxidase MP-7402 (Vector Laboratories, Ltd.)

3.2.6 Histological scoring system

In the literature, there are no references to a method for comparing histological evaluations related to incisional hernia examinations. We suggest a novel scoring system, which is described in detail below.

Two tissue blocks were examined in each animal, one representing the medial region of the abdominal wall with the healing incision, and the other approx. 20 mm laterally to the median incision. Six serial histological sections 5 μm in thickness were processed. Two sections were stained with hematoxylin-eosin (Merck KGaA,

Darmstadt, Germany), two sections were stained with Verhoeff's hematoxylin (Merck KGaA, Darmstadt, Germany) and green trichrome (DiaPath, Martinengo, Italy) to visualize the connective tissue (Kocova J., 1970), and two sections were processed immunohistochemically in order to reveal the presence of micro vessels, smooth (SMC) and myofibroblasts. We used α-smooth muscle actin as a marker of the contractile SMC phenotype and myofibroblasts, and CD31 as an endothelial marker. All sections were counterstained with Gill's hematoxylin.

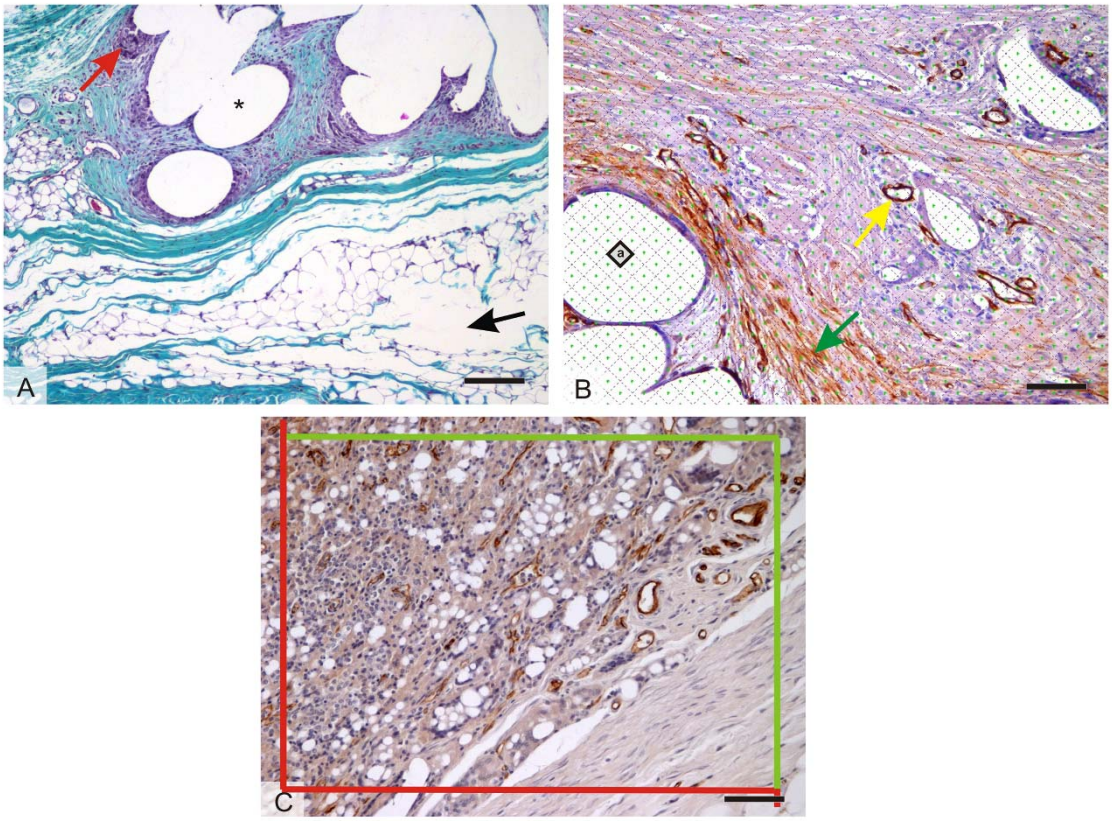

Figure 18. Histological quantification. (A) In sections stained with Verhoeff's hematoxylin (Merck KGaA, Darmstadt, Germany) and green trichrome (DiaPath, Martinengo, Italy), the area fraction of collagen (stained green), adipose tissue, and granulomatous infiltrates (red arrow) was quantified. The area occupied by dissolved tissue scaffolds (asterisk) or by artificial microcracks (black arrow) was excluded from the reference area. (B) For all area quantifications, stereological point grids were superimposed on histological micrographs, points striking the structures of interest within the total area were counted, and the sum of these points was multiplied by the area corresponding to each point (marked "a" within the square). This is illustrated in an immunohistochemical section showing

α-smooth muscle actin-positive vascular smooth muscle cells (yellow arrow) and myofibroblasts (green arrow). (C) Counting CD31-positive microvessel profiles per section area using projection of an unbiased counting frame consisting of two admittance borders (green) and two forbidden borders (red). (B,C) Counterstaining Gill's hematoxylin (Dr. Kulich Pharma, Otrokovice, Czech Republic).
Notes: (A) magnification × 100, scale bar 200 µm. (B,C) magnification × 200, scale bar 100 µm.

We used five continuous variables describing the tissue reaction of the connective tissue below the dermis and superficial to the abdominal muscle. The presence of collagen, adipose tissue and granulomatous infiltrates was assessed in the sections stained with Verhoeff's hematoxylin and green trichrome (Figure 18A). The presence of α-smooth muscle actin and the presence of CD31-positive micro vessel profiles were assessed in immunohistochemical sections (Figure 18B and C). Two micrographs for each staining and tissue block were taken in a systematic random manner, using a 20× objective (quantification of CD31-positive microvessels) or a 10 × objective (other parameters). Next, a randomly positioned uniform grid of equidistant points was placed on the micrographs in an overlay, so that the number of points striking the collagen, adipose tissue, granulomatous infiltrates and α-smooth muscle actin-positive cells was proportional to their area. We counted the number of points striking these structures within the area of the abdominal scar. The area of each major tissue component *A* was calculated by multiplying the number of counted points by the area corresponding to each point (Gundersen H.J., 1978). The presence of each tissue component in the study was then expressed as their area fraction (A_A) within the connective tissue of the scar and abdominal wall. The area not occupied by connective tissue (tissue micro cracks, dissolved mesh and surgical stitches, borders of the section) was excluded from the reference area. The sum of the area fraction of collagen, adipose tissue, granulomatous infiltrates and α-smooth muscle actin represents the main tissue constituents. The remaining fraction of the tissue was

occupied mostly by fibroblasts and scattered connective tissue cells, individual skeletal muscle fibers, ground substance of the extracellular matrix, immature collagen, and lumina of blood and lymphatic vessels. In sections stained for the α-smooth muscle actin and CD31, we assessed the quantity of micro vessels as the number of micro vessel profiles per section area Q_A, using an unbiased counting frame (Gundersen H.J., 1978). Although the α-smooth muscle actin did not label the capillaries which are lacking smooth muscle cells, we found a strong positive correlation (Spearman R=0.91) between the micro vessels labelled with α-smooth muscle actin and CD31-positive micro vessels in a pilot study based on 12 tissue samples. Due to a stronger immunohistochemical reaction, we decided to consider the number of α-smooth muscle actin-positive micro vessels as an acceptable estimate for the presence of micro vessels. In total, the quantification was based on 220 micrographs. An estimate was made of the density of the micro vessel profiles, and 117 micro vessel profiles per sample were counted on an average.

3.2.7 Statistical analysis for *in vivo* tests

The quantitative histological data were processed using Statistics Base 9 (StatSoft Inc., Tulsa, OK, USA). The Spearman rank order correlations were used as a measure of the statistical relations between the variables, and Kruskal-Wallis ANOVA was used for testing the equality of the population medians between the groups under study. We used the Wilcoxon matched pairs test for paired samples of the medial and lateral abdominal wall of the same animals. Values were considered statistically significant for $p < 0.05$. Only significant findings and findings close to significant values are reported.

3.3 *In vivo* testing of the scaffold based on PCL nanofibers functionalized with adhered human platelets on a minipig model.

3.3.1 Preparation of the functionalised scaffolds

Preparation of the PCL nanofibrous scaffolds is described in the chapter 3.1.1.

For *in vivo* tests on a minipig model PCL nanofibers, PCL nanofibers with adhered human platelets or suture alone were used. Nanofibrous scaffolds were cut into a rectangular shape with sides of 4 cm and 9 cm. The scaffolds were sterilized using ethylene oxide at 37°C. TRS was prepared from human platelets in plasma (volume 283 mL, platelets concentration $100x10^7$ platelets/mL) as described in the chapter 3.1.2. Final washed platelets pellet was resuspended in 50 mL of resuspendation buffer. The final concentration of platelets in TRS was $1x10^9$. PCL scaffolds designated for functionalization were immersed in TRS for 2 hours to enable adhesion of platelets (Figure 12; Jakubova R. et al., 2011). After the incubation time, non-adhered platelets were removed by rinsing twice in PBS (pH 7.4). Scaffolds without adhered platelets were incubated in PBS (pH 7.4) for 2 h. Growth factors were released from the platelets adhered to the nanofibers over a period of 1 - 14 days (Buzgo M. et al., 2013).

3.3.2 Minipig animal model, study groups and animal care

The total of 10 male minipigs was randomly divided into two groups. For the implantation, the PCL nanofibers, PCL nanofibers with adhered human platelets (PCL nanofibers + TRS) or suture alone were used. Scaffold was placed over the fascia in an onlay position, overlapping the incision by 2 cm circumferentially. The scaffold was fixed with a continuous suture technique, using a 4/0 PP suture. The last continuous stitch was used to suture the mesh to the incision line.

10 male minipigs (19-31 kg), 6-8 months old, were obtained from a conventional breed (CB Bio, Prague, Czech Republic) and bred in standard individual boxes. The minipigs were fed with 1 kg of the standard complete feed mixture (A1, Cerea a.s., Pardubice, Czech republic). Quality controlled water was supplied *ad libitum* during the acclimatisation time and during the entire study period. The Ethical Principles and Guidelines for Scientific Experiments on Animals were respected throughout this study. The maintenance and handling of the experimental animals followed EU Council Directive (86/609 EEC), and the animals were treated in accordance with the principles of Care and Use of Animals.

3.3.3 Surgical procedure, euthanasia and sample collection

The animals were premedicated with Atropin (0.05 mg/kg, i.m.), Azaperon (2 mg/kg, i.m.) and Ketamin (15 mg/kg, i.m.). After sedation, the animal was intubated. During the surgery, the anaesthesia was keeping by O_2 + 1.5-2.0% Halothane inhalation. After ensuring a venous access entry with a catheter into the marginal ear vein, a 0.9% saline solution was supplied.

After entering to anaesthesia, the animal was placed to the dorsal location. Its skin was shaved. The surgery site was disinfected with povidone-iodine (Braunol, B.Braun, Melsungen, Germany). Following completion of all the preoperative preparations, a four skin incision of about 8 cm was cut laterally from the nipples in particular quadrant of the abdominal wall (Figure 19). Consequently the incision into the frontal fascia of *rectus abdominis* muscle with the fain immobilisation into the muscle was made (Figure 20). The incision was in the length of 5 cm. The scaffold was placed over the fascia in an onlay position according to the scheme. The numbering of the particular incision is presented in Figure 19. Experimental and control defects were

rotated in the position to avoid affection of the healing process due to the particular position in the abdominal wall. The scaffold was fixed with a continuous suture technique, using a 4/0 Vicryl suture. The last continuous stitch was used to suture the mesh to the incision line. The incisionin the group treated without any scaffold (the control group), the fascia tissue defect was primarily closed using a continuous suture technique using a 3/0 PP suture.

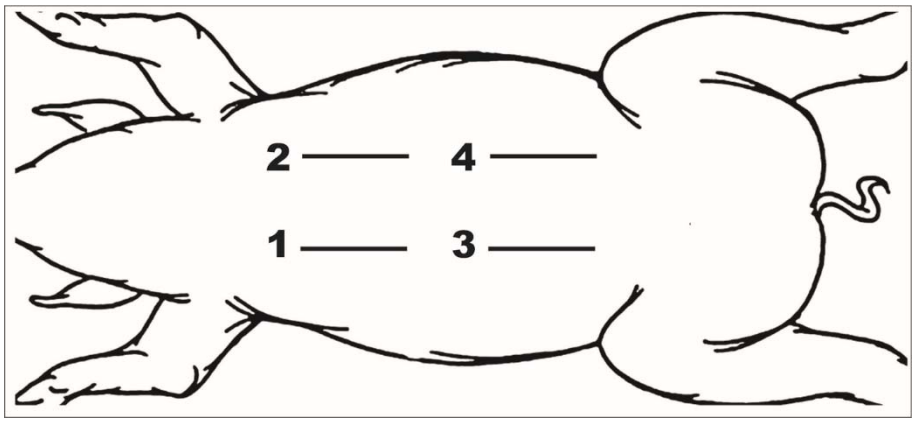

Figure 19. Numbering scheme of particular incision in abdominal wall. Experimental and control defects were rotated in the position to avoid affection of the healing process due to the particular position in the abdominal wall.

Antibiotics (20 mg/kg/day s.c. of Cefalexinum monohydricum, Cefalexin ad us. vet.) and analgesics (0.1mg/kg/day s.c. of Butorphanol tartrate ad us.vet.) were administered during the first 3 days. The minipigs were not limited in their movement after surgery.

The animals in one experimental group were euthanized 6 weeks and in second group 12 weeks after surgery. Euthanasia was realised using premedication of Azaperon (2 mg/kg, i.m.) + Ketamin (15 mg/kg, i.m.) and administration of T61 (10 ml i.v. *pro toto*).

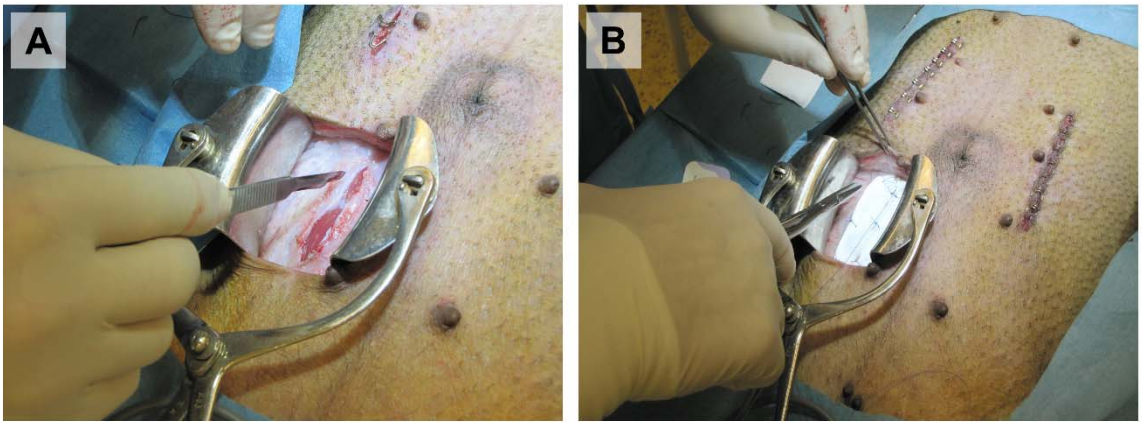

Figure 20. Surgery of the minipigs abdominal wall. (A) Incision in the fascia of *rectus abdominis* muscle. (B) Fixation of the implanted PCL nanofiber mesh.

Samples of 2×6 cm of full layer abdominal wall with scaffold for histological and immunohistochemical analysis were removed and fixed in 10% phosphate-buffered formalin for 48 h. All suturing material was explanted prior to all tests.

3.3.4 Histological evaluation

The tissue samples were fixed in 10% phosphate-buffered formalin, dehydrated and embedded in paraffin blocks. The samples were prepared to represent the places of incision, as well as the abdominal wall approx. 20 mm apart from the incision. Eight serial histological sections 5 μm in thickness were processed from each paraffin-embedded tissue block. Two sections were stained with haematoxylin-eosin, two sections were stained with Verhoeff's haematoxylin and green trichrome (Kocova J., 1970) to visualize the connective tissue, two sections were stained with picrosirius red (Direct Red 80, Sigma Aldrich, Munich, Germany) diluted in saturated picric acid solution for one hour to visualize the type I collagen. The other two sections were processed immunohistochemically in order to reveal the presence of microvessels, SMC and myofibroblasts. We used α-smooth muscle actin as a marker of the contractile SMC phenotype and myofibroblasts. Endogenous peroxidase activity was

blocked with 3% H_2O_2 in PBS. Any unspecific binding activity was blocked with normal goat or horse serum in phosphate-buffered salt solution at room temperature. The sections were incubated overnight with monoclonal mouse anti-human smooth muscle actin primary antibody (dilution 1:1000, clone 1A4, DakoCytomation, Glostrup, Denmark) at 4°C. The products of the immunoreaction were detected using the immunoperoxidase technique (N-Histofine kit, Nichirei Biosciences, Tokyo, Japan) and the reactions were visualized with diaminobenzidine (Fluka, Buchs, Germany). All the sections were counterstained with Gill's haematoxylin.

All quantitative estimates were done using well established stereological methods (Mouton P.R., 2002) and the Ellipse software (ViDiTo, Košice, Slovakia). The new scoring system used in both *in vivo* studies is described in chapter 3.2.6 in more detail. We used six continuous variables describing the tissue reaction of the connective tissue below the dermis and superficial to the abdominal muscle fascia. The presence of type I collagen was assessed in sections stained with picrosirius red using the circularly polarized light. The advantages of this method were described by Rich and Whittaker (Rich L. and Whittaker P., 2005). The picrosirius red enhances the birefringence of co-aligned type I collagen fibrils and fibres. This phenomenon can be used for reproducible morphological quantification of the type I collagen content with high specificity and sensitivity (Junqueira L.C. et al., 1979). According to the thickness, type I collagen fibres appear in yellow (thinner fibres), orange, and red colour (thick bundles of fibres). The presence of α-smooth muscle actin-positive cells was quantified in immunohistochemical sections.

3.3.5 Statistical analysis for *in vivo* tests

The data were processed with the Statistica Base 9 (StatSoft, Inc., Tulsa, OK, USA). As a measure of the statistical relations between the variables, the Spearman rank order correlations were used. Kruskal-Wallis ANOVA and the Mann Whitney U test were used for testing the equality of population medians between the groups under study. For paired samples with and without incision in the same animals, we used the Wilcoxon matched pairs test. Values were considered statistically significant for $p < 0.05$. Only significant findings and finding close to significant values are reported.

3.4 *In vitro* testing of the scaffold base on cryogrinded PCL nanofibers with potential use as a drug delivery system for tissue engineering

3.4.1 Preparation of the microspheres by cryogrinding of PCL nanofibers

The complete preparation process of a potential drug delivery system based on microspeheres derived from the PCL nanofibers by the cryogrinding technique was comprehensively described in our group by Knotek et al. (Knotek P. et al., 2012). Briefly, the PCL nanofibers prepared by a needleless electerospinning method were pulverizing from deep frozen state in cryogenic impact grinder. The cryogrinding process was carried out in different supporting grinding media and, such as mannitol, Pluronic and 2-octanol. The particle size distribution and the morphology were analysed using Mastersizer 2000 MU (Malvern Ins., Malvern, United Kingdom) and SEM Jeol JSM 5500 LV (JEOL Ltd, Tokyo, Japan) respectively.

3.4.2 Cell cultivation and seeding

For *in vitro* testing of cryogrinded microsphere, mouse 3T3 fibroblast were used. Exact procedure of cell cultivation is described in chapter 3.1.5. There were several modifications of the previously described method. Fibroblasts were seeded on the microsphere scaffolds at a density of 6×10^3 cells/cm2. Prior to seeding cells, the microsphere scaffolds (30 mg) were sterilized in 70% ethanol (v/v) for 30 min and put into each well of 96-well plate. In order to prevent cell from adhering to the well surface, wells were modified with 1% Pluronic-127. A 50 µl aliquot of the cell suspension was added into each well and incubated for 2 h. Then 150 µl of cell culture medium was added to the samples and cells were cultured at 37 °C in a humidified atmosphere with 5% CO2.

3.4.3 Cell adhesion on the microspheres by DiOC6 staining

The complete procedure of cell adhesion evaluation by using the confocal microscopy and DiOC6 staining is described in the chapter 3.1.6. Cell adhesion was evaluated on microspheres cryogrinded in all three different supporting grinding media.

3.4.4 Cell proliferation analysis by PicoGreen® assay

The complete cell proliferative PicoGreen® assay is described in chapter 3.1.8. The proliferation of 3T3 fibroblasts on either PCL microspheres cryogrinded in mannitol supporting media or PCL nanofibers was evaluated on days 1, 7, 14 and 21.

3.4.5 Cell metabolic activity analysis by the MTS test

Cell metabolic activity was measured using the 3-[4,5-dimethylthiazol-2-yl]-(3-(4,5-dimethylthiazol-2-yl)-5-(3-carboxymethoxyphenyl)-2-(4-sulfophenyl)-2H-tetrazolium bromid (MTS) test. Samples of either PCL microspheres cryogrinded in

mannitol supporting media or nanofibers on days 1, 7, 14 and 21 were transferred to a new 96-well plate containing 100 µl of fresh full medium per well and 20 µl of CellTiter 96® Aqueous One Solution Reagent was added (CellTiter 96® Aqueous One Solution Cell Proliferation Assay, Promega, Fitchburg, WI, USA). The formazan absorbance in 100 µl of the solution was measured (λ_{sample} = 490 nm, $\lambda_{reference}$ = 690 nm) after 2-h incubation at 37 °C and 5% CO_2 using a microplate reader ELx800. The absorbance of the samples without cells was deducted from the cell-seeded samples. Values represent mean ± SD of four independent measurements.

4 Results

4.1 *In vitro* testing of the composite scaffold based on a polypropylene surgical mesh functionalized with PCL nanofibers and adhered human platelets

4.1.1 SEM and stereological analysis of the scaffolds

The functionalized mesh was prepared by attaching the PP mesh on to the collector before the electrospinning process. PCL nanofibers were deposited on the surface of the PP mesh. The PP mesh with nanofibers was exposed in an aqueous environment for 2 weeks without any visual effect on the functionalized mesh. Three types of functionalised scaffolds were examined using scanning electron microscopy in secondary electron mode. Samples of the PP mesh (Figure 21B) were functionalized with PCL nanofibers (Figure 21A) to create a composite scaffold (Figure 21C).

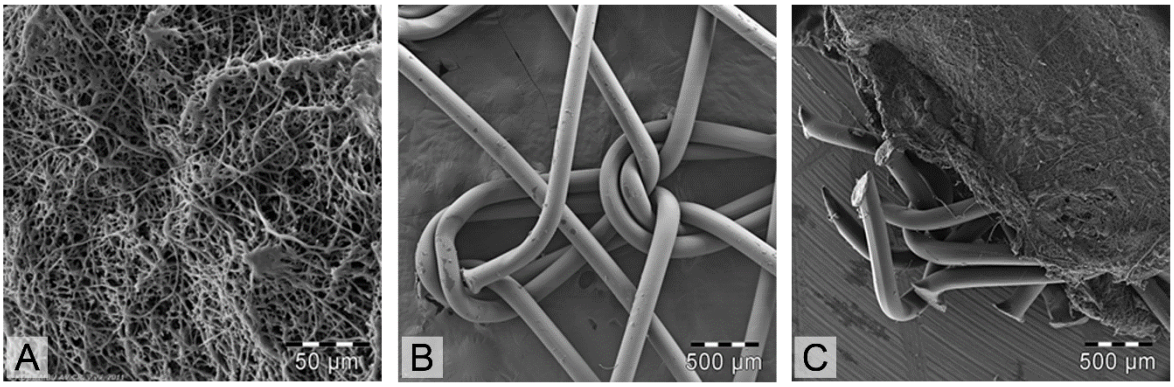

Figure 21. SEM of the scaffolds. (A) PCL nanofibers, (B) PP mesh, (C) PP mesh functionalized with PCL nanofibers.

Notes: (A) magnification × 230, scale bar 50 µm, (B,C) magnification × 18, scale bar 500 µm.

Abbreviations: PP, polypropylene; PCL, poly-ε-caprolactone.

Scanning electron microscopy revealed a randomly-oriented nanofibers and their deposition onto the PP mesh. Stereological analyses divided the nanofibers into two

fractions of PCL fibers. The first fraction contained fibers with an average diameter of $1.29 \times 10^3 \pm 0.33 \times 10^3$ nm, while in the second fraction the average diameter was 466±170 nm. The average diameter of the PP mesh fibers was about $150 \times 10^3 \pm 5.4 \times 10^3$ nm. This kind of system was therefore considered suitable for further cell studies.

4.1.2 PCL nanofibers significantly improved cell adhesion and metabolic activity

Functionalization of the PP mesh significantly improved the adhesion and the metabolic activity of the 3T3 fibroblasts.

First, cell adhesion was evaluated 24 hours after seeding. 3T3 fibroblasts were stained using DiOC6 and propidium iodide, were visualised using confocal microscopy, and areas of the spread cell surface were measured. A significantly larger surface area of the cells was observed on the PP mesh functionalized with PCL nanofibers than on the PP mesh alone (Figure 22). In addition, the largest spreading area was for the cells cultivated on the PP mesh functionalized with PCL nanofibers and TRS. Simultaneously, enrichment of the PP mesh with TRS improved cell adhesion, and the cell spreading area of PP + TRS was significantly larger than for PP ($p < 0.001$). Clearly, PP meshes functionalized with PCL nanofibers alone, and also PP meshes treated with TRS, significantly improved 3T3 adhesion. These two effects seem to be independent, and can therefore result in an additive effect.

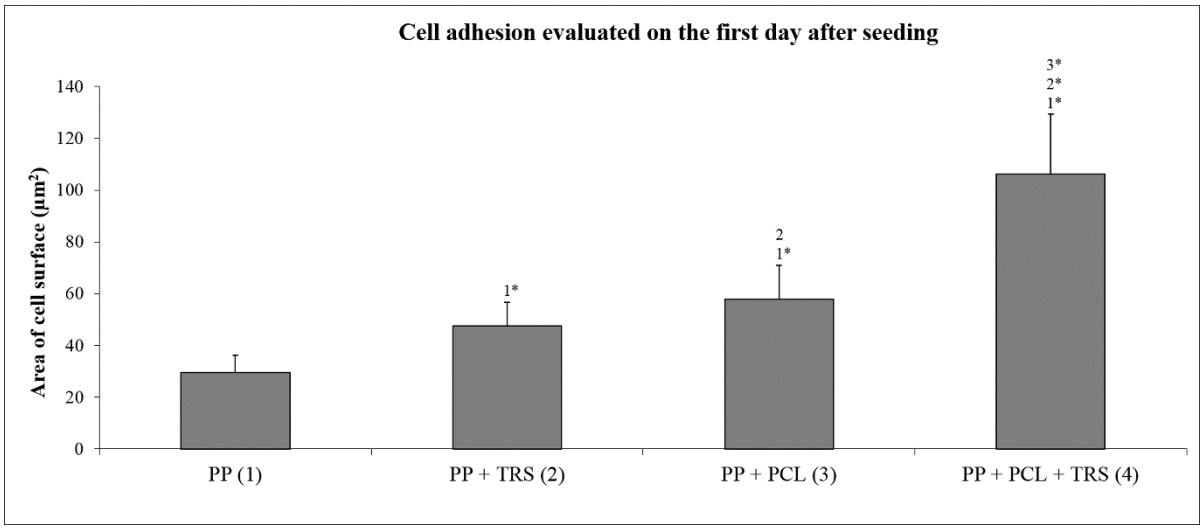

Figure 22. Cell adhesion evaluated on the first day after seeding. Average surface area of spread 3T3 fibroblasts cultivated on the surface of a PP mesh (1), a PP mesh treated with TRS (2), a PP mesh functionalized with PCL nanofibers (3), a PP mesh functionalized with PCL nanofibers treated with TRS (4). A cell adhesion assay revealed a significantly larger surface area of spread 3T3 fibroblasts on scaffolds functionalized with PCL nanofibers (PP + PCL and PP + PCL + TRS) than on scaffolds without functionalization (PP and PP + TRS). Moreover, the average surface area of 3T3 fibroblasts was significantly higher (level of significance at a value of $p < 0.001$) on the PP mesh functionalized with PCL nanofibers treated with TRS than on all other scaffolds.

Notes: The level of statistical significance for the assays is designated above the mean values ($p < 0.05$ indicated by number, $p < 0.001$ indicated by number and *). Day 1: 2 > 1*; 3 > 1*, 2; 4 > 1*, 2*, 3*.

Abbreviations: PP, polypropylene; PCL, poly-ε-caprolactone; TRS, thrombocyte-rich solution; µm2, square micrometre.

3T3 fibroblast metabolic activity was determined by the MTT assay. The MTT assay revealed significantly higher metabolic activity of the cells after the 10th day of cultivation on any composite scaffolds than on the PP mesh alone (Figure 23). Moreover, significantly higher ($p < 0.001$) metabolic activity of the cells was observed on any functionalized composite scaffolds on day 14. Significantly higher metabolic activity was also observed on either a PP mesh functionalized with PCL nanofibers or a PP mesh functionalized with PCL nanofibers treated with TRS after the 7th day of

cultivation. Additionally, a combination of two improvements, namely functionalization of the PP mesh with PCL naofibers and treatment with TRS, led to significantly higher ($p < 0.001$) metabolic activity of the cells on day 14 than on all other scaffolds that were used.

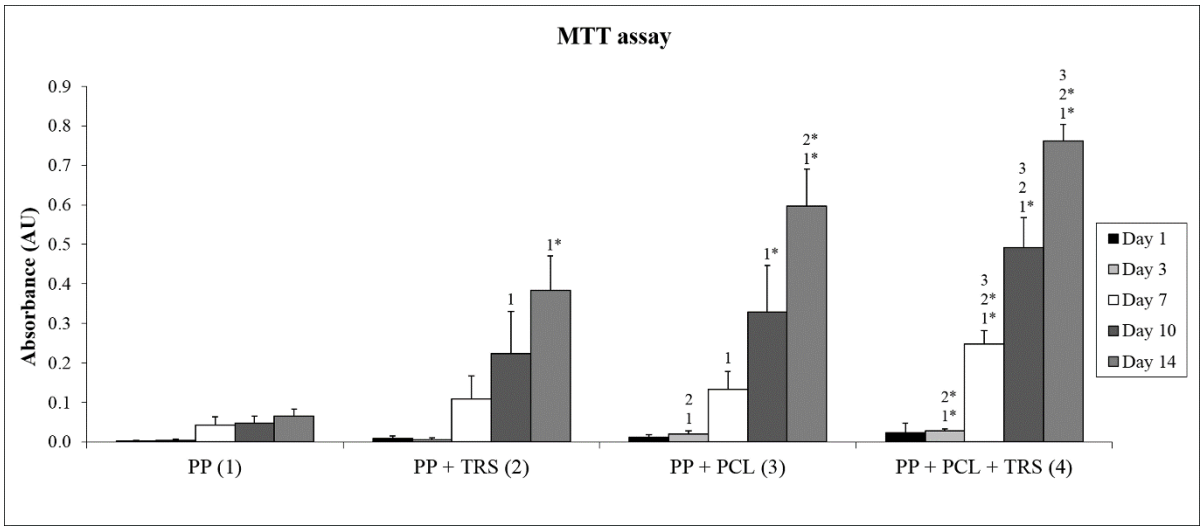

Figure 23. Metabolic activity of 3T3 fibroblasts cultivated on the surface of a PP mesh (1), PP mesh enriched with adhered thrombocytes (2), PP mesh functionalized with PCL nanofibers (3), PP mesh functionalized with PCL nanofibers enriched with adhered thrombocytes (4). The MTT assay revealed significantly higher metabolic activity of 3T3 fibroblasts on scaffolds functionalized with PCL nanofibers (PP + PCL and PP + PCL + TRS) on day 14 than on scaffolds without functionalization (PP). Moreover, the metabolic activity of 3T3 fibroblasts on days 7, 10 and 14 was significantly higher on the PP mesh functionalized with PCL nanofibers treated with TRS than on all other scaffolds.

Notes: The level of statistical significance for the assays is designated above the mean values ($p < 0.05$ indicated by a number, $p < 0.001$ indicated by a number and *). Day 1: without significance. Day 3: 3 > 1, 2; 4 > 1*, 2*. Day 7: 3 > 1; 4 > 1*, 2*, 3. Day 10: 2 > 1; 3 > 1*; 4 > 1*, 2, 3. Day 14: 2 > 1*; 3 > 1*, 2*; 4 > 1*, 2*, 3.

Abbreviations: PP, polypropylene; PCL, poly-ε-caprolactone; TRS, thrombocyte-rich solution; MTT, 3-[4,5-dimethylthiazol-2-yl]-2,5-diphenyltetrazolium bromide; AU, absorbance units.

4.1.3 Increased metabolic activity is accompanied by a larger number of cells

The increase in the number of cells, which is the result of good proliferation, was estimated from the DNA values measured using a PicoGreen assay (Figure 24). The results of the Picogreen assay on days 1, 3, 7, 10, and 14 clearly indicated substantial cell proliferation on the functionalized scaffolds. A significantly higher number of cells were observed on days 10 and 14 on any composite scaffold than on the PP mesh alone. Additionally, the PicoGreen assay confirmed a significantly larger number of cells ($p < 0.001$) on the scaffold with the most advanced improvement, ie the PP mesh functionalized with PCL nanofibers treated with TRS on days 10 and 14 than on all other scaffolds that were investigated. These results are consistent with the results for metabolic activity evaluated by the MTT assay.

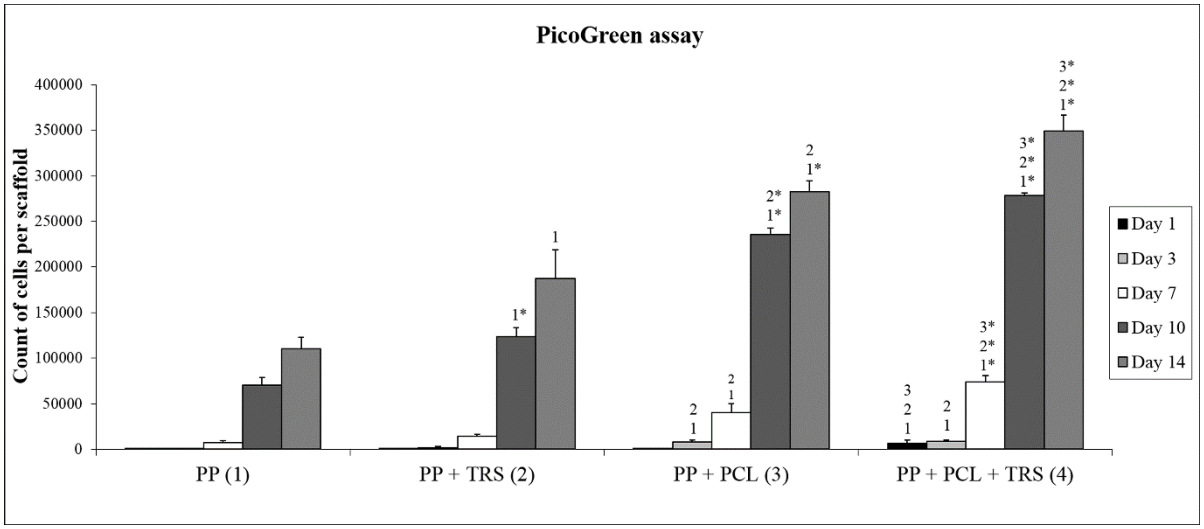

Figure 24. Proliferative activity of 3T3 fibroblasts cultivated on the surface of a PP mesh (1), PP mesh enriched with adhered thrombocytes (2), PP mesh functionalized with PCL nanofibers (3), PP mesh functionalized with PCL nanofibers treated with TRS (4). The PicoGreen assay revealed significantly higher proliferation of 3T3 fibroblasts on scaffolds functionalized with PCL nanofibers (PP + PCL and PP + PCL + TRS) on days 7, 10 and 14 than on scaffolds without functionalization (PP and PP + TRS). In addition, the proliferation of 3T3 fibroblasts on days 7, 10 and 14 was

significantly higher (level of significance at value of $p < 0.001$) on the PP mesh functionalized with PCL nanofibers enriched with adhered thrombocytes than on all other scaffolds.

Notes: The level of statistical significance for the assays is designated above the mean values ($p < 0.05$ indicated by a number, $p < 0.001$ indicated by a number and *). Day 1: 4 > 1, 2, 3. Day 3: 3 > 1, 2; 4 > 1, 2. Day 7: 3 > 1, 2; 4 > 1*, 2*, 3*. Day 10: 2 > 1*; 3 > 1*, 2*; 4 > 1*, 2*, 3*. Day 14: 2 > 1; 3 > 1*, 2; 4 > 1*, 2*, 3*.

Abbreviations: PP, polypropylene; PCL, poly-ε-caprolactone; TRS, thrombocyte-rich solution.

However the concentration of cells does not reflect the ratio of live and dead cells, so a live/dead cell staining assay was performed. The viability of the 3T3 fibroblasts was evaluated on days 1, 3, 7, 10, 14 after seeding. For the simplification only data obtained on day 14 are presented (Figure 25). Live cells were stained by BCECF-AM (green colour) and by propidium iodide (red). Viability was calculated as the percentage of live cells from the total cell count per unit area.

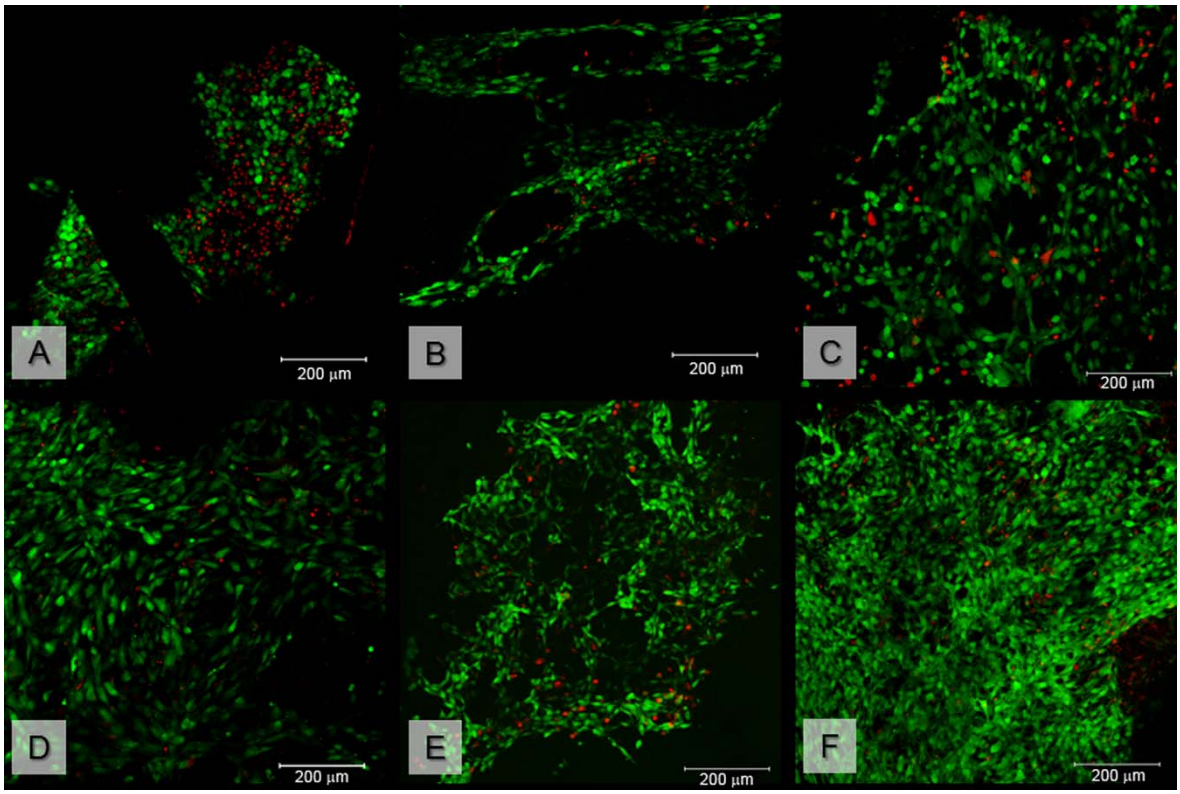

Figure 25. Viability of 3T3 fibroblasts cultivated on the surface of a PP mesh (A), a PP mesh treated with TRS (B), a PP mesh functionalized with PCL nanofibers (C), a PP mesh functionalized with PCL nanofibers treated with TRS (D), PCL nanofibers (E), PCL nanofibers treated with TRS (F) on day

14 after seeding. Live/dead cell staining revealed a higher percentage of viable cells on all scaffolds functionalized either with PCL nanofibers or with TRS than on the scaffold without any functionalization or treatment (PP). The percentage of viable cells cultivated on the surface of scaffold A was: 59,5%, B: 85,4%, C: 88,3%, D: 90,1%, E: 90,3%, F: 94,7%.

Notes: The viability of 3T3 fibroblasts was evaluated on days 1, 3, 7, 10, 14 after seeding. For the simplification only data obtained on day 14 are presented. Viability was calculated as the percentage of live cells from the total cell count per unit area. Live cells are stained green. Dead cells are stained red. Scale bar 200 μm.

Abbreviations: PP, polypropylene; PCL, poly-ε-caprolactone.

Live/dead cell staining revealed a higher percentage of viable cells in all scaffolds either functionalized with PCL nanofibers or treated with TRS than on a PP mesh alone. In particular, the percentage of viable cells on the PP mesh treated only with TRS was 85.4%, on the PP mesh functionalized with PCL nanofibers the value was 88.3%, and the PP mesh functionalized with PCL nanofibers treated with TRS showed 90.1% of viable cells. In the two control groups, the percentage of viable cells was 90.3% for the cells seeded on PCL nanofibers alone, and 94.7% for the cells seeded on PCL nanofibers treated with TRS. Previous results confirmed the conclusion that a PP mesh enriched with either PCL nanofiber functionalization or with TRS treatment improved 3T3 fibroblast viability.

4.1.4 Functionalization of the PP mesh also improved cell proliferation significantly.

Cell metabolic activity can result not only in a larger number of cells, as was confirmed by our study of DNA content, but also in cell proliferation. Cell proliferation was therefore evaluated using a BrdU colorimetric immunoassay. This assay is based on incorporating bromodeoxyuridine only in the active process of DNA synthesis in healthy cells. A BrdU colorimetric immunoassay was performed on days 1, 3, 7, 10 and

14 (Figure 26). The BrdU assay revealed significantly higher proliferation of 3T3 fibroblasts on scaffolds functionalized either with PCL nanofibers or with PCL nanofibers treated with TRS on all evaluation days than on scaffolds without functionalization, namely the PP mesh alone and the PP mesh treated with TRS. Moreover, the proliferation of 3T3 fibroblasts on day 14 was significantly higher ($p < 0.001$) on the PP mesh functionalized with PCL nanofibers treated with TRS than on all other scaffolds. Polypropylene mesh functionalization also significantly improves 3T3 fibroblast proliferation.

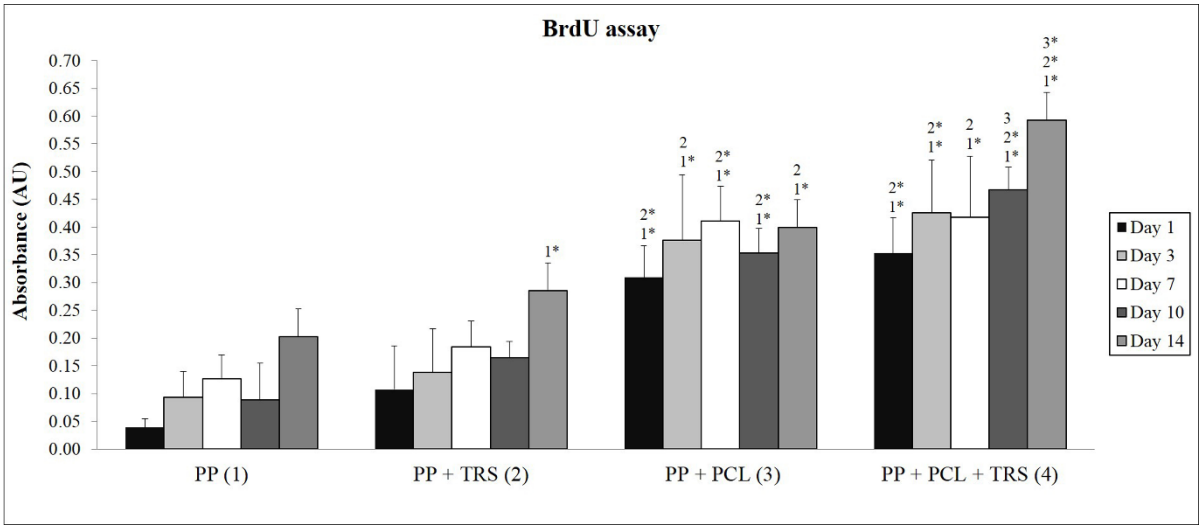

Figure 26. Proliferation of 3T3 fibroblasts cultivated on the surface of a PP mesh (1), PP mesh treated with TRS (2), PP mesh functionalized with PCL nanofibers (3), PP mesh functionalized with PCL nanofibers treated with TRS (4). A BrdU colorimetric immunoassay revealed significantly greater proliferation of 3T3 fibroblasts on scaffolds functionalized with PCL nanofibers (PP + PCL and PP + PCL + TRS) on all days of evaluation than on scaffolds without functionalization (PP and PP + TRS). In addition, the proliferation of 3T3 fibroblasts on day 14 was significantly higher ($p < 0.001$) on the PP mesh functionalized with PCL nanofibers treated with TRS than on all other scaffolds.

Notes: The level of statistical significance for the assays is designated above the mean values ($p < 0.05$ indicated by a number, $p < 0.001$ indicated by a number and *). Day 1: 3 > 1*, 2*; 4 > 1*, 2*. Day 3: 3 > 1*, 2; 4 > 1*, 2*. Day 7: 3 > 1*, 2*; 4 > 1*, 2. Day 10: 3 > 1*, 2*; 4 > 1*, 2*, 3. Day 14: 2 > 1*; 3 > 1*, 2; 4 > 1*, 2*, 3*.

Abbreviations: PP, polypropylene; PCL, poly-ε-caprolactone; TRS, thrombocyte-rich solution; BrdU, 5-bromo-2'-deoxyuridine; AU, absorbance units.

4.2 *In vivo* testing of the composite scaffold based on a polypropylene surgical mesh functionalized with the PCL nanofibers and adhered synthetic growth factors on rabbits as a small animal model.

4.2.1 Clinical postoperative course

The animals were euthanized after 6 weeks. We did not observe any evident changes of condition or weight loss of any animal. A macroscopic evaluation of samples from all groups was made after explanation of abdominal wall (Figure 16). The surface of the regenerated tissue showed no signs of inflammation or infection in any groups. The incidence of hernia was not observed in any samples.

4.2.2 Video-recorded biomechanical assay (tensile strength)

The animals were sacrificed six weeks after surgery and samples of their abdominal wall, including the scar, mesh and healthy tissue were harvested. 1×6 cm strips of regenerated abdominal wall of each animal (Figure 16), as was described in Methods, were tested for hysteresis and maximum tensile strength, using a Micro tester digital tension meter (Figure 17). The tissue samples were individually attached to the branches of the tension meter in longitudinal manner, not including the place covered with scaffolds of a particular type. The samples were stretched by 5 mm at a speed of 10 mm/s ten times and were then pulled at a speed of 0.5 mm/s until the sample broke (Figure 27). The force response of each sample was detected, and both the static and the dynamic properties of each of the samples were analysed. Average

values of all measured data are summarized in Table 5.

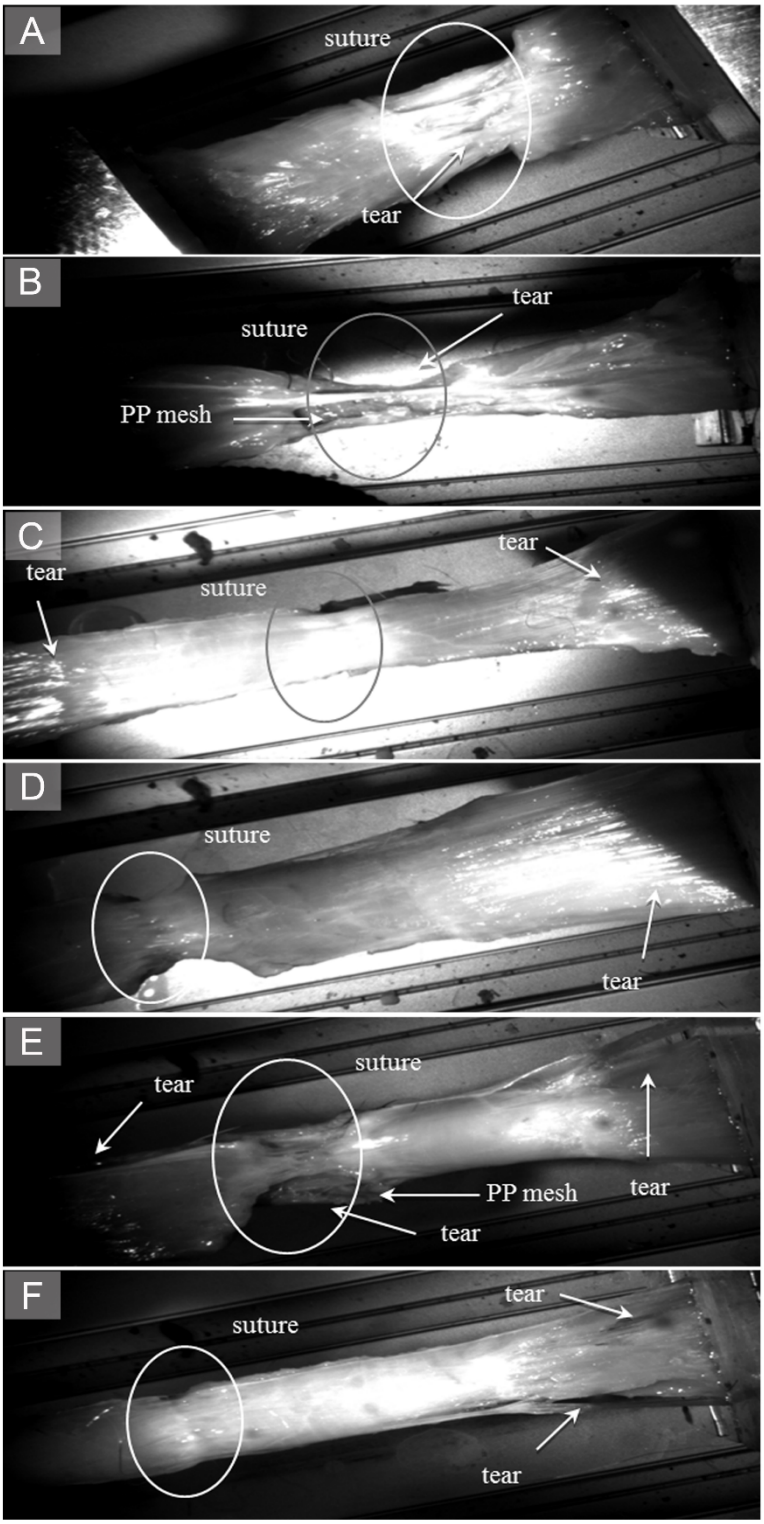

Figure 27. Video-recorded biomechanical assay (tensile strength). (A) Simple suture tears in the line. (B) Healthy muscle broke at the edge and the PP mesh slid on the top of the muscle. (C) Tissue treated by a PP mesh functionalized with PCL nanofibers enriched with adhered GF tore at the edge of the mesh and healthy muscle, and the slide was localized between muscle fibers. (D) In some PCL nanofiber samples with adhered GF, the suture line tore first, but in others a tear occurred between muscle fibers or at the edge of the muscle and the mesh. (E) Healthy muscle tore at the edge and a PP mesh functionalized with PCL nanofibers slid on top of the muscle, or the tear was localized not between the mesh and the muscle layer but in between muscle fibers. (F) In some PCL nanofiber samples, the suture line tore first, but in others a tear occurred between muscle fibers or at the edge of the muscle and the mesh.

Abbreviations: PP, polypropylene; PCL, poly-ε-caprolactone; GF, growth factors.

Values of the variables differed minimally among the groups, because the breach of the tear was almost unconditionally localized at the level of a muscle. The locations of the tear, however, varied significantly among the groups. The suture line broke first if it was not supported by any mesh. Thus, we have confirmed that the suture line is the weakest point of the abdominal wall 6 weeks post-surgery (Figure 27A). In all samples with the PP mesh, the tissue broke first at the edge of the mesh and healthy muscle followed by a slide of the PP mesh on top of a muscle (Figure 27B, C, E). The boundary of the mesh and the muscle created a stress concentration leading to the slip.

Table 5. Average values of the biomechanical quantities

Group	E [N/mm^2]	σ_{max} [N/mm^2]	ε_{max} [-]
I	3.73 ± 1.21	0.50 ± 0.14	0.30 ± 0.04
II	2.55 ± 0.75	0.46 ± 0.07	0.71 ± 0.16
III	2.73 ± 0.20	0.61 ± 0.08	0.61 ± 0.06
IV	2.60 ± 1.23	0.64 ± 0.10	0.61 ± 0.15
V	2.78 ± 1.09	0.63 ± 0.04	0.65 ± 0.10
VI	3.11 ± 1.43	0.68 ± 0.08	0.49 ± 0.08

Notes: Six experimental groups are presented in Methods and in Table1.

Abbreviations: E, elasticity in traction or Young modulus in N/mm^2 (MPa) ; σ_{max}, average values of maximal strength force per square unit in N/mm^2 (MPa); ε_{max}, maximal proportional elongation value.

In the group with PP functionalized with PCL nanofibers (Figure 27E), two types of tear mechanism were recorded. This was the same as in the PP mesh group, but in some samples the slide was localized not between the mesh and the muscle layer but in between the muscle fibers. In the group of PP mesh functionalized with PCL nanofibers enriched with adhered GF (Figure 27C), the tissue also tore at the edge of the mesh and the healthy muscle, and the slide was localized between muscle fibers,

with the exception of one sample, where the recorded mechanism was exactly the same as in the PP mesh group. The PCL nanofibers connected better to the abdominal wall than the PP mesh alone.

In case of pure PCL nanofibers (Figure 27D and F), various types of tear were observed. In some samples the suture line tore first. In other samples a tear occurred between muscle fibers or at the edge of the muscle and the mesh.

Static and dynamic parts of the experiment are documented in Table 5. We compared the average maximal strength force values. All samples functionalized with PCL nanofibers (Groups III – VI), with or without adhered GF, showed a significantly increased average maximal strength force ($\sigma_{max.}$) compared to a simple PP mesh or suture (Groups I and II). Clearly, preserving the elasticity in traction and simultaneously increasing the maximum strength force value indicated a positive effect of nanofibers on fascia healing. Interestingly, PCL nanofibers alone (Group VI) showed the highest average maximal strength force value among all samples. Significant differences of average maximal strength force ($\sigma_{max.}$) among the experimental groups are presented in Figure 28.

Our results also indicated somewhat more elastic samples in the presence of the PP mesh (Groups II-V) compared to samples without the mesh (Groups I and VI), as indicated by their slightly lower Young's modulus. A significantly lower elasticity in traction (E) and higher elongation in Group IV (PCL nanofibers with growth factors) than in Group VI (PCL nanofibers without growth factors) indicated accelerated fascia regeneration, which can undoubtedly be attributed to the presence of growth factors.

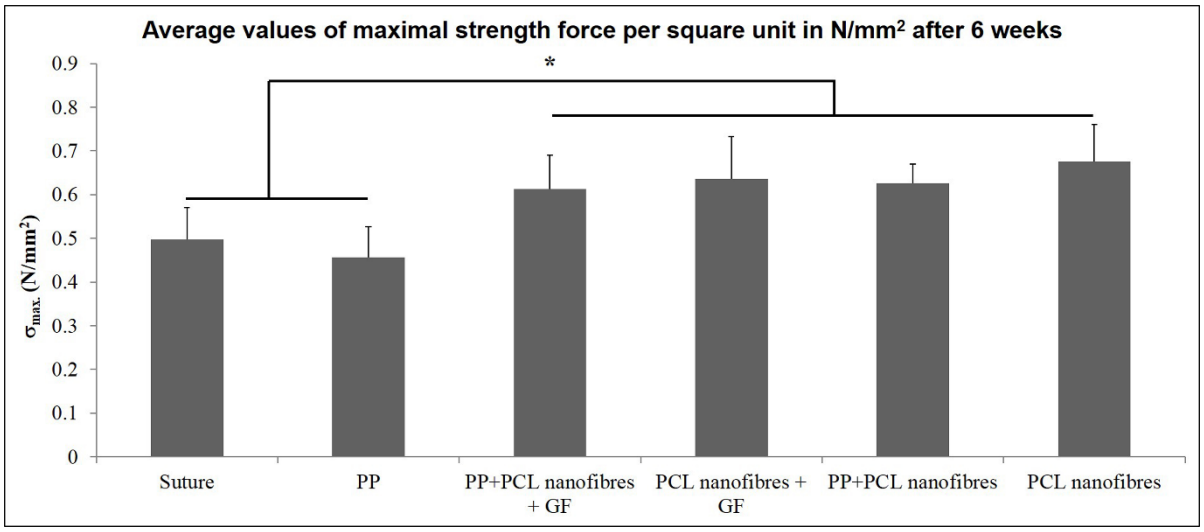

Figure 28. Average values of maximal strength force per square unit in N/mm^2 (MPa) after 6 weeks.

Notes: The level of statistical significance for the measurement is indicated above the mean values: $p < 0.05$ indicated by *.

Abbreviations: σ_{max}, average values of maximal strength force per square unit; N, Newton; mm^2, square millimetre; MPa, megapascal; PP, polypropylene; PCL, poly-ε-caprolactone; GF, growth factors.

4.2.3 Histological evaluation

The implants were prepared and implanted as described in Methods, and were tested in vivo on a small animal model (a rabbit). The animals were sacrificed after 6 weeks. In all groups of scaffolds there were some differences among the groups in the area fraction occupied by granulomatous infiltrate in medial samples taken from the healing incision, but the difference did not reach statistical significance (Figure 29A). Medial samples with the incision had a higher α-smooth muscle actin fraction ($p=0.003$), a lower collagen fraction ($p=0.035$) and a higher density of microvessels ($p<0.001$) in comparison with samples of the lateral abdominal wall without incision.

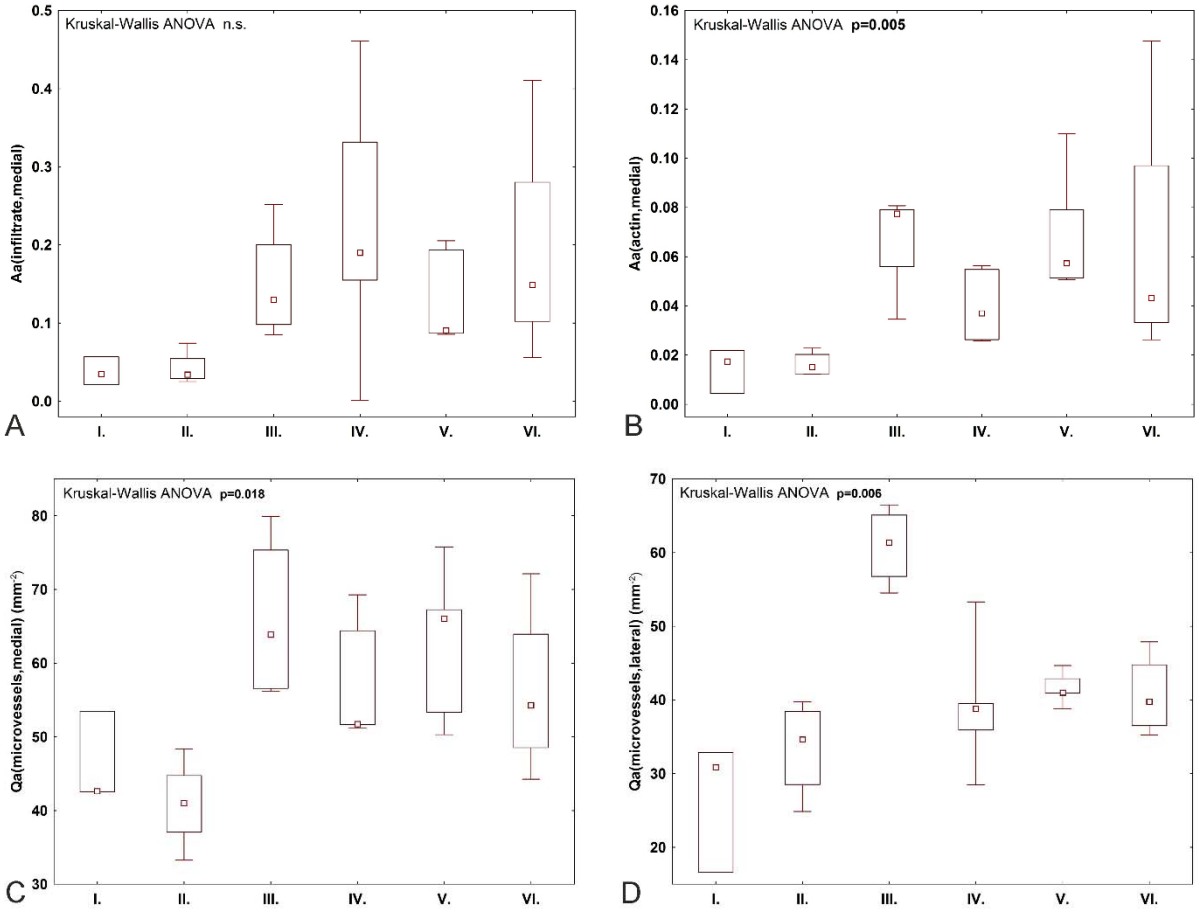

Figure 29. Quantitative histological results. (A) Inflammatory infiltrate in the medial healing incision in group I (suture only), II (PP mesh), III (PP mesh functionalized with PCL nanofibers enriched with adhered GF), IV (PCL nanofibers enriched with adhered GF), V (PP mesh functionalized with PCL nanofibers) and VI (PCL nanofibers alone). (B) Fraction of α-smooth muscle actin positive vascular smooth muscle cells and myofibroblasts in the medial healing incision in groups I-VI (C) Density of microvessel profiles in medial healing incisions in groups I-VI. (D) Density of microvessel profiles in the abdominal wall 20 mm lateral from the incision in groups I-VI.

Notes: The data are presented as medians with boxes spanning the upper limits of the first and third quartiles and with whiskers spanning the minimum and maximum values for each group. P-values of the Kruskal Wallis ANOVA show the differences among the groups under study.

Abbreviations: PP, polypropylene; PCL, poly-ε-caprolactone; GF, growth factors; Aa, area fraction; Qa, section area.

A considerable difference was observed in the area occupied by α-smooth muscle actin-positive cells in medial samples of the healing incision (Figure 29B).

There were more α-smooth muscle actin-positive cells in all samples containing PCL nanofibers than in the controls (simple suture and PP mesh) (Figure 30). There was no significant difference between the groups containing PCL nanofibers, with the exception of the samples from the lateral portion of the healing incision in PCL-only treated specimens.

Significant differences in the density of the microvessel profiles were observed between the groups in both the medial and the lateral parts of the healing fascia (Figure 29C and D). Samples containing PCL nanofibers had a greater density of microvessel profiles than the control groups (simple suture and PP mesh). The density was clearly highest in the lateral portion of samples with a PP mesh functionalized with PCL nanofibers enriched with adhered GF.

PCL nanofiber scaffolds showed beneficial properties in fascia healing, and should be further tested in hernia repair application. From the histological point of view, the highest fraction of collagen was observed in samples with PCL nanofibers enriched with adhered GF, followed by samples with no mesh (incision) and by samples functionalized with PCL nanofibers (Figure 31). Samples functionalized with PCL nanofibers and enriched with adhered GF also contained low fractions of adipose tissue (Figure 31). The presence of PCL nanofibers and GF seemed to increase the granulomatous infiltration and vascularization of the healing tissue, because the remnants of nanofibers were surrounded by granulomatous leukocyte-rich connective tissue at the end of the sixth week after implantation. Tissue samples with heavier granulomatous infiltration also contained more blood vessels and a higher fraction of vascular smooth muscle and myofibroblasts.

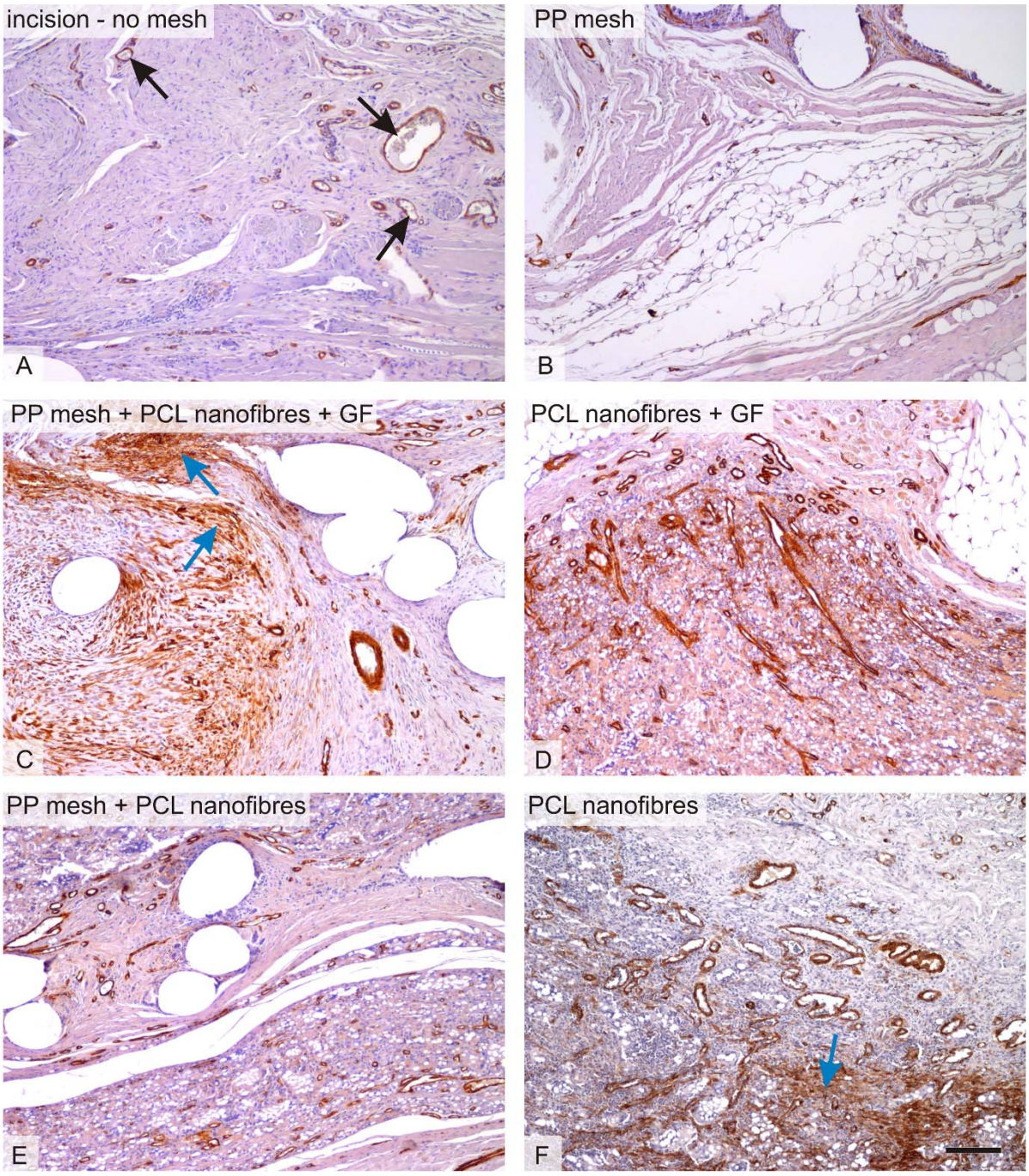

Figure 30. α-smooth muscle positivity in the scaffolds under study. The density of the microvessels (some of them pointed with black arrows) and the area fraction of actin-positive cells (vascular smooth muscle and myofibroblasts, some of the accumulated myofibroblasts highlighted with blue arrows) were highest in the PP mesh samples functionalized with PCL nanofibers enriched with adhered GF (C), followed by the PP mesh functionalized with PCL nanofibers (E), PCL nanofibers (F) and PCL nanofibers enriched with adhered GF (D), while the lowest values were found in samples of pure PP meshes (B) and sham-operated animals with no mesh (A).

Notes: Immunohistochemistry for α-smooth muscle actin, counterstaining Gill's hematoxylin. Magnification × 100, scale bar 200 μm.

Abbreviations: PP, polypropylene; PCL, poly-ε-caprolactone; GF, growth factors.

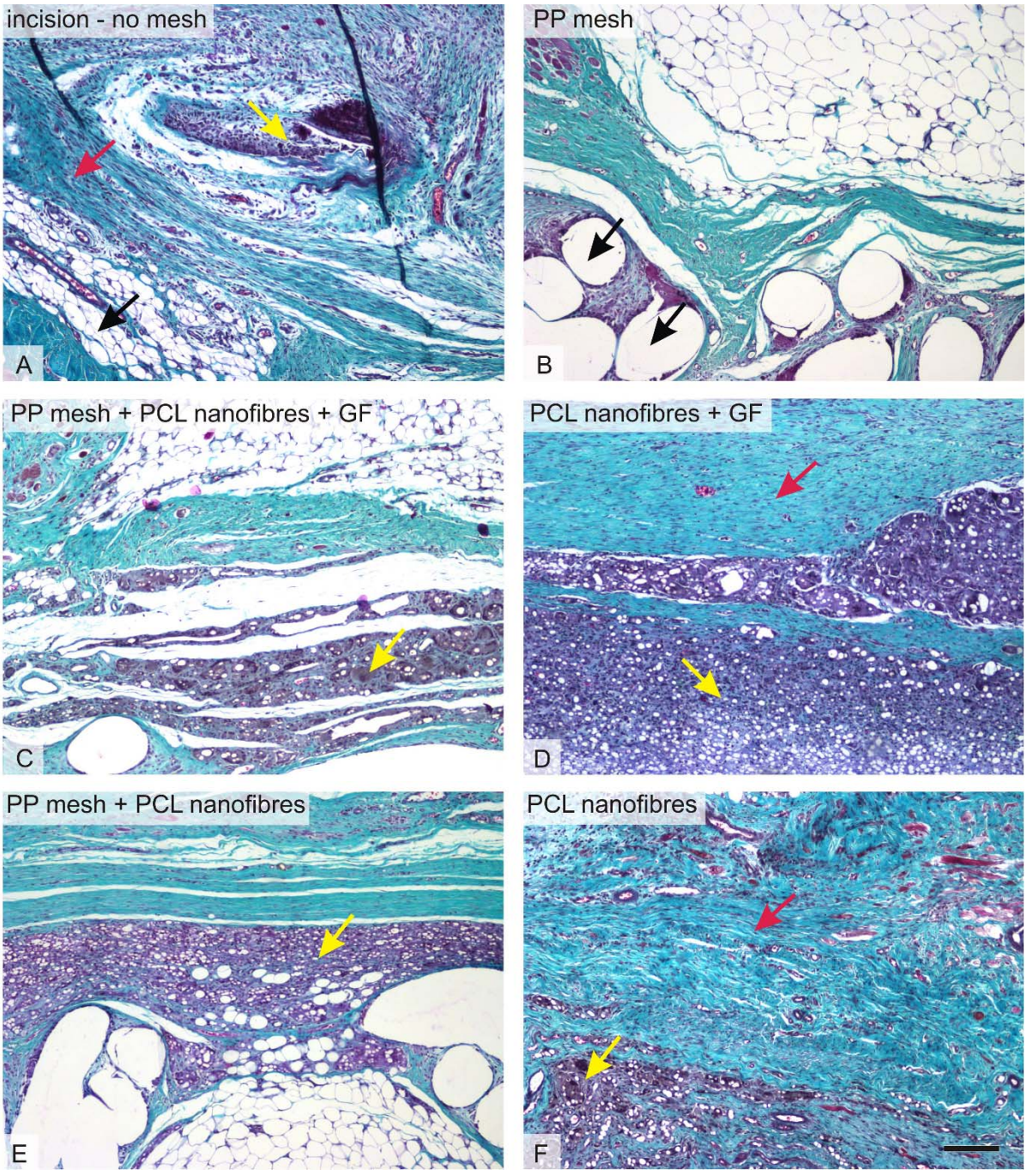

Figure 31. Collagen, adipose tissue, and granulomatous infiltration in the scaffolds under study. In samples without any mesh (A), the incision was healing with a mixture of collagen (red arrow), adipose connective tissue (black arrow) and inflammatory infiltrate (yellow arrow). Samples with PP mesh (B) had a high fraction of adipose tissue, but the spaces showing the dissolved mesh (black

arrows) were surrounded by only a few inflammatory cells. Remnants of the nanofibers (C,D,E,F) were surrounded by granulomatous leukocyte-rich connective tissue (yellow arrows in C,D,E,F). The highest fraction of collagen (red arrow) was in samples of PCL nanofibers with adhered GF (D), followed by samples with no mesh (A) and by samples of PCL nanofibers (F). Low fractions of adipose tissue were found in samples of PCL nanofibers with adhered GF (D), samples with no mesh (A) and in samples of PCL nanofibers (F).

Notes: Verhoeff's hematoxylin and green trichrome staining. Magnification × 100, scale bar 200 μm.

Abbreviations: PP, polypropylene; PCL, poly-ε-caprolactone; GF, growth factors.

The non-parametric Spearman rank order correlations between the quantitative histological parameters are listed in Table 6 (for this purpose, the data were pooled across all groups in the study). Tissue samples with heavier granulomatous infiltration contained more blood vessels and a higher fraction of vascular smooth muscle and myofibroblasts at the site of the healing incision.

Table 6. The non-parametric Spearman rank order correlations between the quantitative parameters at the healing incision (medial side)/without incision (lateral side)

	Aa (adipose)	**Aa (infiltrate)**	**Aa (actin)**	**Qa (microvessel)(mm^{-2})**
Aa (collagen)	**-0.59/-0.42**	**-0.46/-0.50**	n.s./n.s.	n.s./n.s.
Aa (adipose)	-	n.s./n.s.	n.s./n.s.	n.s./n.s.
Aa (infiltrate)	-	-	**0.57/0.47**	**0.50/**n.s.
Aa (actin)	-	-	-	**0.53/0.69**

Notes: Marked correlations are significant at $p < 0.05$, other correlations did not reach statistical significance (n.s.). Autocorrelations and repeating values are replaced by a – sign.

Abbreviations: Aa, area fraction; Qa, section area; n.s., no significance.

4.3 *In vivo* testing of a scaffold based on the PCL nanofibers functionalized with adhered human platelets on minipigs as a large animal model.

4.3.1 Clinical postoperative course

The animals were euthanized either after 6 or 12 weeks. We did not observe any evident changes of condition or weight loss of any animal during the entire study period. One animal underwent on day 14 a dehiscence of the surgical wound with an empyematic discharge. The edges of the wound were treated by curettage and carefully disinfected with povidone-iodine (Braunol). The wounds were stitched with absorbable surgical suture with a temporary drain. The animal was administred Amoxicillin-Clavulanate antibiotics (2.5 mL *i.m., pro toto*; Synulox® RTU, Pfizer Limited, Tadworth, UK). In other animals the post-operative condition was good. Wound healing went with no secondary complication or effect to the animal's day activity, such as movement, liquid and food intake or excretion.

4.3.2 Histological evaluation

The samples contained several layers of subcutaneous fat, abdominal muscles and their fasciae, extraperitoneal fat, and the parietal peritoneum. The deep truncal fascia often contained remnants of elastic fibres. The total thickness of the abdominal wall varied considerably. Although some parts of the abdominal fasciae appeared to be merged, the layers of abdominal skeletal muscles usually kept their organization and only small and sporadic skeletal muscle bundles were found displaced at the healing incision.

4.3.2.1 Differences between experimental groups

Typical histological findings representing the groups under study are summarized in Figures 32, 33 and 34.

Figure 32 shows the presence of collagenous connective tissue and adipose tissue. Nanofiber scaffolds were well integrated to the connective tissue. Their remnants were surrounded with granulomatous leukocyte-rich connective tissue mixed with dense collagenous connective tissue.

In Figure 33 we can observe the lower fraction of α-smooth muscle-positive cells (vascular smooth muscle and myofibroblasts) in the samples with no scaffolds compared to the samples treated with either PCL nanofibers or PCL nanofibers with adhered platelets.

Figure 34 shows the greater fraction of the type I collagen at the site without incision compared to the healing incision.

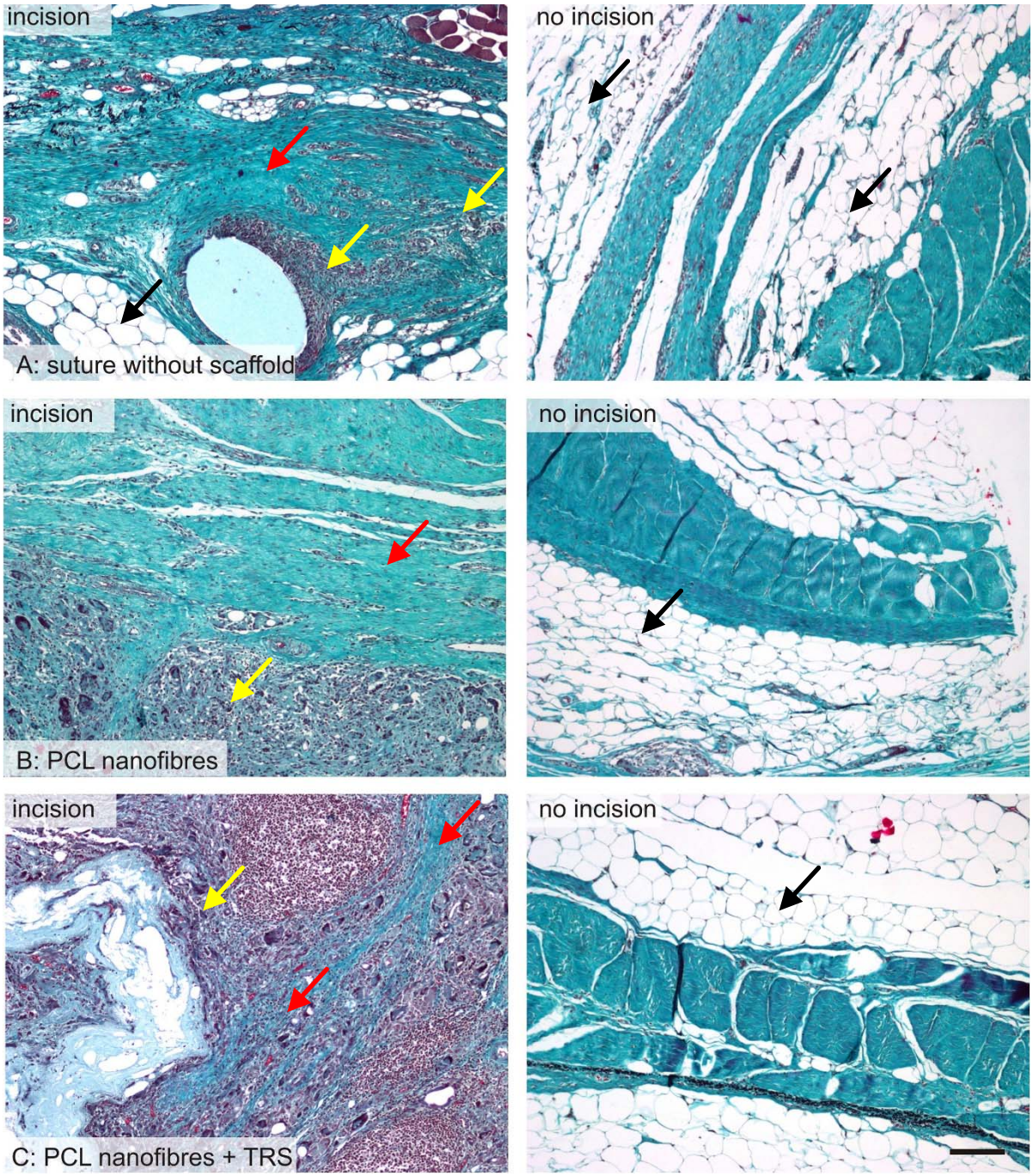

Figure 32. Between-groups comparison and differences between the incision (left) and adjacent region 20 mm apart from the healing incision (right), overall trichrome stain. In samples without any scaffold (A), the stitches were surrounded by collagenous connective tissue (red arrow) and adipose tissue (black arrow). The remnants of nanofibres (B,C) were well integrated to the connective tissue and surrounded with granulomatous leukocyte-rich connective tissue (yellow arrow) mixed with dense collagenous connective tissue (red arrow). In all groups, the abdominal wall without incision consisted mostly of truncal fascia and adipose tissue overlying the abdominal muscles.

Notes: Verhoeff's haematoxylin and green trichrome stain. Magnification × 100, scale bar 200 μm.

Abbreviations: PCl, poly-ε-caprolactone; TRS, thrombocyte-rich solution.

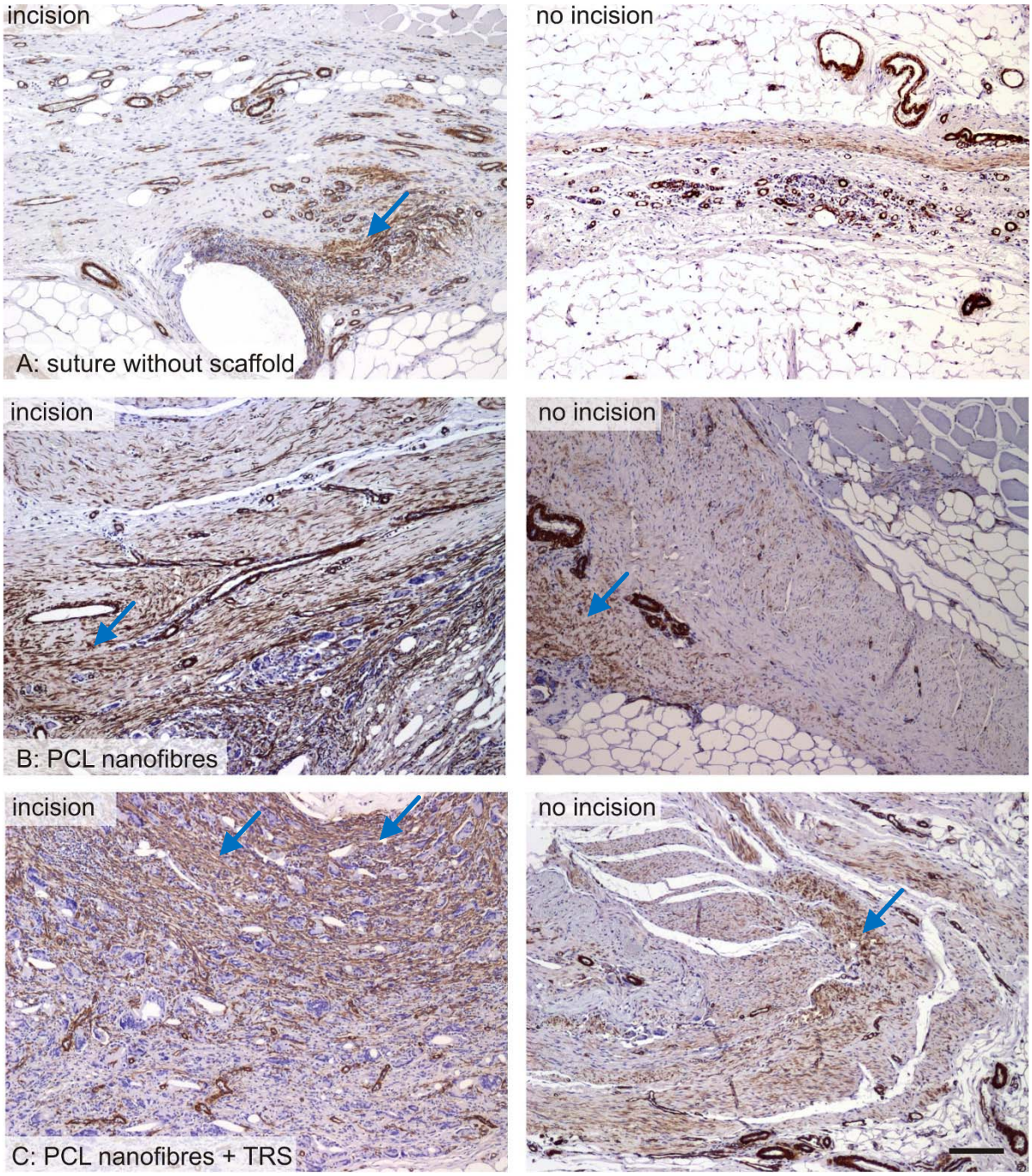

Figure 33. Between-groups comparison and differences between the incision (left) and adjacent region 20 mm apart from the healing incision (right), α-smooth muscle actin immunohistochemistry. In samples without any scaffold (A), the fraction of α-smooth muscle-positive cells (vascular smooth muscle and myofibroblasts, some of the fraction pointed with blue arrows) was smaller than in samples with PCL nanofibres (B) and PCL nanofibres with TRS (C).

Notes: Immunohistochemistry for α-smooth muscle actin showing positive myofibroblasts and vascular smooth muscle cells, counterstaining Gill's haematoxylin. Magnification × 100, scale bar 200 μm.

Abbreviations: PCl, poly-ε-caprolactone; TRS, thrombocyte-rich solution.

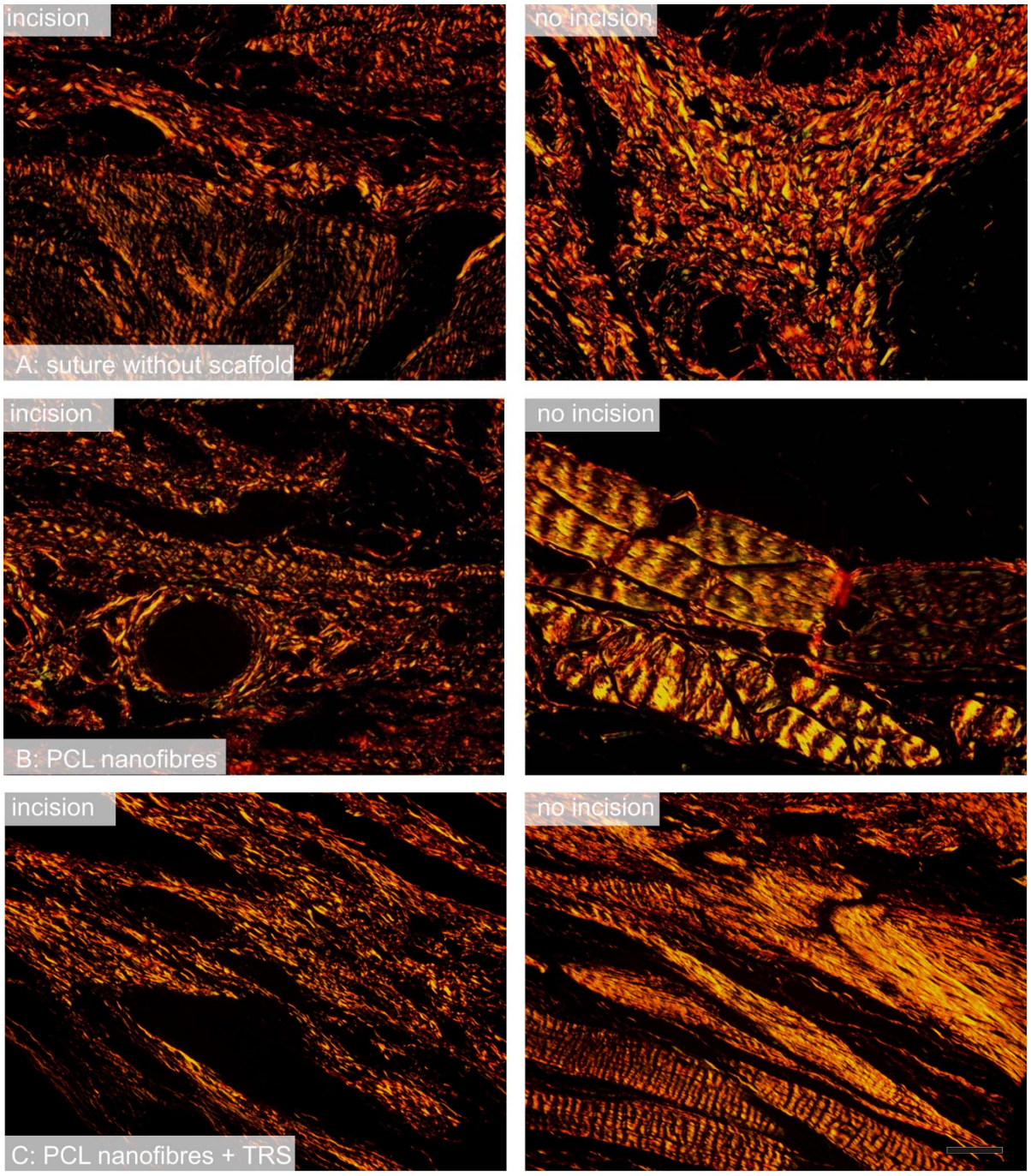

Figure 34. Between-groups comparison and differences between the incision (left) and adjacent region 20 mm apart from the healing incision (right), picrosirius red observed in circular polarization. In all groups under study (A-C), the fraction of type I collagen (red and yellow fibres) was greater at the site without incision (right) than within the healing incision (left).

Notes: Picrosirius red, polarized light. Magnification × 100, scale bar 200 µm.

Abbreviations: PCL, poly-ε-caprolactone; TRS, thrombocyte-rich solution.

From histological point of view, both types of scaffolds (PCL and PCL+TRS) were well and uniformly integrated within the collagenous connective tissue of the healing incision. The most convincing finding was that the presence of both PCL nanofiber and PCL nanofiber + TRS scaffolds led to increased amount of contractile myofibroblasts within the healing incision, but the amount of microvessels in samples with scaffolds was comparable with samples without scaffolds. In PCL scaffold, the microvessel density was positively correlated with the fraction of type I collagen.

We found no differences when comparing the PCL vs. PCL+TRS scaffolds. No differences were found in any of the parameters when comparing samples after 6 weeks of healing vs. 12 weeks of healing.

Tissue samples without any scaffold had more type I collagen after 12 weeks than samples with PCL+TRS. However, the mechanical properties of the abdominal wall and the differences caused by the amount of type I collagen and contractile myofibroblasts should be tested using biomechanics. The total thickness of the abdominal wall varied considerably and it exceeded the size of histological tissue samples in some cases.

4.3.2.2 Quantitative histological results - grouping according to the scaffold type

The quantitative histological results grouped according to the type of the scaffold are presented in Figure 35. Results in Figure 35A evaluated by ANOVA showed considerable differences among the groups in the area fraction occupied by α-smooth muscle actin-positive cells at the site of incision. The area fraction occupied by α-smooth muscle actin-positive cells was greater in samples with PCL nanofibers and PCL nanofibers + TRS compared to samples treated with suture alone. Statistical

analysis of the result using the Mann Whitney U test showed a greater fraction occupied by α-smooth muscle actin-positive cells at the site of incision in samples with PCL nanofibres when compared with samples with no scaffold at 6 weeks (Figure 35B). The same statistical method showed also a greater fraction occupied by α-smooth muscle actin-positive cells at the site of incision in samples with PCL nanofibres + TRS when compared with samples with no scaffold when the samples from the 6 and 12 weeks healing were pooled (Figure 35C).

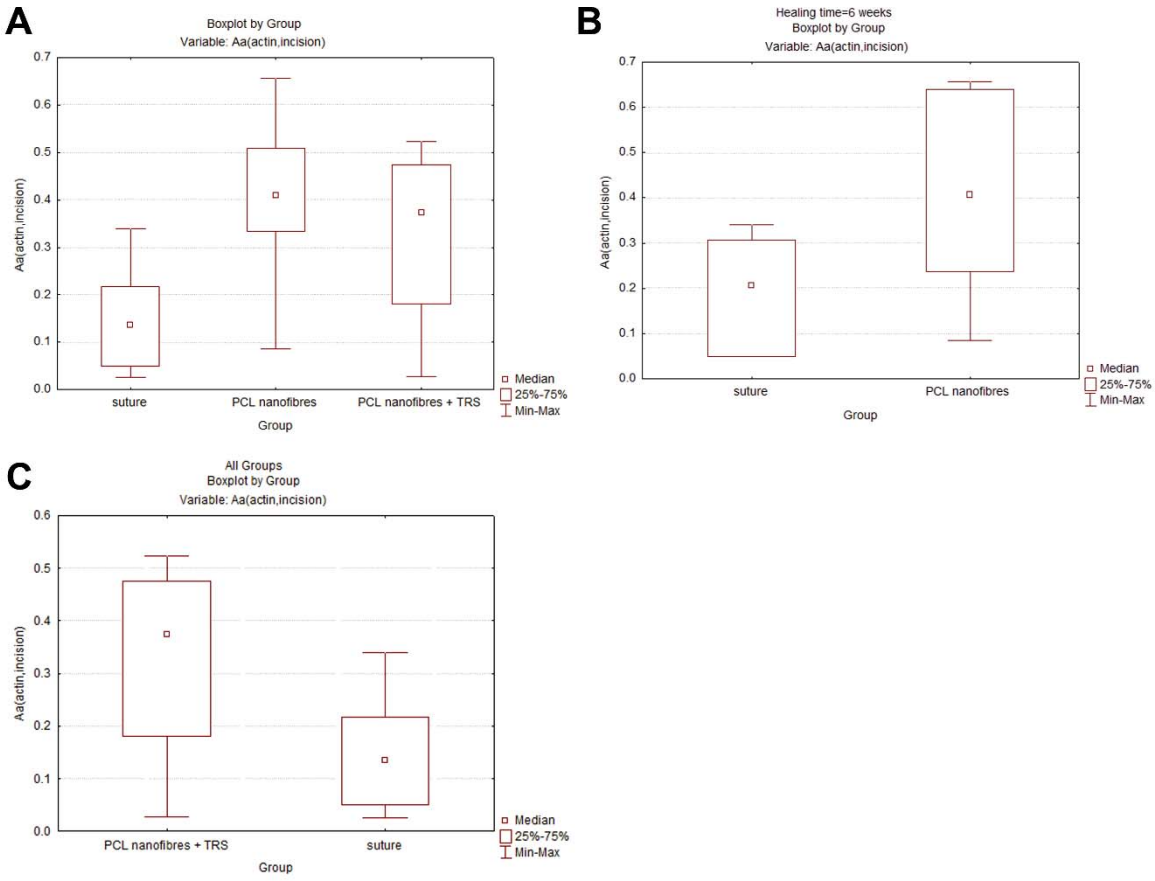

Figure 35. The quantitative histological results grouped according to the type of the scaffold. (A) Considerable differences among the groups in the area fraction occupied by α-smooth muscle actin-positive cells at the site of incision. (B) Greater fraction occupied by α-smooth muscle actin-positive cells at the site of incision in samples with PCL nanofibres when compared with samples with no scaffold at 6 weeks. (C) Greater fraction occupied by α-smooth muscle actin-positive cells at the site

of incision in samples with PCL nanofibres + TRS when compared with samples with no scaffold (the samples 6+12 weeks pooled)

Notes: (B) p=0.035. (C) p=0.015.

Abbreviations: PCL, poly-ε-caprolactone; TRS, thrombocyte-rich solution; Aa, area fraction.

4.3.2.3 Quantitative histological results - grouping according to the healing time

No differences were found in any of the parameters when comparing samples after 6 weeks of healing vs. 12 weeks of healing. For the statistical evaluation the Mann Whitney U test was used.

4.4 *In vitro* testing of the scaffold base on cryogrinded PCL nanofibers with potential use as a drug delivery system for tissue engineering

4.4.1 Cell adhesion on the microsphere system

To evaluate the potential of prepared new drug delivery systems for tissue engineering, mouse 3T3 fibroblasts were seeded on microparticles and cell adhesion was analyzed after one day by confocal microscopy. Cell membranes were stained by DiOC6 and propidium iodide was used as a counterstain for cell nuclei. Results of confocal microscopy showed adhesion of cells to all three samples. Particles grinded in mannitol (Figure 36A) and 2-octanol (Figure 36B) showed good cell adhesion. Biocompatibility of particles ground in 2-octanol is quite surprising and could be explained by 2-octanol washing out during the sterilization of particles in ethanol. Interestingly, the sample grounded in Pluronic F-68 (Figure 36C) exhibited the lowest cell adhesion.

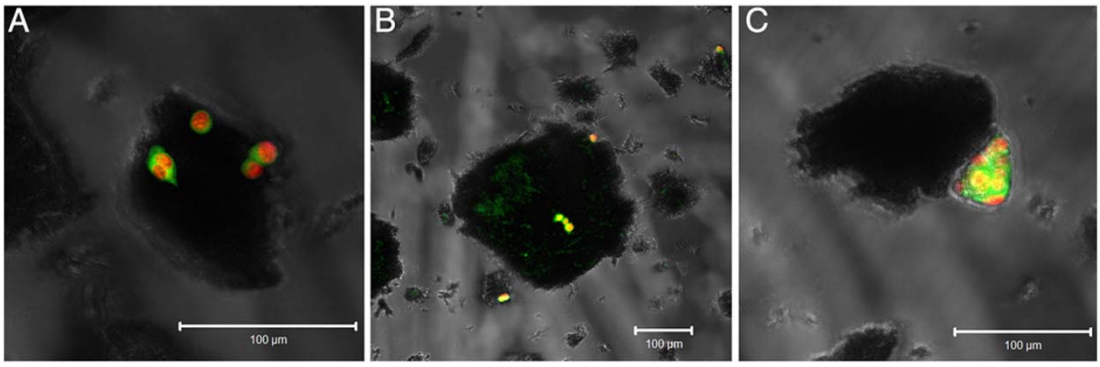

Figure 36. Adhesion of 3T3 fibroblasts on microparicles. (A) Microparticles cryogrinded in 10% mannitol. (B) Microparticles cryogrinded in 2-octanol. (C) Microparticles cryogrinded in 10% Pluronic F-68.

Notes: Cell membranes are stained green with DiOC6 and nucleus red with propidium iodide. Morphology of microparticles is visualized with passing through light. Scale bar 100 µm.

4.4.2 Proliferation and metabolic activity of the cells cultivated on the microsphere system

In order to examine the cell proliferation and metabolic activity of 3T3 fibroblasts on PCL microparticles, 21 - day cultivation testing was performed. Cells were directly seeded on PCL microspheres cryogrinded in mannitol and ungrinded PCL mesh was used as a control. Quantification of DNA concentration in samples was measured on days 1, 7,14 and 21 by PicoGreen® assay (Figure 37). Results showed similar cell adhesion on day 1 on microspheres and nanofibers. Interestingly cell proliferation on days 7 and 14 was higher on microspheres. This result could be caused by higher free surface of microparticles. On day 21 the number of cells on microspheres decreased due to metabolic deprivation. On other hand, the number of cells on nanofibers increased even on day 21.

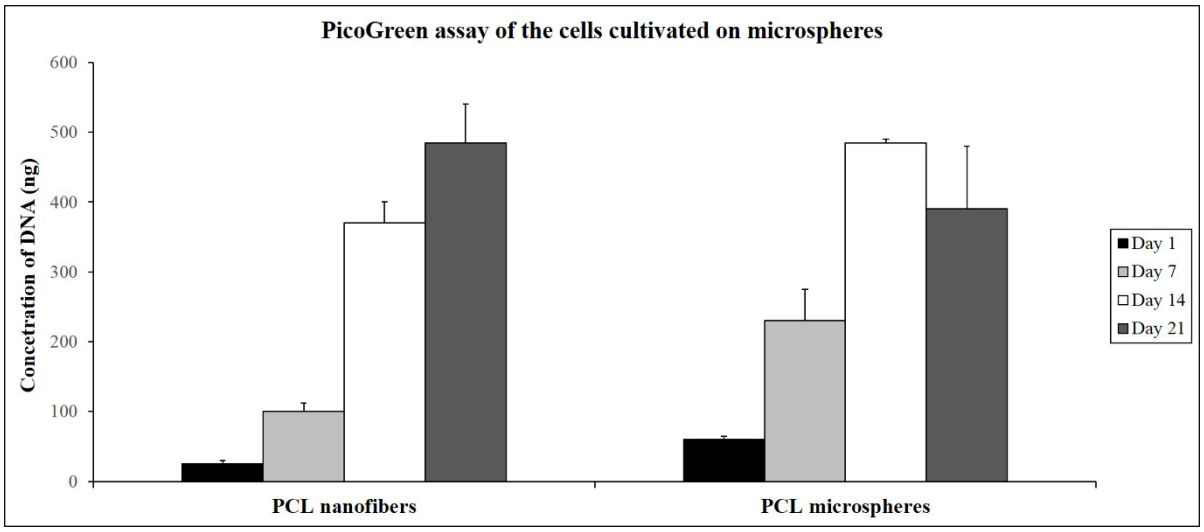

Figure 37. Proliferation of 3T3 fibroblast cultivated on either PCL nanofibers or PCL microspheres. Microspheres were cryogrinded in 10% mannitol.

Abbreviations: PCL, poly-ε-caprolactone; ng, nanograms.

Metabolic activity of cells was measured by MTS assay (Figure 38). Cells on microspheres showed higher activity on day 7 which is in agreement with results of PicoGreen® assay. Interestingly, metabolic activity on microspheres was lower compared to nanofibers on days 14 and 21. This result could be explained by higher shear stress on microspheres and depletion of nutrients.

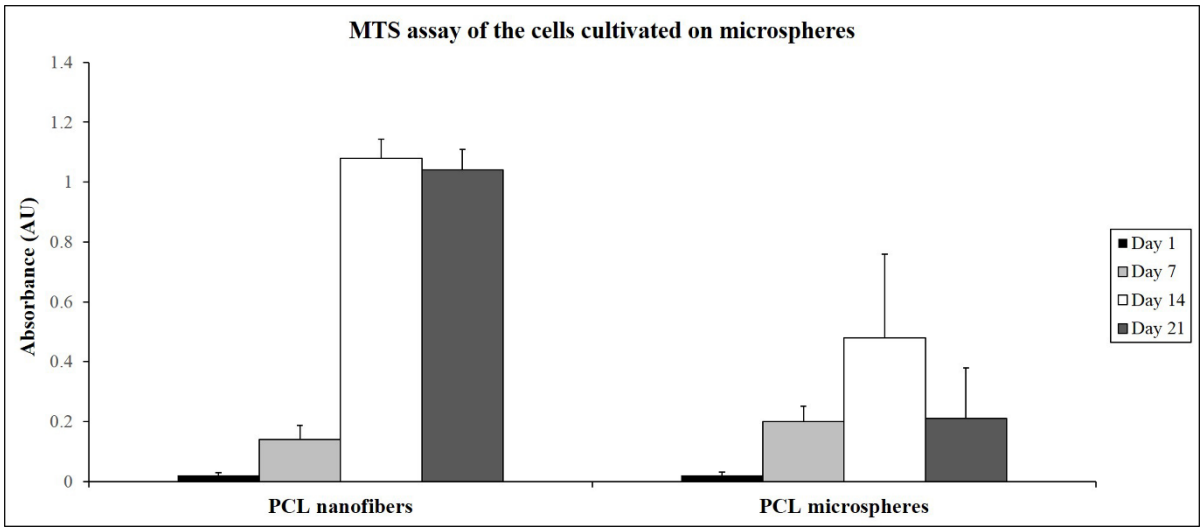

Figure 38. Metabolic activity of 3T3 fibroblast cultivated on either PCL nanofibers or PCL microspheres. Microspheres were cryogrinded in 10% mannitol.

Abbreviations: PCL, poly-ε-caprolactone; AU, absorbance units.

In general, porous microspheres produced by cryogenic grinding are suitable for the cultivation of cells. They could serve as a scaffolding system and even adherent cells could be cultured in suspensions. Proliferation rate and metabolic activity was higher on the first 7 cultivation days and peaked on day 14. This result could be explained by the higher shear stress on microspheres and depletion of nutrients. Interestingly, standard deviation of microsphere samples was higher due to the size diversity of the system. Thus microsphere–cell interaction should be further examined in future experiments after size separation.

5 Discussion

Incisional hernia is the most common postoperative complication following abdominal surgery, affecting up to 20% of patients after midline incision (Sugerman H.J. et al., 1996; Hoer J. et al., 2002). Insertion of a synthetic material has become the standard for care in abdominal wall hernia repair. More than a hundred surgical meshes have been developed by now, still there is no ideal mesh among those yet (Shankaran V. et al., 2011). The aim of the present study was to develop a composite functionalized nanofiber scaffold for preventing or repairing incisional hernias and *in vitro* testing of the new microsphere system with potential use as a drug delivery system in tissue engineering.

Polypropylene is the most widely-used prosthetic material for repairing abdominal wall hernia (Cobb W.S. et al., 2009). A combination of PCL nanofibers with a polypropylene surgical mesh (Prolene™) was chosen as a suitable material for our studies. Nowadays, PCL seems to be used more often as a biocompatible soft and hard tissue material, and it also includes a resorbable suture, a drug delivery system and bone graft substitutes, but only few studies have investigated PCL for abdominal wall hernia repairs (Kweon H. et al., 2003; Williams J.M. et al., 2005). Guillaume et al. used PCL as a coating agent and a drug reservoir for anti-infective drugs by heating deposition onto polypropylene prostheses (Guillaume O. et al., 2011). Another study using PCL in the form of nanofibers as a carrier for antibiotics was evaluated by Bolgen et al. (Bolgen N. et al., 2007). The antibiotic embedded PCL membranes eliminated post-surgery adhesions and improved healing in rats. In the most recent study, Zhao et al used an electrospun PCL/collagen hybrid scaffold for congenital diaphragmatic hernia reconstruction in rats. The aligned scaffolds allowed muscle cell migration and tissue formation (Zhao W. et al., 2013).

In general, nanofibers have recently been used in various tissue engineering applications (Ma Z. et al., 2005a). An advantage of using nanofibers for hernia regeneration lies in the simplicity of the process for preparing submicron-scale fibers, and their low cost. In addition, manufactured nanofibers can easily be modified and functionalized to refine their biological and biomechanical properties. Various studies have proved that nanofibers, namely PCL nanofibers, support the adhesion, growth and proliferation of fibroblasts, chondrocytes and MSCs (Jakubova R. et al., 2011; Chen M. et al., 2007; Rampichova M. et al., 2013).

In the first part of the present study, we have tested a new composite scaffold based on a PP surgical mesh, PCL nanofibers and adhered platelets. We have evaluated the effect of released natural GFs from platelets and the effect of PCL nanofiber functionalization on 3T3 fibroblast proliferation *in vitro*. In extensive tests, we have proved that PCL nanofibers have excellent biocompatible properties. We have confirmed that PCL nanofibers deposited on a PP mesh promote better adhesion, growth, metabolic activity, proliferation and viability of 3T3 fibroblasts in all tests than a PP mesh alone.

The second part of the study has proven the suitability of a composite scaffold based on PCL nanofibers deposited on a PP mesh for hernia regeneration in a rabbit model. A histological and biomechanical evaluation revealed better healing capacity of PCL nanofibers than of a conventional PP mesh for preventing hernia formation. PCL nanofibers as novel absorbable scaffolds for hernia repair application were biomechanically tested by Ebersole et al. (Ebersole G.C. et al., 2012). The authors have shown that electrospun PCL scaffolds retain suture material and possess tensile strength appropriate for hernia repair, and therefore have the potential to be a novel class of hernia repair materials. Our scaffold combined good biocompatible properties,

environment-promoting cell growth, adherence due to the PCL nanofibers, and tensile strength due to the PP mesh. This part of the study has confirmed that adhesion of various synthetic growth factors on the surface of our nanofibers increased their regenerative potential. GF such as bFGF, IGF-I and TGF-β2 may stimulate angiogenesis, fibroblast proliferation and collagen synthesis, thus enhancing tissue stability (Hant T.K. et al., 1984; Mustoe T.A. et al., 1987; Yaeger P.C. et al., 1997). Their concentration ratio and their positive effect on cultivated cells were evaluated in our group by Filova et al. (Filova E. et al., 2008).

The groups of Ebersole et al. and Deeken et al. measured the tensile strength and other biomechanical parameters of the prosthetic material used in ventral (incisional) hernia repair without implantation into animal models or human patients (Ebersole G.C. et al., 2012; Deeken C.R. et al., 2011). These studies showed that the tensile strength of PCL nanofibers was appropriate for most hernia repairs. Electrospun scaffolds possessing mechanical properties within the predefined range may be suitable for further evaluation in preclinical trials (Deeken C.R. et al., 2011). In another study, Melman et al biomechanically tested samples implanted into a porcine model (Melman N. et al., 2011). Samples were attached into the tension meter branches over the entire thickness of the abdominal wall including the prosthetic material. We suggest a new biomechanical testing method, where the results reflect the real state the repaired abdominal wall. In our design the attachment points were adjacent to the implanted mesh, so we tested not only the strength of the implant but also the properties of mesh-fascia interface and its resistance to distracting forces. We did not test the tensile strength of our samples alone, because the biomechanical parameters of PP meshes are well known (Melman N. et al., 2011). We modified this

prosthetic PP material with PCL nanofibers, thus it was not necessary to evaluate the biomechanical parameters before implantation.

Biomechanical testing 6 weeks post implantation in the rabbit model showed that the PCL nanofibers improved the biomechanical properties of the healed tissue, as evidenced by a higher average maximal strength force. This applies not only to the nanofibers in combination with a PP mesh, but also to the suture alone. The group treated with suture and PCL nanofibers with or without adhered synthetic GFs showed a modulus of elasticity comparable with that of the PP mesh, but higher average maximal strength force. This could reflect lower fibroblast proliferation around the PP mesh, which might be caused by a reduction in the mechanical signals that arise as the structural soft tissue fails (Franz M.G., 2006). In addition to these results, video analysis of the biomechanical testing of the samples from *in vivo* study on rabbits revealed in most cases that if the tissue tore first between the edge of the mesh and healthy tissue, the PP mesh slid off the surface of the muscle. In samples functionalized with PCL nanofibers, we observed two types of tear mechanism. Some were like in the PP mesh group, but in other samples the slide was localized between muscle fibers. When the PCL nanofibers were used, different types of tear were observed. In some samples, the suture line tore first, whereas in others a tear occurred between muscle fibers or at the edge of the muscle and the PCL nanofibers. This indicates that PCL nanofibers provide support for fusion of fascia without causing a significant increase in local stiffness, or the formation of a major tension concentrator, as in the case of a PP mesh. Finally, as we had expected, the suture line broke first if it was not supported by any mesh.

The third part of the present study proved the suitability of a nanofiber scaffold based on PCL nanofibers and PCL nanofibers with adhered platelets for hernia

regeneration in a minipig model. Both scaffold types were well and uniformly integrated within the collagenous connective tissue of the healing incision. In adition, the presence of both PCL nanofiber and PCL nanofiber + TRS scaffolds led to increased amount of contractile myofibroblasts within the healing incision. In PCL nanofiber scaffold, the microvessel density was positively correlated with the fraction of type I collagen. On the other hand, unfortunately, we did not observe any differences in any assessed parameters in the samples after 6 weeks of healing compared to samples after 12 weeks of healing. We also did not observe increase of any parameters with using PCL nanofibers functionalised with adhered platelets. Probably the concentration of the platelets in the TRS at the level of five times physiological concentration was not sufficient to cause any changes.

The quality of the ECM deposition is dependent among others on the content of collagen, which influenced the mechanical properties of the tissue and is notably influenced by the kind of mesh material (Junge K. et al., 2002). In the all examined samples either in rabbit study or in minipig study, there were no significant differences among the groups in the area fraction of total collagen. However, the analysis of the main tissue constituents, i.e., the collagen fraction, the adipose tissue fraction, and leukocyte infiltration suggested that the presence of either a simple suture or a PP mesh resulted in the formation of a scar with a greater adipose tissue fraction (Figure 31 and 32). Tissue samples with heavier granulomatous infiltration also contained more blood vessels and a higher fraction of vascular smooth muscle and myofibroblasts. This finding supports the hypothesis mentioned above that there is lower fibroblast proliferation (Franz M.G., 2006). Simple sutures contained a large amount of collagen. This supports the hypothesis of tissue flexibility, but these samples also contained a decreased amount of α-smooth muscle actin positive cells. There

were more actin positive cells in both the medial and the lateral parts of samples containing PCL nanofibers than in the other groups. In *in vivo* tests on rabbit model, the samples with a PP mesh functionalized with PCL nanofibers with adhered GFs included also more α-smooth muscle actin positive cells in a part distant from the incision. This could be explained by chemotaxis in this area. In both *in vivo* studies we have proven that nanofibers are a good substrate for cell attachment, and thus they promote cell proliferation and ECM synthesis.

Advanced improvement of our composite scaffolds seems to be promising for regenerating ventral or incisional hernias. We used a simple drug delivery system developed in our group, based on either platelets or synthetic GFs adhered onto PCL nanofibers (Jakubova R. et al., 2011). The approaches that have been used so far, in which simple GFs or platelets are administered, may tend to diffuse active substances away from the site of the injury (Tabata I.I., 2000). The problem of refusing of active substances can be solved by using suitable biocompatible scaffolds, to which the desired drugs could be attached. One of the first attempts to set up a dual drug delivery system based on polymeric scaffolds was reported by Richardson et al (Richardson T.P. et al., 2001). Better control of either drug or GF pharmacokinetics could be achieved by using a combination of active substances with natural or synthetic biomaterials, such as collagen or PCL composite scaffolds (Rai B. et al., 2005). Previous studies have mentioned various drug delivery systems based on a PCL composite scaffold successfully used for hernia regeneration (Guillaume O. et al., 2011; Bolgen N. et al., 2007).

In the last part of our study we demonstrated that the PCL microspheres prepared by cryogrinding is a promising system potentially exploitable as a drug delivery system in tissue engineering. In general, porous PCL microspheres produced by cryogenic

grinding are suitable for cell cultivation. We have proved it by using metabolic activity, adhesion and proliferation assay.

PCL nanofibers were used in all parts of our study as a carrier or a potential carrier of GFs gradually released either from platelets adhered on the nanofiber surface or directly from nanofibers, with the aim of using the material in hernia regeneration. The use of this system enabled us to avoid the complications caused by a burst release of high doses of GFs. In addition, the GFs are prevented from proteolysis and loss in bioactivity both by the scaffold and by the platelets themselves (Babensee J.E. et al., 2000). This enables a prolonged therapeutic effect of GFs. GFs naturally occurring in platelets have been shown to be effective in promoting wound healing and regeneration (Nauta A. et al., 2011). Platelets in the form of TRS or PRP have been playing a rapidly growing role in tissue engineering (Tonti G.A. et al, 2008.). The positive effect of PRP on fibroblast proliferation has already been described by Anitua et al, Creeper et al and Passaretti et al. (Anitua E. et al., 2009; Creeper F. and Ivanovski S., 2012; Passaretti F. et al., 2014). Unfortunately these teams did not use a polymeric scaffold, so it was not possible to observe the benefits from the multiplication of the positive effect on the fibroblasts from both the polymer scaffold and the PRP. Platelets were shown to release numerous growth factors with mitogenic and anabolic function (e.g. PDGF, EGF, TGF-β; Plachokova A.S. et al., 2008; Nikolidakis D. and Jansen J.A. 2012). Our observation of increased proliferation, metabolic activity and DNA synthesis of the 3T3 fibroblasts in TRS containing samples groups in the present study is explained by stimulatory effect of such active molecules. In addition platelets upon activation form protein layer consist of fibrinogen, von Willebrand factor (VWF) and other proteins (Blair P. and Flaumenhaft R., 2009), which together with the PCL nanofibers mimicking ECM has a possible stimulatory effect on

cell adhesion. Moreover, we used in our study TRS which does not include leukocytes and erythrocytes in comparison to PRP obtained from whole blood. Prosecka et al showed that even human TRS promote tissue regeneration in rabbit model with a minimal immunological negative response (Prosecka E. et al., 2014). That kind of results favour TRS for further preclinical and clinical studies.

6 Conclusion

In the present study, we have confirmed the biocompatibility of PCL nanofibers with adhered platelets in the form of TRS deposited on a PP mesh. This composite scaffold provided better adhesion, growth, metabolic activity, proliferation and viability of 3T3 fibroblasts in all tests than on a PP mesh alone, and even better than on a PP mesh functionalised by PCL nanofibers. The gradual release of growth factors from biocompatible scaffolds is a promising approach in tissue engineering and regenerative medicine.

Our experiments have also proved that the composite scaffolds based on polypropylene surgical mesh functionalized with PCL nanofibers and adhered synthetic growth factors positively affected the fascia healing in a rabbit model. Thanks to their nanofiber structure, PCL nanofibers provide a better environment for cell growth and proliferation, either in combination with a PP mesh or alone, and are therefore are a suitable alternative to a standard hernia mesh. Surprisingly, scaffolds with no PP mesh showed even better fascia healing and higher elasticity than a widely-used surgical mesh. PCL nanofiber scaffolds are promising materials for use in hernia repair. By adhering GF into their structure we can further improve several parameters, especially in the quantity of collagen that is produced compared to the adipose tissue content.

In vivo tests on minipig model have proved, that the composite scaffolds based on either PCL nanofibers or PCL nanofibers functionalised with adhered human platelets obtained from TRS improved tissue healing. Scaffolds well integrated into the collagenous connective tissue of the healing incision and using of them led to increased amount of contractile myofibroblast at the site of incision.

The last system tested in the present study has proven its potential use as a drug delivery system in tissue engineering. The microsphere system based on cryogrinded PCL nanofibers has supported cell adhesion and proliferation. In the future a big potential of this system lies in the possibility of replacement of simple PCL nanofibers with either coaxial nanofibers with PCL as a shell part or with PCL nanofibers prepared by emulsion electrospinning with using active substances incorporation. Cryogrinded microspheres are a suitable and promising scaffolding system for use in tissue engineering and regenerative medicine.

7 Summary

Incisional hernia is the most common postoperative complication which affects up to 20% of patients after abdominal surgery. Insertion of a synthetic surgical mesh has become the standard for care in abdominal wall hernia repair. However, implementation of a mesh does not reduce the risk of recurrence and the onset of hernia recurrence is only delayed by 2-3 years. Nowadays, more than one hundred surgical meshes are available on the market from which the polypropylene is most widely used for abdominal wall hernia repair. Nonetheless, the ideal mesh does not exist yet - it still needs to be developed. The aim of the present study was to develop a functionalized scaffold for abdominal wall hernia regeneration and *in vitro* testing of the new microsphere system with potential use as a drug delivery system in tissue engineering. We prepared novel composite scaffolds based on a polypropylene surgical mesh functionalized with polycaprolactone nanofibers and adhered either platelet as a natural source of growth factors or a synthetic growth factor. In extensive in vitro tests, we have proven the biocompatibility of polycaprolactone nanofibers with adhered platelets on a polypropylene mesh. A histological and biomechanical evaluation from *in vivo* tests revealed better healing capacity of our composite functionalized scaffolds in comparison with either a conventional polypropylene surgical mesh or a simple suture for preventing hernia formation. The microsphere system based on cryogrinded PCL nanofibers has proven its potential to be used as a drug delivery system in biomedical application. The gradual release of growth factors from biocompatible nanofiber-modified scaffolds seems to be a promising approach in tissue engineering and regenerative medicine.

8 Abstrakt

Incizionální kýla postihuje víc než 20% pacientů, kteří podstoupili operaci břicha. Implantace syntetických materiálů se stala standardem v reparaci kýl břišní stěny. Nicméně implantace kýlních sítěk nezaručuje trvalé zhojení, jen oddaluje riziko recidivy vzniku kýly o 2-3 roky. V současnosti je na trhu dostupná víc jak stovka chirurgických sítěk. Nejčastěji používané síťky pro reparaci ventrální kýly jsou vyrobené z polypropylénu. Ideální síťka dodnes neexistuje a je tudíž zapotřebí ji vyvinout. Cílem této studie bylo vyvinout funkcionalizovaný nosič pro reparaci kýl břišní stěny. Připravili jsme nový kompozitní nosič na bázi polypropylénové chirurgické síťky funkcionalizovaný pomocí poly-ε-kaprolaktonových nanovláken připravených elektrostatickým zvlákňováním. Na nanovlákna byly adherovány buď trombocyty, jako přirozený zdroj růstových faktorů, nebo syntetické růstové faktory. V rozsáhlých *in vitro* testech jsme jednoznačně prokázali biokompatibilitu tohoto nového systému. Histologické a biomechanické hodnocení v *in vivo* testech na modelu králíka a miniprasete odhalilo lepší regenerační schopnost našeho kompozitního funkcionalizovaného nosiče ve srovnání s konvenčně používanou polypropylénovou chirurgickou síti a samotnou suturou. Dále byl testován systém mikročástic vyrobený pomocí kryomletí poly-ε-kaprolaktonových nanovláken sloužící jako systém dodávání léčiv v biomedicínských aplikacích. Postupné uvolňování růstových faktorů z biokompatibilních nanovlákenných nosičů, se jeví jako slibný přistup v tkáňovém inženýrství a regenerativní medicíně.

9 References

1. Abaza R, Perring P, Sferra JJ. Novel parastomal hernia repair using a modified polypropylene and PTFE mesh. *J Am Coll Surg.* Aug 2005;201(2):316-317.

2. Adler RH, Firme CN. The use of nylon prostheses for diaphragmatic defects. *Surgery, gynecology & obstetrics.* Jun 1957;104(6):669-674.

3. Agarwal S, Greiner A. On the way to clean and safe electrospinning-green electrospinning: emulsion and suspension electrospinning. *Polymers for Advanced Technologies.* Mar 2011;22(3):372-378.

4. Agarwal S, Wendorff JH, Greiner A. Use of electrospinning technique for biomedical applications. *Polymer.* Dec 8 2008;49(26):5603-5621.

5. Amid PK, Shulman AG, Lichtenstein IL, Hakakha M. [Biomaterials and hernia surgery. Rationale for using them]. *Rev Esp Enferm Dig.* Aug 1995;87(8):582-586.

6. Anitua E. Plasma rich in growth factors: preliminary results of use in the preparation of future sites for implants. *Int J Oral Maxillofac Implants.* Jul-Aug 1999;14(4):529-535.

7. Anitua E, Andia I, Sanchez M, et al. Autologous preparations rich in growth factors promote proliferation and induce VEGF and HGF production by human tendon cells in culture. *Journal of Orthopaedic Research.* Mar 2005;23(2):281-286.

8. Anitua E, Sanchez M, Orive G, Andia I. The potential impact of the preparation rich in growth factors (PRGF) in different medical fields. *Biomaterials.* Nov 2007;28(31):4551-4560.

9. Anitua E, Sanchez M, Zalduendo MM, et al. Fibroblastic response to treatment with different preparations rich in growth factors. *Cell Prolif.* Apr 2009;42(2):162-170.

10. Antoniou GA, Georgiadis GS, Antoniou SA, Granderath FA, Giannoukas AD, Lazarides MK. Abdominal aortic aneurysm and abdominal wall hernia as manifestations of a connective tissue disorder. *Journal of vascular surgery.* Oct 2011;54(4):1175-1181.

11. Aquaviva D, Bounet P. [Cure d'une volumineuse eventration par plaque de Crinofil]. *Extraits Bull Soc Chir De Marseille.* 1944;17.

12. Ather S, Harding KG. Wound management and dressings. In: Rajendran S, ed. *Advanced Textiles for Wound Care*. 1 ed. Cambridge: Woodhead Publishing Limited and CRC Press LLC; 2009: Chapter 1, p. 3-19.

13. Babensee JE, McIntire LV, Mikos AG. Growth factor delivery for tissue engineering. *Pharmaceutical research.* May 2000;17(5):497-504.

14. Bachman S, Ramshaw B. Prosthetic material in ventral hernia repair: how do I choose? *Surg Clin North Am.* Feb 2008;88(1):101-112, ix.

15. Baenziger NL, Brodie GN, Majerus PW. A thrombin-sensitive protein of human platelet membranes. *Proceedings of the National Academy of Sciences of the United States of America.* Jan 1971;68(1):240-243.

16. Ballem N, Parikh R, Berber E, Siperstein A. Laparoscopic versus open ventral hernia repairs: 5 year recurrence rates. *Surgical endoscopy.* Sep 2008;22(9):1935-1940.

17. Barrientos S, Stojadinovic O, Golinko MS, Brem H, Tomic-Canic M. Growth factors and cytokines in wound healing. *Wound repair and regeneration : official*

publication of the Wound Healing Society [and] the European Tissue Repair Society. Sep-Oct 2008;16(5):585-601.
18. Bay-Nielsen M. Complications of Hernia in General. In: Kingsnorth A, LeBlanc KA, eds. *Management of Abdominal Hernias*. 1 ed. London: Management of Abdominal Hernias; 2013: p. 171-184.
19. Bellon JM, Contreras LA, Bujan J, et al. A new type of polytetrafluoroethylene prosthesis (Mycro Mesh): An experimental study. *Journal of Materials Science-Materials in Medicine.* Aug 1996;7(8):475-478.
20. Bendavid R, Abrahamson J, Arregui ME, Flament JB, Phillips EH. *Abdominal Wall Hernias.* 1 ed. New York: Springer Science+Buisness Media New York 2001: p. 792.
21. Bhardwaj N, Kundu SC. Electrospinning: A fascinating fiber fabrication technique. *Biotechnol Adv.* May-Jun 2010;28(3):325-347.
22. Binnebosel M, Klink CD, Otto J, et al. Impact of mesh positioning on foreign body reaction and collagenous ingrowth in a rabbit model of open incisional hernia repair. *Hernia : the journal of hernias and abdominal wall surgery.* Feb 2010;14(1):71-77.
23. Birk DE, Mayne R. Localization of collagen types I, III and V during tendon development. Changes in collagen types I and III are correlated with changes in fibril diameter. *Eur J Cell Biol.* Apr 1997;72(4):352-361.
24. Bittner R, Bingener-Casey J, Dietz U, et al. Guidelines for laparoscopic treatment of ventral and incisional abdominal wall hernias (International Endohernia Society (IEHS)-part 1. *Surgical endoscopy.* Jan 2014;28(1):2-29.
25. Blair P, Flaumenhaft R. Platelet alpha-granules: basic biology and clinical correlates. *Blood reviews.* Jul 2009;23(4):177-189.
26. Blatnik J, Jin J, Rosen M. Abdominal hernia repair with bridging acellular dermal matrix--an expensive hernia sac. *American journal of surgery.* Jul 2008;196(1):47-50.
27. Blokhuis TJ. Formulations and delivery vehicles for bone morphogenetic proteins: latest advances and future directions. *Injury-International Journal of the Care of the Injured.* Dec 2009;40:8-11.
28. Bolgen N, Vargel I, Korkusuz P, Menceloglu YZ, Piskin E. In vivo performance of antibiotic embedded electrospun PCL membranes for prevention of abdominal adhesions. *Journal of biomedical materials research. Part B, Applied biomaterials.* May 2007;81(2):530-543.
29. Bothra R. Late onset small bowel fistula due to tantalum mesh. *American journal of surgery.* May 1973;125(5):649-650.
30. Brem H, Tomic-Canic M. Cellular and molecular basis of wound healing in diabetes. *The Journal of clinical investigation.* May 2007;117(5):1219-1222.
31. Burger JW, Halm JA, Wijsmuller AR, ten Raa S, Jeekel J. Evaluation of new prosthetic meshes for ventral hernia repair. *Surgical endoscopy.* Aug 2006;20(8):1320-1325.
32. Burger JW, Luijendijk RW, Hop WC, Halm JA, Verdaasdonk EG, Jeekel J. Long-term follow-up of a randomized controlled trial of suture versus mesh repair of incisional hernia. *Ann Surg.* Oct 2004;240(4):578-583; discussion 583-575.
33. Burke GL. THE CORROSION OF METALS IN TISSUES; AND AN INTRODUCTION TO TANTALUM. In: Bendavid R, Abrahamson J, Arregui ME, Flament JB, Phillips EH, eds. *Abdominal Wall Hernias*. 1 ed. New York: Springer Science+Buisness Media New York; 2001: p. 792.

34. Butler CE, Prieto VG. Reduction of adhesions with composite AlloDerm/polypropylene mesh implants for abdominal wall reconstruction. *Plast Reconstr Surg.* Aug 2004;114(2):464-473.
35. Buzgo M, Jakubova R, Mickova A, et al. Time-regulated drug delivery system based on coaxially incorporated platelet alpha-granules for biomedical use. *Nanomedicine (London, England).* Jul 2013;8(7):1137-1154.
36. Canbolat MF, Celebioglu A, Uyar T. Drug delivery system based on cyclodextrin-naproxen inclusion complex incorporated in electrospun polycaprolactone nanofibers. *Colloids and Surfaces B-Biointerfaces.* Mar 2014;115:15-21.
37. Carbajo MA, Martin del Olmo JC, Blanco JI, et al. Laparoscopic treatment vs open surgery in the solution of major incisional and abdominal wall hernias with mesh. *Surgical endoscopy.* Mar 1999;13(3):250-252.
38. Carlisle CR, Coulais C, Namboothiry M, Carroll DL, Hantgan RR, Guthold M. The mechanical properties of individual, electrospun fibrinogen fibers. *Biomaterials.* Feb 2009;30(6):1205-1213.
39. Chen M, Patra PK, Warner SB, Bhowmick S. Role of fiber diameter in adhesion and proliferation of NIH 3T3 fibroblast on electrospun polycaprolactone scaffolds. *Tissue Eng.* Mar 2007;13(3):579-587.
40. Chevrel JP, Rath AM. Classification of incisional hernias of the abdominal wall *Hernia : the journal of hernias and abdominal wall surgery.* Jan 2000;4:7-11.
41. Chuangchote S, Supaphol P. Fabrication of aligned poly (vinyl alcohol) nanofibers by electrospinning. *Journal of nanoscience and nanotechnology.* Jan 2006;6(1):125-129.
42. Cipitria A, Skelton A, Dargaville TR, Dalton PD, Hutmacher DW. Design, fabrication and characterization of PCL electrospun scaffolds-a review. *Journal of Materials Chemistry.* Mar 2011;21(26):9419-9453.
43. Clausen C, Hermund NU, Donatsky O, Nielsen H, Osther K. Homologous activated platelets stimulate differentiation and proliferation of primary human bone cells. *Cells, tissues, organs.* Oct 2006;184(2):68-75.
44. Cobb WS, Kercher KW, Heniford BT. The argument for lightweight polypropylene mesh in hernia repair. *Surgical innovation.* Mar 2005;12(1):63-69.
45. Cobb WS, Peindl RM, Zerey M, Carbonell AM, Heniford BT. Mesh terminology 101. *Hernia : the journal of hernias and abdominal wall surgery.* Feb 2009;13(1):1-6.
46. Coda A, Lamberti R, Martorana S. Classification of prosthetics used in hernia repair based on weight and biomaterial. *Hernia : the journal of hernias and abdominal wall surgery.* Feb 2012;16(1):9-20.
47. Conze J, Klinge U, Schumpelick V. [Incisional hernia]. *Der Chirurg; Zeitschrift fur alle Gebiete der operativen Medizen.* Sep 2005;76(9):897-909; quiz 910.
48. Costello CR, Bachman SL, Ramshaw BJ, Grant SA. Materials characterization of explanted polypropylene hernia meshes. *Journal of biomedical materials research. Part B, Applied biomaterials.* Oct 2007;83(1):44-49.
49. Cozad MJ, Grant DA, Bachman SL, Grant DN, Ramshaw BJ, Grant SA. Materials characterization of explanted polypropylene, polyethylene terephthalate, and expanded polytetrafluoroethylene composites: spectral and thermal analysis. *Journal of biomedical materials research. Part B, Applied biomaterials.* Aug 2010;94(2):455-462.
50. Creeper F, Ivanovski S. Effect of autologous and allogenic platelet-rich plasma on human gingival fibroblast function. *Oral Diseases.* Jul 2012;18(5):494-500.

51. Cui WG, Zhou Y, Chang J. Electrospun nanofibrous materials for tissue engineering and drug delivery. *Science and Technology of Advanced Materials.* Feb 2010;11(1).
52. Dave R, Jayaraj P, Ajikumar PK, Joshi H, Mathews T, Venugopalan VP. Endogenously triggered electrospun fibres for tailored and controlled antibiotic release. *Journal of Biomaterials Science-Polymer Edition.* Aug 2013;24(11):1305-1319.
53. Deeken CR, Abdo MS, Frisella MM, Matthews BD. Physicomechanical evaluation of polypropylene, polyester, and polytetrafluoroethylene meshes for inguinal hernia repair. *J Am Coll Surg.* Jan 2011;212(1):68-79.
54. Deitzel JM, Kleinmeyer J, Harris D, Tan NCB. The effect of processing variables on the morphology of electrospun nanofibers and textiles. *Polymer.* Jan 2001;42(1):261-272.
55. den Hartog D, Dur AH, Tuinebreijer WE, Kreis RW. Open surgical procedures for incisional hernias. *The Cochrane database of systematic reviews.* Jul 2008(3):CD006438.
56. Di Cera E. Thrombin. *Molecular Aspects of Medicine.* Aug 2008;29(4):203-254.
57. Doshi J, Reneker DH. ELECTROSPINNING PROCESS AND APPLICATIONS OF ELECTROSPUN FIBERS. *Journal of Electrostatics.* Aug 1995;35(2-3):151-160.
58. Dosunmu OO, Chase GG, Kataphinan W, Reneker DH. Electrospinning of polymer nanofibres from multiple jets on a porous tubular surface. *Nanotechnology.* Feb 28 2006;17(4):1123-1127.
59. Drengk A, Zapf A, Sturmer EK, Sturmer KM, Frosch KH. Influence of platelet-rich plasma on chondrogenic differentiation and proliferation of chondrocytes and mesenchymal stem cells. *Cells, tissues, organs.* Aug 2009;189(5):317-326.
60. Dror Y, Kuhn J, Avrahami R, Zussman E. Encapsulation of enzymes in biodegradable tubular structures. *Macromolecules.* Jun 2008;41(12):4187-4192.
61. Ebersole GC, Buettmann EG, MacEwan MR, et al. Development of novel electrospun absorbable polycaprolactone (PCL) scaffolds for hernia repair applications. *Surgical endoscopy.* Oct 2012;26(10):2717-2728.
62. Ehrenfest DMD, Rasmusson L, Albrektsson T. Classification of platelet concentrates: from pure platelet-rich plasma (P-PRP) to leucocyte- and platelet-rich fibrin (L-PRF). *Trends in Biotechnology.* Mar 2009;27(3):158-167.
63. Ekberg O, Kesek P. Herniographic appearance of the lateral inguinal fossa. *Acta radiologica (Stockholm, Sweden : 1987).* Sep-Oct 1987;28(5):563-569.
64. Etherington RJ, Williams JG, Hayward MW, Hughes LE. Demonstration of para-ileostomy herniation using computed tomography. *Clinical radiology.* May 1990;41(5):333-336.
65. Filova E, Jelinek F, Handl M, et al. Novel composite hyaluronan/type I collagen/fibrin scaffold enhances repair of osteochondral defect in rabbit knee. *Journal of biomedical materials research. Part B, Applied biomaterials.* Nov 2008;87(2):415-424.
66. Filova E, Rampichova M, Litvinec A, et al. A cell-free nanofiber composite scaffold regenerated osteochondral defects in miniature pigs. *Int J Pharm.* Apr 15 2013;447(1-2):139-149.
67. Fisch AE, Brodey PA. Computed tomography of the anterior abdominal wall: normal anatomy and pathology. *Journal of computer assisted tomography.* Oct 1981;5(5):728-733.

68. Flaumenhaft R. Molecular basis of platelet granule secretion. *Arteriosclerosis Thrombosis and Vascular Biology.* Jul 2003;23(7):1152-1160.
69. Flum DR, Horvath K, Koepsell T. Have outcomes of incisional hernia repair improved with time? A population-based analysis. *Ann Surg.* Jan 2003;237(1):129-135.
70. Franz MG. The biology of hernias and the abdominal wall. *Hernia : the journal of hernias and abdominal wall surgery.* Dec 2006;10(6):462-471.
71. Friesel RE, Maciag T. Molecular mechanisms of angiogenesis: fibroblast growth factor signal transduction. *FASEB journal : official publication of the Federation of American Societies for Experimental Biology.* Jul 1995;9(10):919-925.
72. Gaertner WB, Bonsack ME, Delaney JP. Experimental evaluation of four biologic prostheses for ventral hernia repair. *Journal of gastrointestinal surgery : official journal of the Society for Surgery of the Alimentary Tract.* Oct 2007;11(10):1275-1285.
73. Gilbert TW, Freund JM, Badylak SF. Quantification of DNA in biologic scaffold materials. *The Journal of surgical research.* Mar 2009;152(1):135-139.
74. Gleissner CA, von Hundelshausen P, Ley K. Platelet chemokines in vascular disease. *Arteriosclerosis, thrombosis, and vascular biology.* Nov 2008;28(11):1920-1927.
75. Goepel R. Ueber die verschliessung von bruchpforten durch ein heilung geflochtener, fertiger silberdrahtnetze (silberdrahtpelotten). *Verh Dsch Ges Chir.* 1900;29:174-177.
76. Gonzalez R, Fugate K, McClusky D, 3rd, et al. Relationship between tissue ingrowth and mesh contraction. *World J Surg.* Aug 2005;29(8):1038-1043.
77. Gore RW, Inventor; W. L. Gore & Associates, Inc., assignee. Process for producing porous products. US patent US3953566A. Apr 1976.
78. Goutallier D, Postel JM, Gleyze P, Leguilloux P, Van Driessche S. Influence of cuff muscle fatty degeneration on anatomic and functional outcomes after simple suture of full-thickness tears. *Journal of shoulder and elbow surgery / American Shoulder and Elbow Surgeons ... [et al.].* Nov-Dec 2003;12(6):550-554.
79. Grafahrend D, Heffels KH, Beer MV, et al. Degradable polyester scaffolds with controlled surface chemistry combining minimal protein adsorption with specific bioactivation. *Nature Materials.* Jan 2011;10(1):67-73.
80. Graziani F, Ivanovski S, Cei S, Ducci F, Tonetti M, Gabriele M. The in vitro effect of different PRP concentrations on osteoblasts and fibroblasts. *Clinical oral implants research.* Apr 2006;17(2):212-219.
81. Guillaume O, Lavigne JP, Lefranc O, Nottelet B, Coudane J, Garric X. New antibiotic-eluting mesh used for soft tissue reinforcement. *Acta Biomater.* Sep 2011;7(9):3390-3397.
82. Gundersen HJ. Estimators of the number of objects per area unbiased by edge effects. *Microsc Acta.* Nov 1978;81(2):107-117.
83. Haghi AK, Akbari M. Trends in electrospinning of natural nanofibers. *Physica Status Solidi a-Applications and Materials Science.* Jun 2007;204(6):1830-1834.
84. Handley WS. A method for the radical cure of inguinal hernia (darn and stay-lace method). *The Practitioner.* 1918;100:466-471.
85. Harrison LA, Keesling CA, Martin NL, Lee KR, Wetzel LH. Abdominal wall hernias: review of herniography and correlation with cross-sectional imaging. *Radiographics : a review publication of the Radiological Society of North America, Inc.* Mar 1995;15(2):315-332.

86. Heldin CH, Westermark B. Platelet-derived growth factor: mechanism of action and possible in vivo function. *Cell regulation.* Jul 1990;1(8):555-566.
87. Heniford BT, Park A, Ramshaw BJ, Voeller G. Laparoscopic repair of ventral hernias: nine years' experience with 850 consecutive hernias. *Ann Surg.* Sep 2003;238(3):391-399; discussion 399-400.
88. Hers I. Insulin-like growth factor-1 potentiates platelet activation via the IRS/PI3K alpha pathway. *Blood.* Dec 2007;110(13):4243-4252.
89. Hiles M, Record Ritchie RD, Altizer AM. Are biologic grafts effective for hernia repair?: a systematic review of the literature. *Surgical innovation.* Mar 2009;16(1):26-37.
90. Hiller N, Alberton Y, Shapira Y, Hadas-Halpern I. Richter's hernia strangulated in a spigelian hernia: ultrasonic diagnosis. *Journal of clinical ultrasound : JCU.* Oct 1994;22(8):503-505.
91. Hoer J, Lawong G, Klinge U, Schumpelick V. [Factors influencing the development of incisional hernia. A retrospective study of 2,983 laparotomy patients over a period of 10 years]. *Der Chirurg; Zeitschrift fur alle Gebiete der operativen Medizen.* May 2002;73(5):474-480.
92. Hokugo A, Ozeki M, Kawakami O, et al. Augmented bone regeneration activity of platelet-rich plasma by biodegradable gelatin hydrogel. *Tissue Eng.* Jul-Aug 2005;11(7-8):1224-1233.
93. Hromadka M, Collins JB, Reed C, et al. Nanofiber applications for burn care. *Journal of burn care & research : official publication of the American Burn Association.* Sep-Oct 2008;29(5):695-703.
94. Hunt TK, Knighton DR, Thakral KK, Goodson WH, 3rd, Andrews WS. Studies on inflammation and wound healing: angiogenesis and collagen synthesis stimulated in vivo by resident and activated wound macrophages. *Surgery.* Jul 1984;96(1):48-54.
95. Hutmacher DW, Schantz T, Zein I, Ng KW, Teoh SH, Tan KC. Mechanical properties and cell cultural response of polycaprolactone scaffolds designed and fabricated via fused deposition modeling. *Journal of biomedical materials research.* May 2001;55(2):203-216.
96. Ianora AA, Midiri M, Vinci R, Rotondo A, Angelelli G. Abdominal wall hernias: imaging with spiral CT. *European radiology.* Aug 2000;10(6):914-919.
97. Italiano JE, Richardson JL, Patel-Hett S, et al. Angiogenesis is regulated by a novel mechanism: pro- and antiangiogenic proteins are organized into separate platelet alpha granules and differentially released. *Blood.* Feb 2008;111(3):1227-1233.
98. Jacob BP, Hogle NJ, Durak E, Kim T, Fowler DL. Tissue ingrowth and bowel adhesion formation in an animal comparative study: polypropylene versus Proceed versus Parietex Composite. *Surgical endoscopy.* Apr 2007;21(4):629-633.
99. Jacob BP, Ramshaw B. *The SAGES Manual of Hernia Repair.* New York: Springer Science+Buisness Media New York 2013: p. 610.
100. Jakubova R, Mickova A, Buzgo M, et al. Immobilization of thrombocytes on PCL nanofibres enhances chondrocyte proliferation in vitro. *Cell Proliferation.* 2011;44(2):183-191.
101. Jarman-Smith ML, Bodamyali T, Stevens C, Howell JA, Horrocks M, Chaudhuri JB. Porcine collagen crosslinking, degradation and its capability for fibroblast adhesion and proliferation. *J Mater Sci Mater Med.* Aug 2004;15(8):925-932.

102. Jayakumar R, Prabaharan M, Nair SV, Tamura H. Novel chitin and chitosan nanofibers in biomedical applications. *Biotechnol Adv.* Jan-Feb 2010;28(1):142-150.
103. Jefferson NC, Dailey UG. Incisional hernia repaired with tanatalum gauze; preliminary report. *American journal of surgery.* Apr 1948;75(4):575-579.
104. Jezupovs A, Mihelsons M. The analysis of infection after polypropylene mesh repair of abdominal wall hernia. *World J Surg.* Dec 2006;30(12):2270-2278; discussion 2279-2280.
105. Ji W, Yang F, van den Beucken J, et al. Fibrous scaffolds loaded with protein prepared by blend or coaxial electrospinning. *Acta Biomater.* Nov 2010;6(11):4199-4207.
106. Jiang HL, Hu YQ, Zhao PC, Li Y, Zhu KJ. Modulation of protein release from biodegradable core-shell structured fibers prepared by coaxial electrospinning. *Journal of Biomedical Materials Research Part B-Applied Biomaterials.* Oct 2006;79B(1):50-57.
107. Jirsak O, Hanuš J, Kotek V, Sanetrnik F, Krčma R, Inventors. Device for perpendicular stratification of planary fibrous shapes. US patent 6,983,515. 2006.
108. Judge TW, Parker DM, Dinsmore RC. Abdominal wall hernia repair: a comparison of sepramesh and parietex composite mesh in a rabbit hernia model. *J Am Coll Surg.* Feb 2007;204(2):276-281.
109. Junge K, Klinge U, Klosterhalfen B, et al. Influence of mesh materials on collagen deposition in a rat model. *J Invest Surg.* Nov-Dec 2002;15(6):319-328.
110. Junqueira LC, Bignolas G, Brentani RR. Picrosirius staining plus polarization microscopy, a specific method for collagen detection in tissue sections. *The Histochemical journal.* Jul 1979;11(4):447-455.
111. Khil MS, Bhattarai SR, Kim HY, Kim SZ, Lee KH. Novel fabricated matrix via electrospinning for tissue engineering. *Journal of Biomedical Materials Research Part B-Applied Biomaterials.* Jan 2005;72B(1):117-124.
112. Khil MS, Cha DI, Kim HY, Kim IS, Bhattarai N. Electrospun nanofibrous polyurethane membrane as wound dressing. *Journal of Biomedical Materials Research Part B-Applied Biomaterials.* Nov 2003;67B(2):675-679.
113. Kim GH. Electrospun PCL nanofibers with anisotropic mechanical properties as a biomedical scaffold. *Biomedical materials (Bristol, England).* Jun 2008;3(2):025010.
114. Kim SH, Turnbull J, Guimond S. Extracellular matrix and cell signalling: the dynamic cooperation of integrin, proteoglycan and growth factor receptor. *J Endocrinol.* May 2011;209(2):139-151.
115. Kim TG, Park TG. Surface functionalized electrospun biodegradable nanofibers for immobilization of bioactive molecules. *Biotechnol Prog.* Jul-Aug 2006;22(4):1108-1113.
116. King SM, Reed GL. Development of platelet secretory granules. *Seminars in Cell & Developmental Biology.* Aug 2002;13(4):293-302.
117. Klinge U. Mesh for hernia repair. *Br J Surg.* May 2008;95(5):539-540.
118. Klinge U, Conze J, Limberg W, Brucker C, Ottinger AP, Schumpelick V. [Pathophysiology of the abdominal wall]. *Der Chirurg; Zeitschrift fur alle Gebiete der operativen Medizen.* Mar 1996;67(3):229-233.
119. Klinge U, Klosterhalfen B. Modified classification of surgical meshes for hernia repair based on the analyses of 1,000 explanted meshes. *Hernia : the journal of hernias and abdominal wall surgery.* Jun 2012;16(3):251-258.

120. Klinge U, Klosterhalfen B, Conze J, et al. Modified mesh for hernia repair that is adapted to the physiology of the abdominal wall. *The European journal of surgery = Acta chirurgica.* Dec 1998b;164(12):951-960.
121. Klinge U, Klosterhalfen B, Muller M, Ottinger AP, Schumpelick V. Shrinking of polypropylene mesh in vivo: an experimental study in dogs. *The European journal of surgery = Acta chirurgica.* Dec 1998a;164(12):965-969.
122. Klinge U, Klosterhalfen B, Muller M, Schumpelick V. Foreign body reaction to meshes used for the repair of abdominal wall hernias. *The European journal of surgery = Acta chirurgica.* Jul 1999;165(7):665-673.
123. Klosterhalfen B, Junge K, Klinge U. The lightweight and large porous mesh concept for hernia repair. *Expert review of medical devices.* Jan 2005;2(1):103-117.
124. Klosterhalfen B, Klinge U. Retrieval study at 623 human mesh explants made of polypropylene - impact of mesh class and indication for mesh removal on tissue reaction. *Journal of biomedical materials research. Part B, Applied biomaterials.* Nov 2013;101(8):1393-1399.
125. Knotek P, Pouzar M, Buzgo M, et al. Cryogenic grinding of electrospun poly-epsilon-caprolactone mesh submerged in liquid media. *Materials Science & Engineering C-Materials for Biological Applications.* Aug 2012;32(6):1366-1374.
126. Knott JI. MERSILENE MESH FOR POST-THROMBOTIC LEG - CASE REPORT. *Angiology.* 1961;12(12):607-&.
127. Knuutinen A, Kokkonen N, Risteli J, et al. Smoking affects collagen synthesis and extracellular matrix turnover in human skin. *The British journal of dermatology.* Apr 2002;146(4):588-594.
128. Kobsa S, Kristofik NJ, Sawyer AJ, Bothwell ALM, Kyriakides TR, Saltzman WM. An electrospun scaffold integrating nucleic acid delivery for treatment of full-thickness wounds. *Biomaterials.* May 2013;34(15):3891-3901.
129. Kocova J. Overall staining of connective tissue and the muscular layer of vessels. *Folia Morphol (Praha).* 1970;18(3):293-295.
130. Koontz AR. Preliminary Report on the Use of Tantalum Mesh in the Repair of Ventral Hernias. *Ann Surg.* May 1948;127(5):1079-1085.
131. Koontz AR, Kimberly RC. Further experimental work on prostheses for hernia repair. *Surgery, gynecology & obstetrics.* Sep 1959;109:321-327.
132. Korenkov M, Paul A, Sauerland S, et al. Classification and surgical treatment of incisional hernia. Results of an experts' meeting. *Langenbeck's archives of surgery / Deutsche Gesellschaft fur Chirurgie.* Feb 2001;386(1):65-73.
133. Kweon H, Yoo MK, Park IK, et al. A novel degradable polycaprolactone networks for tissue engineering. *Biomaterials.* Feb 2003;24(5):801-808.
134. Lawrence DA. Transforming growth factor-beta: a general review. *European cytokine network.* Sep 1996;7(3):363-374.
135. LeBlanc KA. Prostheses and Products for Hernioplasty. In: Kingsnorth A, LeBlanc KA, eds. *Management of Abdominal Hernias*. 4 ed. London: Management of Abdominal Hernias; 2013: p. 103-150.
136. Lee GH, Cohen AJ. CT imaging of abdominal hernias. *AJR. American journal of roentgenology.* Dec 1993;161(6):1209-1213.
137. Li WJ, Danielson KG, Alexander PG, Tuan RS. Biological response of chondrocytes cultured in three-dimensional nanofibrous poly(epsilon-caprolactone) scaffolds. *J Biomed Mater Res A.* Dec 2003;67(4):1105-1114.

138. Li WJ, Tuli R, Okafor C, et al. A three-dimensional nanofibrous scaffold for cartilage tissue engineering using human mesenchymal stem cells. *Biomaterials.* Feb 2005;26(6):599-609.
139. Liang D, Luu YK, Kim K, Hsiao BS, Hadjiargyrou M, Chu B. In vitro non-viral gene delivery with nanofibrous scaffolds. *Nucleic acids research.* Nov 2005;33(19):e170.
140. Liu X, Lin T, Fang J, et al. In vivo wound healing and antibacterial performances of electrospun nanofibre membranes. *J Biomed Mater Res A.* Aug 2010;94(2):499-508.
141. Lo B, Li L, Gissen P, et al. Requirement of VPS33B, a member of the Sec1/Munc18 protein family, in megakaryocyte and platelet alpha-granule biogenesis. *Blood.* Dec 2005;106(13):4159-4166.
142. Losanoff JE, Richman BW, Jones JW. Entero-colocutaneous fistula: a late consequence of polypropylene mesh abdominal wall repair: case report and review of the literature. *Hernia : the journal of hernias and abdominal wall surgery.* Sep 2002;6(3):144-147.
143. Loscertales IG, Barrero A, Marquez M, Spretz R, Velarde-Ortiz R, Larsen G. Electrically forced coaxial nanojets for one-step hollow nanofiber design. *Journal of the American Chemical Society.* May 2004;126(17):5376-5377.
144. Lu Y, Jiang HL, Tu KH, Wang LQ. Mild immobilization of diverse macromolecular bioactive agents onto multifunctional fibrous membranes prepared by coaxial electrospinning. *Acta Biomater.* Jun 2009;5(5):1562-1574.
145. Luijendijk RW, Hop WC, van den Tol MP, et al. A comparison of suture repair with mesh repair for incisional hernia. *N Engl J Med.* Aug 2000;343(6):392-398.
146. Lukas D, Sarkar A, Chaloupek J. Principles of Electrospinning. In: Kothari VK, ed. *Nonwoven Fabrics*. 1 ed. New Delhi: IAFL Publications; 2008.
147. Lukas D, Sarkar A, Martinova L, et al. Physical principles of electrospinning (electrospinning as a nano-scale technology of the twenty-first century). *Textile Progress.* Mar 2009;41(2):59-140.
148. Lukas D, Sarkar A, Pokorny P. Self-organization of jets in electrospinning from free liquid surface: A generalized approach. *Journal of Applied Physics.* Apr 2008b;103(8).
149. Ma Z, Kotaki M, Inai R, Ramakrishna S. Potential of nanofiber matrix as tissue-engineering scaffolds. *Tissue Eng.* Jan-Feb 2005a;11(1-2):101-109.
150. Ma ZW, Kotaki M, Ramakrishna S. Electrospun cellulose nanofiber as affinity membrane. *Journal of Membrane Science.* Nov 2005b;265(1-2):115-123.
151. Madry H, Zurakowski D, Trippel SB. Overexpression of human insulin-like growth factor-I promotes new tissue formation in an ex vivo model of articular chondrocyte transplantation. *Gene therapy.* Oct 2001;8(19):1443-1449.
152. Manakhov A, Necas D, Cechal J, Pavlinak D, Elias M, Zajickova L. Deposition of stable amine coating onto polycaprolactone nanofibers by low pressure cyclopropylamine plasma polymerization. *Thin Solid Films.* Apr 2015;581:7-13.
153. Matlock-Colangelo L, Baeumner AJ. Biologically Inspired Nanofibers for Use in Translational Bioanalytical Systems. *Annual Review of Analytical Chemistry,* 2014;7:23-42.
154. Matthews JA, Wnek GE, Simpson DG, Bowlin GL. Electrospinning of collagen nanofibers. *Biomacromolecules.* Mar-Apr 2002;3(2):232-238.
155. Mayo WJ. IV. Remarks on the Radical Cure of Hernia. *Ann Surg.* Jan 1899;29(1):51-61.

156. McGavin L. An Address ON THE USE OF FILIGREES OF SILVER WIRE IN THE CURE OF HERNIAE USUALLY CONSIDERED INOPERABLE: Read before the Norwood Division of the British Medical Association. In: Bendavid R, Abrahamson J, Arregui ME, Flament JB, Phillips EH, eds. *Abdominal Wall Hernias*. 1 ed. New York: Springer Science+Buisness Media New York; 2001: p. 792.
157. Melick DW. Nylon sutures. *Annals of Surgery.* 1942;115:475-476.
158. Melman L, Jenkins ED, Hamilton NA, et al. Histologic and biomechanical evaluation of a novel macroporous polytetrafluoroethylene knit mesh compared to lightweight and heavyweight polypropylene mesh in a porcine model of ventral incisional hernia repair. *Hernia : the journal of hernias and abdominal wall surgery.* Aug 2011;15(4):423-431.
159. Meyer W. The implantation of silver filigree for the closure of large hernial apertures. In: Bendavid R, Abrahamson J, Arregui ME, Flament JB, Phillips EH, eds. *Abdominal Wall Hernias*. 1 ed. New York: Springer Science+Buisness Media New York; 2001: p. 792.
160. Mickova A, Buzgo M, Benada O, et al. Core/shell nanofibers with embedded liposomes as a drug delivery system. *J Tissue Eng Regen M.* Oct 2012;6:35-35.
161. Milburn ML, Holton LH, Chung TL, et al. Acellular dermal matrix compared with synthetic implant material for repair of ventral hernia in the setting of peri-operative Staphylococcus aureus implant contamination: a rabbit model. *Surg Infect (Larchmt).* Aug 2008;9(4):433-442.
162. Miller PA, Mezwa DG, Feczko PJ, Jafri ZH, Madrazo BL. Imaging of abdominal hernias. *Radiographics : a review publication of the Radiological Society of North America, Inc.* Mar 1995;15(2):333-347.
163. Moloney GE, Gill WG, Barclay RC. OPERATIONS FOR HERNIA - TECHNIQUE OF NYLON DARN. *Lancet.* Jul 1948;255:45-48.
164. Monteiro N, Martins M, Martins A, et al. Antibacterial activity of chitosan nanofiber meshes with liposomes immobilized releasing gentamicin. *Acta Biomater.* May 2015;18:196-205.
165. Mouton PR. *Principles and Practices of Unbiased Stereology: An Introduction for Bioscientists.* 1 ed. Baltimore: Johns Hopkins University Press; 2002, p. 232.
166. Mustoe TA, Pierce GF, Thomason A, Gramates P, Sporn MB, Deuel TF. Accelerated healing of incisional wounds in rats induced by transforming growth factor-beta. *Science.* Sep 1987;237(4820):1333-1336.
167. Muysoms F, Campanelli G, Champault GG, et al. EuraHS: the development of an international online platform for registration and outcome measurement of ventral abdominal wall hernia repair. *Hernia : the journal of hernias and abdominal wall surgery.* Jun 2012;16(3):239-250.
168. Muysoms FE, Miserez M, Berrevoet F, et al. Classification of primary and incisional abdominal wall hernias. *Hernia : the journal of hernias and abdominal wall surgery.* Aug 2009;13(4):407-414.
169. Nakahata N. Thromboxane A2: physiology/pathophysiology, cellular signal transduction and pharmacology. *Pharmacology & therapeutics.* Apr 2008;118(1):18-35.
170. Nauta A, Gurtner GC, Longaker MT. Wound healing and regenerative strategies. *Oral Diseases.* Sep 2011;17(6):541-549.
171. Ng KW, Achuth HN, Moochhala S, Lim TC, Hutmacher DW. In vivo evaluation of an ultra-thin polycaprolactone film as a wound dressing. *Journal of Biomaterials Science-Polymer Edition.* Jul 2007;18(7):925-938.

172. Ng KW, Hutmacher DW, Schantz JT, et al. Evaluation of ultra-thin poly(epsilon-caprolactone) films for tissue-engineered skin. *Tissue Eng.* Aug 2001;7(4):441-455.
173. Nikolidakis D, Jansen JA. Biology of platelet-rich plasma and its application in oral surgery: Literature review. *Tissue Engineering Part B-Reviews.* Sep 2008;14(3):249-258.
174. Niu HT, Lin T, Wang XG. Needleless Electrospinning. I. A Comparison of Cylinder and Disk Nozzles. *Journal of Applied Polymer Science.* Dec 2009;114(6):3524-3530.
175. Ohgo K, Zhao CH, Kobayashi M, Asakura T. Preparation of non-woven nanofibers of Bombyx mori silk, Samia cynthia ricini silk and recombinant hybrid silk with electrospinning method. *Polymer.* Feb 2003;44(3):841-846.
176. Oktay B, Demir S, Kayaman-Apohan N. Immobilization of alpha-amylase onto poly(glycidyl methacrylate) grafted electrospun fibers by ATRP. *Materials Science & Engineering C-Materials for Biological Applications.* May 2015;50:386-393.
177. Panseri S, Cunha C, Lowery J, et al. Electrospun micro- and nanofiber tubes for functional nervous regeneration in sciatic nerve transections. *BMC biotechnology.* Apr 2008;8:39-51.
178. Park A, Birch DW, Lovrics P. Laparoscopic and open incisional hernia repair: a comparison study. *Surgery.* Oct 1998;124(4):816-821; discussion 821-812.
179. Passaretti F, Tia M, D'Esposito V, et al. Growth-promoting action and growth factor release by different platelet derivatives. *Platelets.* Jan 2014;25(4):252-256.
180. Patel AC, Li SX, Yuan JM, Wei Y. In situ encapsulation of horseradish peroxidase in electrospun porous silica fibers for potential biosensor applications. *Nano Letters.* May 2006;6(5):1042-1046.
181. Paul A, Korenkov M, Peters S, Kohler L, Fischer S, Troidl H. Unacceptable results of the Mayo procedure for repair of abdominal incisional hernias. *The European journal of surgery = Acta chirurgica.* May 1998;164(5):361-367.
182. Peppas G, Gkegkes ID, Makris MC, Falagas ME. Biological mesh in hernia repair, abdominal wall defects, and reconstruction and treatment of pelvic organ prolapse: a review of the clinical evidence. *Am Surg.* Nov 2010;76(11):1290-1299.
183. Pietrzak WS, An YH, Kang QK, Demos HA, Ehrens KH. Platelet-rich and platelet-poor plasma: development of an animal model to evaluate hemostatic efficacy. *Journal of Craniofacial Surgery.* May 2007;18(3):559-567.
184. Plachokova AS, Nikolidakis D, Mulder J, Jansen JA, Creugers NH. Effect of platelet-rich plasma on bone regeneration in dentistry: a systematic review. *Clinical oral implants research.* Jun 2008;19(6):539-545.
185. Prosecka E, Rampichova M, Litvinec A, et al. Collagen/hydroxyapatite scaffold enriched with polycaprolactone nanofibers, thrombocyte-rich solution and mesenchymal stem cells promotes regeneration in large bone defect in vivo. *J Biomed Mater Res A.* May 16 2014.
186. Qi HX, Hu P, Xu J, Wang AJ. Encapsulation of drug reservoirs in fibers by emulsion electrospinning: Morphology characterization and preliminary release assessment. *Biomacromolecules.* Aug 2006;7(8):2327-2330.
187. Rai B, Teoh SH, Ho KH. An in vitro evaluation of PCL-TCP composites as delivery systems for platelet-rich plasma. *J Control Release.* Oct 2005;107(2):330-342.
188. Rampichova M, Chvojka J, Buzgo M, et al. Elastic three-dimensional poly (epsilon-caprolactone) nanofibre scaffold enhances migration, proliferation and

osteogenic differentiation of mesenchymal stem cells. *Cell Prolif.* Feb 2013;46(1):23-37.
189. Ramshaw BJ, Esartia P, Schwab J, et al. Comparison of laparoscopic and open ventral herniorrhaphy. *Am Surg.* Sep 1999;65(9):827-831; discussion 831-822.
190. Read RC. Milestones in the history of hernia surgery: prosthetic repair. *Hernia : the journal of hernias and abdominal wall surgery.* Feb 2004;8(1):8-14.
191. Reznik SN, Yarin AL, Zussman E, Bercovici L. Evolution of a compound droplet attached to a core-shell nozzle under the action of a strong electric field. *Physics of Fluids.* Jun 2006;18(6).
192. Rich L, Whittaker P. Collagen and Picrosirius Red staining: a polarized light assessment of fibrillar hue and spatial distribution. *Braz J Morphol Sci.* 2005;22(2):97-104.
193. Richardson TP, Peters MC, Ennett AB, Mooney DJ. Polymeric system for dual growth factor delivery. *Nat Biotechnol.* Nov 2001;19(11):1029-1034.
194. Rives J. Surgical treatment of the inguinal hernia with dacron patch. *International surgery.* Apr 1967;47(4):360-361.
195. Roberts DE, McNicol A, Bose R. Mechanism of collagen activation in human platelets. *Journal of Biological Chemistry.* May 2004;279(19):19421-19430.
196. Rodriguez A, Anastassov GE, Lee H, Buchbinder D, Wettan H. Maxillary sinus augmentation with deproteinated bovine bone and platelet rich plasma with simultaneous insertion of endosseous implants. *Journal of oral and maxillofacial surgery : official journal of the American Association of Oral and Maxillofacial Surgeons.* Feb 2003;61(2):157-163.
197. Rosen MJ. Biologic mesh for abdominal wall reconstruction: a critical appraisal. *Am Surg.* Jan 2010;76(1):1-6.
198. Rubert M, Dehli J, Li YF, et al. Electrospun PCL/PEO coaxial fibers for basic fibroblast growth factor delivery. *Journal of Materials Chemistry B.* Oct 2014;2(48):8538-8546.
199. Sahoo S, Ang LT, Goh JCH, Toh SL. Growth factor delivery through electrospun nanofibers in scaffolds for tissue engineering applications. *Journal of Biomedical Materials Research Part A.* Jun 2010;93A(4):1539-1550.
200. Sandor M, Xu H, Connor J, et al. Host response to implanted porcine-derived biologic materials in a primate model of abdominal wall repair. *Tissue engineering. Part A.* Dec 2008;14(12):2021-2031.
201. Saraf A, Lozier G, Haesslein A, et al. Fabrication of Nonwoven Coaxial Fiber Meshes by Electrospinning. *Tissue Engineering Part C-Methods.* Sep 2009;15(3):333-344.
202. Sato T, Chen G, Ushida T, et al. Evaluation of PLLA-collagen hybrid sponge as a scaffold for cartilage tissue engineering. *Materials Science and Engineering: C.* Dec 2004;24(3):365-372.
203. Scheidbach H, Tamme C, Tannapfel A, Lippert H, Kockerling F. In vivo studies comparing the biocompatibility of various polypropylene meshes and their handling properties during endoscopic total extraperitoneal (TEP) patchplasty: an experimental study in pigs. *Surgical endoscopy.* Feb 2004;18(2):211-220.
204. Schmidbauer S, Ladurner R, Hallfeldt KK, Mussack T. Heavy-weight versus low-weight polypropylene meshes for open sublay mesh repair of incisional hernia. *European journal of medical research.* Jun 22 2005;10(6):247-253.
205. Schnell E, Klinkhammer K, Balzer S, et al. Guidance of glial cell migration and axonal growth on electrospun nanofibers of poly-epsilon-caprolactone and a

collagen/poly-epsilon-caprolactone blend. *Biomaterials.* Jul 2007;28(19):3012-3025.
206. Schoenmaeckers EJ, van der Valk SB, van den Hout HW, Raymakers JF, Rakic S. Computed tomographic measurements of mesh shrinkage after laparoscopic ventral incisional hernia repair with an expanded polytetrafluoroethylene mesh. *Surgical endoscopy.* Jul 2009;23(7):1620-1623.
207. Schreinemacher MH, Emans PJ, Gijbels MJ, Greve JW, Beets GL, Bouvy ND. Degradation of mesh coatings and intraperitoneal adhesion formation in an experimental model. *Br J Surg.* Mar 2009;96(3):305-313.
208. Shankaran V, Weber DJ, Reed RL, 2nd, Luchette FA. A review of available prosthetics for ventral hernia repair. *Ann Surg.* Jan 2011;253(1):16-26.
209. Sill TJ, von Recum HA. Electrospinning: Applications in drug delivery and tissue engineering. *Biomaterials.* Feb 2008;29:1989-2006
210. Stellos K, Langer H, Daub K, et al. Platelet-derived stromal cell-derived factor-1 regulates adhesion and promotes differentiation of human CD34+ cells to endothelial progenitor cells. *Circulation.* Jan 2008;117(2):206-215.
211. Stoppa RE. The treatment of complicated groin and incisional hernias. *World J Surg.* Sep-Oct 1989;13(5):545-554.
212. Sugerman HJ, Kellum JM, Jr., Reines HD, DeMaria EJ, Newsome HH, Lowry JW. Greater risk of incisional hernia with morbidly obese than steroid-dependent patients and low recurrence with prefascial polypropylene mesh. *American journal of surgery.* Jan 1996;171(1):80-84.
213. Sun ZC, Zussman E, Yarin AL, Wendorff JH, Greiner A. Compound core-shell polymer nanofibers by co-electrospinning. *Advanced Materials.* Nov 2003;15(22):1929-1932.
214. Tabata II. The importance of drug delivery systems in tissue engineering. *Pharmaceutical science & technology today.* Mar 2000;3(3):80-89.
215. Teo WE, Ramakrishna S. A review on electrospinning design and nanofibre assemblies. *Nanotechnology.* Jul 2006;17(14):R89-R106.
216. Thapa A, Webster TJ, Haberstroh KM. Polymers with nano-dimensional surface features enhance bladder smooth muscle cell adhesion. *J Biomed Mater Res A.* Dec 2003;67(4):1374-1383.
217. Thorbjarnarson B, Goulian D. Complications from use of surgical mesh in repair of hernias. *New York state journal of medicine.* May 1967;67(9):1189-1192.
218. Tonti GA, Mannello F. From bone marrow to therapeutic applications: different behaviour and genetic/epigenetic stability during mesenchymal stem cell expansion in autologous and foetal bovine sera? *The International journal of developmental biology.* Nov 2008;52(8):1023-1032.
219. Townsend-Nicholson A, Jayasinghe SN. Cell electrospinning: a unique biotechnique for encapsulating living organisms for generating active biological microthreads/scaffolds. *Biomacromolecules.* Dec 2006;7(12):3364-3369.
220. Tuli R, Tuli S, Nandi S, et al. Transforming growth factor-beta-mediated chondrogenesis of human mesenchymal progenitor cells involves N-cadherin and mitogen-activated protein kinase and Wnt signaling cross-talk. *The Journal of biological chemistry.* Oct 17 2003;278(42):41227-41236.
221. Um IC, Fang DF, Hsiao BS, Okamoto A, Chu B. Electro-spinning and electro-blowing of hyaluronic acid. *Biomacromolecules.* Jul-Aug 2004;5(4):1428-1436.
222. Usher FC, Ochsner J, Tuttle LL, Jr. Use of marlex mesh in the repair of incisional hernias. *Am Surg.* Dec 1958;24(12):969-974.

223. Vasita R, Katti DS. Nanofibers and their applications in tissue engineering. *Int J Nanomedicine.* 2006;1(1):15-30.
224. Vavken P, Sadoghi P, Murray MM. The effect of platelet concentrates on graft maturation and graft-bone interface healing in anterior cruciate ligament reconstruction in human patients: a systematic review of controlled trials. *Arthroscopy : the journal of arthroscopic & related surgery : official publication of the Arthroscopy Association of North America and the International Arthroscopy Association.* Nov 2011;27(11):1573-1583.
225. Venugopal JR, Zhang Y, Ramakrishna S. In vitro culture of human dermal fibroblasts on electrospun polycaprolactone collagen nanofibrous membrane. *Artif Organs.* Jun 2006;30(6):440-446.
226. Voskerician G, Jin J, White MF, Williams CP, Rosen MJ. Effect of biomaterial design criteria on the performance of surgical meshes for abdominal hernia repair: a pre-clinical evaluation in a chronic rat model. *J Mater Sci Mater Med.* Jun 2010;21(6):1989-1995.
227. Vrijland WW, Bonthuis F, Steyerberg EW, Marquet RL, Jeekel J, Bonjer HJ. Peritoneal adhesions to prosthetic materials: choice of mesh for incisional hernia repair. *Surgical endoscopy.* Oct 2000;14(10):960-963.
228. Wang ZG, Wan LS, Liu ZM, Huang XJ, Xu ZK. Enzyme immobilization on electrospun polymer nanofibers: An overview. *Journal of Molecular Catalysis B-Enzymatic.* Apr 2009;56(4):189-195.
229. Wantz GE. Incisional hernioplasty with Mersilene. *Surgery, gynecology & obstetrics.* Feb 1991;172(2):129-137.
230. White JG. An overview of platelet structural physiology. *Scanning microscopy.* Dec 1987;1(4):1677-1700.
231. Williams JM, Adewunmi A, Schek RM, et al. Bone tissue engineering using polycaprolactone scaffolds fabricated via selective laser sintering. *Biomaterials.* Aug 2005;26(23):4817-4827.
232. Williamson MR, Adams EF, Coombes AG. Gravity spun polycaprolactone fibres for soft tissue engineering: interaction with fibroblasts and myoblasts in cell culture. *Biomaterials.* Mar 2006;27(7):1019-1026.
233. Witzel O. Uber den verschluss von bauchwunden und bruchpforten durch versenkte silverdrahtnetze. (Einheilung von filigran-pelotten). *Centralb Chir.* 1900;27:257-260.
234. Wolstenholme JT. Use of commercial dacron fabric in the repair of inguinal hernias and abdominal wall defects. *A.M.A. archives of surgery.* Dec 1956;73(6):1004-1008.
235. Woodward SC, Brewer PS, Moatamed F, Schindler A, Pitt CG. The intracellular degradation of poly(epsilon-caprolactone). *Journal of biomedical materials research.* Apr 1985;19(4):437-444.
236. Wutticharoenmongkol P, Sanchavanakit N, Pavasant P, Supaphol P. Preparation and characterization of novel bone scaffolds based on electrospun polycaprolactone fibers filled with nanoparticles. *Macromolecular bioscience.* Jan 5 2006;6(1):70-77.
237. Xie J, Wang CH. Electrospun micro- and nanofibers for sustained delivery of paclitaxel to treat C6 glioma in vitro. *Pharmaceutical research.* Aug 2006;23(8):1817-1826.
238. Yaeger PC, Masi TL, de Ortiz JL, Binette F, Tubo R, McPherson JM. Synergistic action of transforming growth factor-beta and insulin-like growth factor-I induces

expression of type II collagen and aggrecan genes in adult human articular chondrocytes. *Exp Cell Res.* Dec 1997;237(2):318-325.
239. Yamaguchi R, Terashima H, Yoneyama S, Tadano S, Ohkohchi N. Effects of platelet-rich plasma on intestinal anastomotic healing in rats: PRP concentration is a key factor. *The Journal of surgical research.* Apr 2012;173(2):258-266.
240. Yang F, Murugan R, Wang S, Ramakrishna S. Electrospinning of nano/micro scale poly(L-lactic acid) aligned fibers and their potential in neural tissue engineering. *Biomaterials.* May 2005;26(15):2603-2610.
241. Yarin AL. Coaxial electrospinning and emulsion electrospinning of core-shell fibers. *Polymers for Advanced Technologies.* Mar 2011;22(3):310-317.
242. Yarin AL, Zussman E. Upward needleless electrospinning of multiple nanofibers. *Polymer.* Apr 2004;45(9):2977-2980.
243. Yuan XY, Zhang YY, Dong CH, Sheng J. Morphology of ultrafine polysulfone fibers prepared by electrospinning. *Polymer International.* Nov 2004;53(11):1704-1710.
244. Zeng J, Aigner A, Czubayko F, Kissel T, Wendorff JH, Greiner A. Poly(vinyl alcohol) nanofibers by electrospinning as a protein delivery system and the retardation of enzyme release by additional polymer coatings. *Biomacromolecules.* May-Jun 2005;6(3):1484-1488.
245. Zhang YZ, Huang ZM, Xu XJ, Lim CT, Ramakrishna S. Preparation of core-shell structured PCL-r-gelatin Bi-component nanofibers by coaxial electrospinning. *Chemistry of Materials.* Sep 2004;16(18):3406-3409.
246. Zhao W, Ju YM, Christ G, Atala A, Yoo JJ, Lee SJ. Diaphragmatic muscle reconstruction with an aligned electrospun poly(epsilon-caprolactone)/collagen hybrid scaffold. *Biomaterials.* Nov 2013;34(33):8235-8240.

Reprints of papers published by the author

1. Knotek P., Pouzar M., Buzgo M., Krizkova B., Vlcek M., Mickova A., Plencner M., Navesnik J., Amler E., Belina P. Cryogenic grinding of electrospun poly-ε-caprolactone mesh submerged in liquid media. *Materials Science and Engineering C.* 2012; 32(6): 1366-1374. IF: 2.40 (12)

2. Plencner M.,* East B.,* Tonar Z., Otáhal M., Prosecká E., Rampichová M., Krejčí T., Litvinec A., Buzgo M., Míčková A., Nečas A., Hoch J., Amler E. Abdominal closure reinforcement by using polypropylene mesh functionalized with PCL nanofibers and growth factors for prevention of incisional hernia formation. *Int J Nanomedicine.* 2014;9:3263-3277. IF: 4.2 (13).

3. Plencner M., Prosecka E., Rampichova M., East B., Buzgo M., Vyslouzilova L., Hoch J., Amler E. Significant improvement of biocompatibility of polypropylene mesh for incisional hernia repair by using poly-epsilon-caprolactone nanofibers functionalized with thrombocyte-rich solution. *Int J Nanomedicine.* 2015;10:2635-2646. IF: 4.2 (13).

Articles not directly related to the topic of this thesis

1. Míčková A., Tománková K., Kolářová H., Bajgar R., Šunka P., Plencner M., Jakubová R., Beneš J., Koláčná L. Plánka L., Nečas A., Amler E. Ultrasonic shock - wave as a control mechanism for liposome drug delivery system for possible use in scaffold implanted to animals with iatrogenic articular cartilage defects. *Acta Vet. Brno*. 2008; 77: 285-289, IF: 0.395 (08)

2. Rampichová M., Košťáková E., Filová E., Prosecká E., Plencner M., Ocheretná L., Lytvynets L., Lukáš D., Amler E. Non-woven PGA/PVA fibrous mesh as an appropriate scaffold for chondrocyte proliferation. *Physiol Res.* 2010; 59: 773-781.IF: 1,65 (10)

3. Prosecká E., Rampichová M., Vojtová L., Tvrdík D., Melčáková Š., Juhasová J., Plencner M., Jakubová R., Jančář J., Nečas A., Kochová P., Klepáček J., Tonar Z., Amler E. Optimized conditions for mesenchymal stem cells to differentiate into osteoblasts on acollagen/hydroxyapatite matrix. *Journal of Biomedical Materials Research Part A.* 2011; 99(2): 307-315. IF: 2.63 (11)

4. Prosecká E., Rampichová M., Litvinec A., Tonar Z., Králíčková M., Vojtová L., Kochová P., Plencner M., Buzgo M., Míčková A., Jančář J., Amler E. Collagen/hydroxyapatite scaffold enriched with polycaprolactone nanofibers, thrombocyte-rich solution and mesenchymal stem cells promotes regeneration in large bone defect in vivo. *Journal of Biomedical Materials Research Part A.* 2015;103(2):671-682. IF: 2.84 (13)

Acknowledgments

This work was supported by the Academy of Sciences of the Czech Republic (the Institutional Research Concept RVO 68378041), The Ministry of Education Youth and Sports of the Czech Republic (project IPv6), The Grant Agency of the Charles University (grant No., 545313, 384311, 270513, 424213, 648112), Internal Grant Agency of the Ministry of Health of the Czech Republic (grant No. NT12156) and University Hospital in Motol (grant number 9775). Histological quantification was supported by European Regional Development Fund project ED2.1.00/03.0076. CEITEC - Central European Institute of Technology (CZ.1.05/1.1.00/02.0068) from the European Regional Development Fund.

The authors would like to acknowledge O. Kofroňová and O. Benada from the Laboratory of Molecular Structure Characterization, Institute of Microbiology, Academy of Sciences of the Czech Republic, Prague, Czech Republic, for performing SEM analyses.